

MICROWAVE SPECTRAL STUDIES  
ON NITROSYL CYANIDE  
AND OTHER MOLECULES

Submitted to the University of Glasgow  
in part fulfillment of the requirements  
for the degree of Doctor of Philosophy  
in the Faculty of Science

by

RONALD DICKINSON, B.Sc.

ProQuest Number: 13804110

All rights reserved

INFORMATION TO ALL USERS

The quality of this reproduction is dependent upon the quality of the copy submitted.

In the unlikely event that the author did not send a complete manuscript and there are missing pages, these will be noted. Also, if material had to be removed, a note will indicate the deletion.



ProQuest 13804110

Published by ProQuest LLC (2018). Copyright of the Dissertation is held by the Author.

All rights reserved.

This work is protected against unauthorized copying under Title 17, United States Code  
Microform Edition © ProQuest LLC.

ProQuest LLC.  
789 East Eisenhower Parkway  
P.O. Box 1346  
Ann Arbor, MI 48106 – 1346

## ACKNOWLEDGEMENTS

My sincere thanks go to my supervisor, Dr. J.K. Tyler, for his advice and guidance during the course of the work described in this thesis, and for his critical reading of the text.

I am grateful to Dr. D.D. MacNicol for supplying a sample of 9-thiabicyclo[3,3,1]nona-2,6-diene.

I am indebted to Dr. R.V. Emanuel and Mr. B. Jack for their assistance in the theoretical calculations described in Chapter 2.

I thank the Science Research Council for the award of a maintenance grant, and my wife, whose support helped us to survive on it.

## SUMMARY

Microwave spectral studies on nitrosyl cyanide, maleimide, p-fluoroaniline and 9-thiabicyclo[3,3,1]nona-2,6-diene, and a discussion on the microwave analysis of deuteropropene mixtures are presented. A brief introduction, Chapter 1, has been included to provide information on the general structure of the thesis and bibliography.

Nitrosyl cyanide is an interesting molecule which has not previously been isolated or characterised. A comprehensive investigation of its physical properties has been carried out by microwave spectroscopy. In Chapter 2, the molecular structure, dipole moment and  $^{14}\text{N}$  nuclear quadrupole coupling constants are presented and discussed. Also included is information on molecular vibrations. Theoretical calculations of physical properties have been performed, the results of which are compared with experimental values.

The microwave spectra of normal and N-deutero maleimide have been analysed. The spectra, in particular the inertial defects, are discussed in terms of molecular planarity. The dipole moment has been determined. This forms the substance of Chapter 3.

In the fourth chapter, the microwave spectrum of  $\text{ND}_2$ -p-fluoroaniline is presented. Spectra of the normal and NHD species have been analysed previously, allowing calculation of the amine group geometry, which is discussed in relation to those of aniline and p-chloroaniline.

The microwave spectrum of 9-thiabicyclo[3,3,1]nona-2,6-diene has been measured and analysed, as detailed in Chapter 5.

Microwave spectroscopy has an important application in the analysis of deuteropropene mixtures formed by heterogeneous catalysis. In Chapter 6 the theoretical and practical considerations involved in this procedure, with examples of two mechanistic studies, are presented. This technique is not restricted to propene and may be applied to other catalytic reactions.

# CONTENTS.

	page
<u>Chapter 1.</u>	
Introduction	1
References	2
 <u>Chapter 2.</u>	
The Microwave Spectrum of Nitrosyl Cyanide	
2.1 Introduction	3
2.2 Observation and analysis of the Spectrum	6
2.3 Centrifugal distortion	16
2.4 Structure	20
2.5 Stark effect and dipole moment	24
2.6 Quadrupole coupling in nitrosyl cyanide	28
2.7 The vibrational spectrum	40
2.8 Theoretical calculations	44
2.9 Preparation of NO.CN and isotopically substituted species	49
References	51
 <u>Chapter 3.</u>	
The Microwave Spectrum of Maleimide	
3.1 Introduction	54
3.2 Observation and analysis of the spectrum	55
3.3 Structure	68
3.4 Dipole moment	72
References	75
 <u>Chapter 4.</u>	
The Effect of p-Halogen Substituents on the Amine Group Geometry of Aniline; the Microwave Spectrum of ND <sub>2</sub> -p-Fluoroaniline	
4.1 Introduction	78
4.2 Analysis of the spectrum of ND <sub>2</sub> -p-fluoroaniline	79

4.3	Calculation of the NH <sub>2</sub> -group geometry	82
4.4	The configuration of the amine group in aniline and its p-fluoro- and p-chloro-derivatives	89
	References	93
<u>Chapter 5.</u>	The Microwave Spectrum of 9-Thia-bicyclo[3,3,1] nona-2,6-diene	
5.1	Introduction	94
5.2	Observation and analysis of the spectrum	96
5.3	General conclusions	103
	References	105
<u>Chapter 6.</u>	Application of Microwave Spectroscopy to Analysis of Deuteropropene Mixtures formed by Heterogeneous Catalysis	
6.1	Introduction	106
6.2	Factors governing line intensities	109
6.3	Example of mechanistic studies of catalytic exchange reactions by the tracer/microwave technique	119
	References	122

---

Appendices I - III.

## CHAPTER 1.

### INTRODUCTION.

In this thesis are presented microwave spectral studies on nitrosyl cyanide, maleimide, p-fluoroaniline, and 9-thia-bicyclo[3,3,1]nona-2,6-diene, and a procedure for the analysis of deuteropropene mixtures. Each of the following chapters is devoted to one molecular study.

Where appropriate, theory relevant to a particular section is included in the text. General accounts of the theory of microwave spectroscopy are available in the standard reference books.<sup>1-7</sup> A detailed quantum mechanical treatment of rotational spectroscopy and vibration-rotation interactions is presented in reference 1, while references 2-6 are more broadly based with some attention to practical details.

Spectra were observed in the conventional Stark modulation spectrometer which has been in use at Glasgow for some time, and is described in detail elsewhere.<sup>8-10</sup> The only difference between the current system and that described previously is use of a backward wave oscillator (b.w.o.) as a microwave source, with tubes for operation in J-, K-, and Q-bands. The b.w.o. has the advantage that it can easily be adjusted over many GHz. In addition, a ferrite isolator has been introduced to reduce reflections in the cell. Measurements with this system are usually accurate to within  $\sim 0.1$  MHz. Where particularly high resolution is required, for example in the analysis of nuclear quadrupole hyperfine structure, reflex klystrons may be used. Aspects of instrumentation pertaining to the measurement

of transition intensities are discussed in Chapter 6.

The  $^{12}\text{C}$  mass scale was used throughout the work in this thesis with  $\frac{h}{8\pi^2} = 505376 \text{ MHz amu } \text{\AA}^2$ .

#### REFERENCES.

1. H.C. Allen Jr. and P.C. Cross, "Molecular Vib-rotors", John Wiley and Sons, Inc., New York, 1963.
2. W. Gordy, W.V. Smith and R.F. Trambarulo, "Microwave Spectroscopy", Dover Publications Inc., New York, 1953.
3. C.H. Townes and A.L. Schawlow, "Microwave Spectroscopy", McGraw-Hill Book Co. Inc., New York, 1955.
4. T.M. Sugden and C.N. Kenney, "Microwave Spectroscopy of Gases", D. Van Nostrand Co. Ltd., London, 1966.
5. J.E. Wollrab, "Rotational Spectra and Molecular Structure", Academic Press Inc., New York, 1967.
6. H.W. Krato, "Molecular Rotation Spectra", John Wiley and Sons Ltd., London, 1975.
7. W. Gordy and R.L. Cook, "Microwave Molecular Spectra", Vol. IX part II, "Techniques of Organic Chemistry", ed. Weissberger, John Wiley and Sons, Inc., New York, 1970.
8. D.G. Lister, Ph.D. Thesis, University of Glasgow, 1968.
9. J.N. Macdonald, Ph.D. Thesis, University of Glasgow, 1969.
10. S.A. Mackay, Ph.D. Thesis, University of Glasgow, 1971.

## CHAPTER 2.

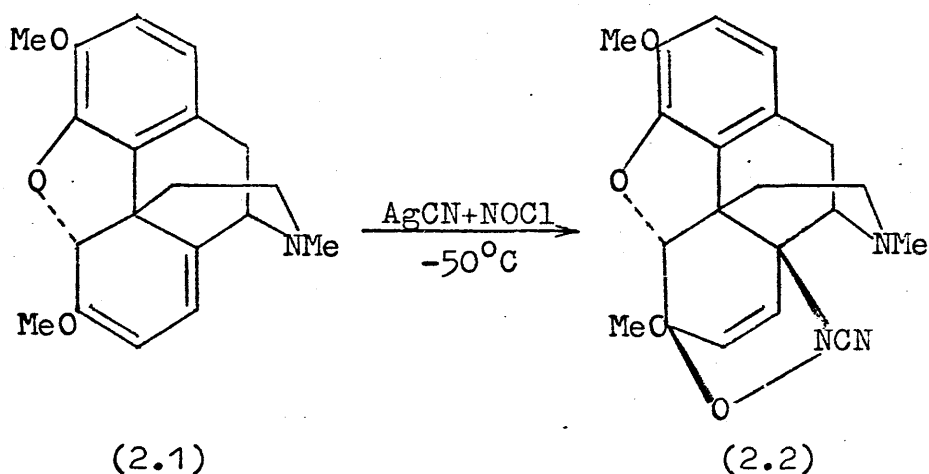
### THE MICROWAVE SPECTRUM OF NITROSYL CYANIDE.

#### 1. Introduction.

Nitrosyl cyanide, NO.CN, has been suggested as an unstable intermediate in the photolysis of cyanogen / nitric oxide mixtures containing a trace of nitrogen dioxide.<sup>1</sup> The evidence for the existence of NO.CN in this system was based on an analysis of pressure / time measurements. The mass spectrometric detection of nitrosyl cyanide has also been reported in photolysis experiments on cyanogen halide / nitric oxide mixtures.<sup>2</sup> However the isolation and characterisation of this interesting substance have not been achieved until recently, as will now be detailed.

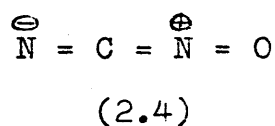
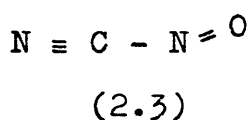
Nitrosyl chloride has been shown by Kirby and co-workers to react with silver cyanide at  $-20^{\circ}\text{C}$  to form silver chloride and a blue-green gas, stable in a glass vessel at room temperature for several hours.<sup>3</sup> The structure NO.CN was proposed for this gas on the basis of its colour, ( $\lambda_{\text{max}} = 738 \text{ nm}$ ),<sup>4</sup> typical of C-nitroso compounds, and its cycloaddition to conjugated dienes to form N-cyano-3,6-dihydro-2H-1,2-oxazines. This work originated in reactions of the alkaloid thebaine (2.1) with a range of C-nitroso compounds to give Diels-Alder adducts, readily convertible into 14-aminocodeinone derivatives, several of which have analgaesic properties.<sup>5</sup> The adducts of thebaine and nitrosoarenes, however, dissociated in solution over prolonged periods at room temperature. The high electronegativity of the nitrile group, which would

facilitate electrophilic addition, led to the reaction of thebaine with nitrosyl chloride and silver cyanide to give the stable adduct (2.2).



The initial object of the present study was to provide conclusive evidence for the existence of nitrosyl cyanide in the products of the  $\text{NO} \cdot \text{Cl} / \text{AgCN}$  reaction. This has been successfully achieved and subsequently an extensive microwave spectral investigation was carried out.

$\text{NO} \cdot \text{CN}$  is a chemically interesting molecule suitable for microwave work. In addition, it is small, allowing theoretical calculation of its structural and electronic properties. Of particular interest in this microwave investigation are the relative contributions of the valence bond canonical forms (2.3) and (2.4).



Five isotopic species of this molecule have been studied; these are normal  $\text{NO} \cdot \text{CN}$ ,  $^{15}\text{NO} \cdot \text{CN}$ ,  $\text{N}^{18}\text{O} \cdot \text{CN}$ ,  $\text{NO} \cdot ^{13}\text{CN}$  and  $\text{NO} \cdot \text{C}^{15}\text{N}$ . Rotational constants and centrifugal distortion

constants were obtained for each species. A planar equilibrium conformation of the molecule in the ground vibrational state has been established by accurate determination of the inertial defect of the normal species. Structural parameters of the molecule have been evaluated, the internuclear distances suggesting a small amount of delocalisation of the N=O and C≡N  $\pi$ -electron systems.

The dipole moment of nitrosyl cyanide, and its components along the principal inertial axes, have been determined from Stark effect measurements. The value of the dipole moment,  $\mu$ , is  $1.365 \pm 0.03$  D, with  $\mu_a = 1.241 \pm 0.003$  D and  $\mu_b = 0.57 \pm 0.08$  D.

$^{14}\text{N}$ -quadrupole hyperfine structures have been resolved in the spectra of NO.CN,  $^{15}\text{NO.CN}$  and  $\text{NO.C}^{15}\text{N}$ . Analysis of these hyperfine patterns yielded coupling constants  $\chi_{aa}$  and  $\chi_{bb}$  for each nitrogen. These are discussed in terms of the electronic configuration of the molecule.

Theoretical calculations have been performed on NO.CN using INDO and extended basis SCF ab initio (Atmol) methods. Values for the dipole moment and quadrupole coupling constants from these calculations are compared with experimental results. The preferred conformation of the N-C-N fragment was calculated by both methods.

Attempts to repeat the experiments of Norrish et al using the Stark spectrometer to monitor formation of nitrosyl cyanide were unsuccessful. Nor was any NO.CN obtained on passing an electric discharge through the cyanogen / nitric oxide mixtures. A discharge on a

mixture of NO.Cl and cyanogen produced cyanogen chloride, but again no nitrosyl cyanide was detected in the spectrometer.

Preliminary reports have been made on the structure<sup>6</sup> and dipole moment<sup>6(b)</sup> of NO.CN.

## 2. Observation and Analysis of the Spectrum.

The spectrum of nitrosyl cyanide was predicted using a planar model in which  $r(\text{C}\equiv\text{N}) = 1.16 \text{ \AA}$ ,  $r(\text{N}-\text{C}) = 1.35 \text{ \AA}$ ,  $r(\text{N}=\text{O}) = 1.20 \text{ \AA}$  and the angle  $\text{CNO} = 120^\circ$ , the  $\text{N}\equiv\text{C}-\text{N}$  fragment being assumed linear. Predictions were made of the  $\mu_a$ , R-branch transitions expected to be the most intense in the spectrum of a molecule of this type. A search was made for these lines. The predominant species in the reaction gases was nitrosyl chloride, but some weaker lines, due to nitrosyl cyanide, were observed. Impurities detected included ClCN, NO, NO<sub>2</sub>, H<sub>2</sub>O and HCN. The transitions of NO.CN were assigned on the basis of their Stark effects and their deviation from predicted frequencies. Assignment was facilitated by the fact that there is no overlap of the R-branch centres of NO.CN and NO.Cl in the K- and Q-band regions in which initial observations were made.

Spectra were observed in the Stark modulation spectrometer, the absorption cell being cooled with solid CO<sub>2</sub> to slow decomposition of nitrosyl cyanide. Under these conditions, it is possible to observe a sample for a period of about thirty minutes without renewal. The pressure of gas in the cell was generally in the range

0.01 - 0.08 torr.

Rotational constants were calculated from the expressions of Polo.<sup>7</sup> For a near-prolate rotor, these may be written;-

$$\underline{K_{-1}=0} \quad \frac{\nu}{J+1} = B+C-8R_6 + \frac{B-C}{2}\epsilon - (J+1)^2 \cdot \frac{B-C}{2}\epsilon - 4D_J(J+1)^2.$$

$$\underline{\langle K_{-1}=1 \rangle} \quad \frac{\nu}{J+1} = B+C-8R_6 - 2D_{JK} + \frac{B-C}{2}\epsilon - (J+1)^2 \cdot \frac{B-C}{8}\epsilon - 4D_J(J+1)^2.$$

$$\underline{\langle K_{-1}=2 \rangle} \quad \frac{\nu}{J+1} = B+C-8R_6 - 16D_{JK} + \frac{B-C}{2}\epsilon + (J+1)^2 \cdot \frac{B-C}{6}\epsilon - 4D_J(J+1)^2.$$

The separation of the  $K_{-1}=1$  lines is given by;-

$$\frac{\Delta\nu}{J+1} = B-C + 8R_5 - 8(J+1)^2\delta_J. \quad (2.1)$$

where  $\langle K_{-1}=1 \rangle$  denotes the mean of the  $J_{1,J} - (J+1)_{1,J+1}$  and  $J_{1,J-1} - (J+1)_{1,J}$  lines,

$\epsilon$  is an asymmetry parameter =  $\frac{B-C}{2(2A-B-C)}$ ,

and  $D_J$ ,  $D_{JK}$ ,  $\delta_J$ ,  $R_5$ , and  $R_6$  are centrifugal distortion constants,  $\delta_J$ ,  $R_5$ , and  $R_6$  being zero at the symmetric top limit.

Rotational constants were obtained by simultaneous solution of these equations, graphical methods being used where possible.

It was evident from a comparison of predicted and observed frequencies of NO.CN that the model required improvement before being used to predict spectra of the isotopically substituted species. The parameters thought to be least reliable, the central N-C internuclear

distance and the CNO angle, were fitted to  $I_a (= I_c - I_b)$  and  $I_b$ , giving  $r(\text{N-C}) = 1.42 \text{ \AA}$  and angle  $\text{CNO} = 118^\circ$ . This optimised model was used in calculation of moments of inertia for the isotopically substituted species. The differences between these and the moments of normal nitrosyl cyanide gave  $\Delta B$  and  $\Delta C$  for each species, which were used to predict the spectra by calculating corrections required to the normal NO.CN frequencies from Polo's expressions (equations 2.1). This method is more precise than direct prediction, due to inaccuracies in the model.

The spectra of the isotopically substituted species were analysed using Polo's expressions as described above. A full structure calculation, making use of the  $I_c - I_b$  and  $I_b$  values, was then possible, provided planarity could be established.<sup>8</sup> To assess planarity, an accurate value of the inertial defect is required. It was necessary therefore, to make a precise determination of the rotational constant A. In the spectrum of a near-prolate rotor, this is not available from the strong  $\mu_a$  transitions. Consequently, a search was undertaken for some  $\mu_b$  lines.

An attempt was made to measure the  $0_{00}-1_{11}$  transition which was predicted to be at approximately 86 GHz. A source modulated spectrometer was used to search for this line, as too much power is lost along the Stark cell at these frequencies. Harmonics of K-band radiation (ca. 29 GHz) from a Klystron were generated using a silicon crystal multiplier. A short section of O-band waveguide was used to filter out the fundamental frequency. How-

ever most of the transmitted microwave power was at twice the fundamental frequency and no line was found. Some improvement was made on A by measuring the  $J = 5-6 \mu_a$  transitions at about 60 GHz by doubling from Q-band in the same apparatus, and some high J,  $K_{-1} = 1$ , Q-branch lines in the Stark spectrometer. This fixed A to within 100 MHz and gave  $\Delta = +0.177 \pm 0.005 \text{ amu } \text{\AA}^2$ . This improved value of A was used to predict several  $\mu_b$ , R-branch lines in the 18-40 GHz range to an accuracy of approximately 150 MHz. These lines were identified on the basis of their Stark effects and their deviation from prediction.

The rotational constant A was then determined to within 0.1 MHz, and a value for  $\Delta$  of  $+0.1799 \pm 0.0003 \text{ amu } \text{\AA}^2$  was obtained. This value is close to that expected for such a molecule if planar.<sup>9</sup> It is also very near the value of  $+0.1769 \text{ amu } \text{\AA}^2$  reported for the inertially similar, planar molecule, propynal.<sup>10</sup> A calculation of  $\Delta$  from the vibrational spectrum of nitrosyl cyanide, (section 7 in this chapter) by the method of Herschbach and Laurie<sup>11</sup> using the uniform coupling and average frequency approximations, gave a value of  $+0.16 \text{ amu } \text{\AA}^2$ , which is within the 10-20% accuracy claimed for this method. These calculations show the molecule to be planar.

Analysis of  $^{14}\text{N}$ -quadrupole hyperfine structure enabled the theoretical line centre of each transition to be used in calculation of rotational constants rather than the point of maximum intensity. This was achieved by calculation of the hyperfine pattern of each transition and computer simulation of the line shape as detailed

in section 6. It was then possible to measure, from the calculated line shape, the deviation of the line centre from the point of maximum intensity. This procedure effected considerable improvement in the centrifugal distortion constants as it removes small systematic errors, particularly at low J. As no quadrupole analysis was carried out on the  $^{13}\text{C}$ - and  $^{18}\text{O}$ -species, the normal NO.CN corrections were applied. This approximation is extremely good for NO. $^{13}\text{C}$ N due to the position of the carbon near the a-axis. On substitution of  $^{18}\text{O}$ , however, a significant axis swing occurs ( $\sim 40^\circ$ ). Since the off-diagonal quadrupole tensor components,  $\chi_{ab}$ , are unknown, it is not possible to correct for this effect. The approximation is thought to be justifiable as the N $^{18}\text{O}$ .CN line shapes are very similar to those of the normal species. The small, negative value of  $\delta_J$  indicates the slightly greater uncertainty in the constants of the  $^{18}\text{O}$ -species.

The rotational constants calculated from Polo's equations for all five isotopic species are given in table 2.1. These were used in calculation of the molecular structure. Measured and calculated transition frequencies are given in tables 2.2 to 2.6. The frequencies calculated for normal NO.CN were obtained using rotational constants from the least squares fit, which is discussed in the following section.

Table 2.1.

Rotational Constants of Nitrosyl Cyanide (in MHz)  
from Polo's Expressions.

	NO.CN	N <sup>18</sup> O.CN	<sup>15</sup> NO.CN	NO. <sup>13</sup> CN	NO.C <sup>15</sup> N
A	81216.2	(80021)	(79293)	(80662)	(80011)
B	5384.554	5144.93	5359.70	5359.48	5205.99
C	5040.663	4819.26	5005.37	5018.56	4882.72
D <sub>J</sub>	0.0029	0.0028	0.0049	0.0010	0.0044
D <sub>JK</sub>	-0.2292	-0.236	-0.199	-0.206	-0.222
δ <sub>J</sub>	0.000487	-0.0008	0.000537	0.000483	0.000427

Table 2.2.

Observed and Calculated Transition Frequencies  
of Normal Nitrosyl Cyanide in MHz.

Transition	$\nu_{\text{obs}}$	$\nu_{\text{calc}}$	$\nu_{\text{obs}} - \nu_{\text{calc}}$
$0_{00} - 1_{01}$	10425.26	10425.20	0.06
$1_{01} - 2_{02}$	20849.14	20849.17	-0.03
$1_{11} - 2_{12}$	20507.45	20507.38	0.07
$1_{10} - 2_{11}$	21195.04	21195.13	-0.09
$2_{02} - 3_{03}$	31270.70	31270.66	0.04
$2_{12} - 3_{13}$	30760.23	30760.19	0.04
$2_{11} - 3_{12}$	31791.72	31791.75	-0.03
$2_{21} - 3_{22}$	31280.73	31280.83	-0.10
$2_{20} - 3_{21}$	31285.41	31285.50	-0.09
$3_{13} - 4_{04}$	33275.49	33275.52	0.03
$4_{14} - 5_{05}$	22186.19	22186.20	0.01
$5_{05} - 6_{06}$	62507.86	62507.93	-0.07
$5_{15} - 6_{16}$	61510.91	61510.98	-0.07
$5_{14} - 6_{15}$	63573.36	63573.34	0.02
$5_{24} - 6_{25}$	62554.60	62554.51	0.09
$5_{23} - 6_{24}$	62595.37	62595.30	0.07
$5_{33} - 6_{34}$	62579.96	62579.85	0.11
$5_{32} - 6_{33}$	62579.96	62579.99	-0.03
$5_{42} - 6_{43}$	62596.79	62596.73	0.06
$5_{41} - 6_{42}$			
$5_{51} - 6_{52}$	62620.39	62620.45	-0.06
$5_{50} - 6_{51}$			
$8_{18} - 9_{09}$	23672.82	23672.87	-0.05
$9_{19} - 10_{010}$	35478.27	35478.26	0.01

cotd.

Table 2.2, contd.

Transition	$\nu_{\text{obs}}$	$\nu_{\text{calc}}$	$\nu_{\text{obs}} - \nu_{\text{calc}}$
$10_{110} - 10_{19}$	18898.00	18897.96	0.04
$11_{111} - 11_{110}$	22672.47	22672.39	0.08
$12_{112} - 12_{111}$	26787.30	26787.41	-0.11
$13_{113} - 13_{112}$	31242.01	31242.04	-0.03
$14_{114} - 14_{113}$	36035.12	36035.08	0.04
$16_{115} - 15_{214}$	38299.63	38299.62	0.01
$17_{116} - 16_{215}$	25113.62	25113.63	-0.01

Table 2.3.

Observed and Calculated Transition Frequencies  
of  $\text{N}^{18}\text{O.CN}$  in MHz.

Transition	$\nu_{\text{obs}}$	$\nu_{\text{calc}}$	$\nu_{\text{obs}} - \nu_{\text{calc}}$
$1_{01} - 2_{02}$	19927.24	19927.24	0.00
$1_{11} - 2_{12}$	19603.60	19603.57	0.03
$1_{10} - 2_{11}$	20254.89	20254.92	-0.03
$2_{02} - 3_{03}$	29888.04	29888.04	0.00
$2_{12} - 3_{13}$	29404.51	29404.53	-0.02
$2_{11} - 3_{12}$	30381.56	30381.54	0.02

Table 2.4.

Observed and Calculated Transition Frequencies  
of  $^{15}\text{NO.CN}$  in MHz.

Transition	$\nu_{\text{obs}}$	$\nu_{\text{calc}}$	$\nu_{\text{obs}} - \nu_{\text{calc}}$
$0_{00} - 1_{01}$	10365.10	10365.05	0.05
$1_{01} - 2_{02}$	20728.70	20728.72	-0.02
$1_{11} - 2_{12}$	20376.53	20376.48	0.05
$1_{10} - 2_{11}$	21085.02	21085.09	-0.07
$2_{02} - 3_{03}$	31089.60	31089.60	0.00
$2_{12} - 3_{13}$	30563.76	30563.66	0.10
$2_{11} - 3_{12}$	31626.43	31626.52	-0.09
$10_{110} - 10_{19}$	19469.98	19470.03	-0.05
$11_{111} - 11_{110}$	23358.36	23358.24	0.12
$12_{112} - 12_{111}$	27597.00	27597.06	-0.06

Table 2.5.

Observed and Calculated Transition Frequencies  
of  $\text{NO.}^{13}\text{CN}$  in MHz.

Transition	$\nu_{\text{obs}}$	$\nu_{\text{calc}}$	$\nu_{\text{obs}} - \nu_{\text{calc}}$
$1_{01} - 2_{02}$	20754.86	20754.90	-0.04
$1_{11} - 2_{12}$	20416.00	20415.98	0.02
$1_{10} - 2_{11}$	21097.80	21097.78	0.02
$2_{02} - 3_{03}$	31129.44	31129.41	0.03
$2_{12} - 3_{13}$	30623.21	30623.22	-0.01
$2_{11} - 3_{12}$	31645.85	31645.86	-0.01

Table 2.6.

Observed and Calculated Transition Frequencies  
of NO.C<sup>15</sup>N in MHz.

Transition	$\nu_{\text{obs}}$	$\nu_{\text{calc}}$	$\nu_{\text{obs}} - \nu_{\text{calc}}$
$0_{00} - 1_{01}$	10088.62	10088.70	-0.08
$1_{01} - 2_{02}$	20176.20	20176.24	-0.04
$1_{11} - 2_{12}$	19855.01	19854.92	0.09
$1_{10} - 2_{11}$	20501.45	20501.44	0.01
$2_{02} - 3_{03}$	30261.54	30261.49	0.05
$2_{12} - 3_{13}$	29781.56	29781.48	0.08
$2_{11} - 3_{12}$	30751.06	30751.21	-0.15
$11_{111} - 11_{110}$	21314.85	21314.80	0.05
$12_{112} - 12_{111}$	25183.91	25183.96	-0.05
$13_{113} - 13_{112}$	29372.70	29372.69	0.01

### 3. Centrifugal Distortion.

The problem of studying centrifugal distortion in asymmetric top rotation spectra was first fully discussed by Kivelson and Wilson.<sup>12</sup> They presented an approximate method in which centrifugal distortion is a first order perturbation on the rigid rotor Hamiltonian.

The Hamiltonian for this semi-rigid rotor in the near prolate case is;

$$H = H_0 + H_1, \quad (2.2)$$

$$H_0 = A' P_z^2 + B' P_x^2 + C' P_y^2,$$

$$H_1 = \frac{1}{4} \sum_{\mu\nu} \tau'_{\mu\mu\nu\nu} P_\mu^2 P_\nu^2,$$

where some centrifugal distortion has been included in A', B', C' thus:

$$A' = A + (3\tau_{bcbc} - 2\tau_{abab} - 2\tau_{caca}) \hbar^4 / 4 \quad (2.3)$$

$$B' = B + (3\tau_{caca} - 2\tau_{bcbc} - 2\tau_{abab}) \hbar^4 / 4$$

$$C' = C + (3\tau_{abab} - 2\tau_{caca} - 2\tau_{bcbc}) \hbar^4 / 4$$

where  $A = \frac{\hbar^2}{8\pi^2 I_a}$ , etc.,

and the  $\tau'$  are related to the  $\tau$  constants of Wilson and Howard<sup>13</sup> as follows,

$$\tau'_{\mu\mu\mu\mu} = \tau_{\mu\mu\mu\mu} \hbar^4 \quad (2.4)$$

$$\text{and } \tau'_{\mu\mu\nu\nu} = \tau'_{\nu\nu\mu\mu} = (\tau_{\mu\mu\nu\nu} + 2\tau_{\mu\nu\mu\nu}) \hbar^4$$

The contribution of centrifugal distortion to the rotational energy is, by first order perturbation theory,

$$\Delta E = \frac{1}{4} \sum_{\mu\nu} \tau'_{\mu\mu\nu\nu} \langle P_\mu^2 P_\nu^2 \rangle \quad (2.5)$$

where  $\langle P_\mu^2 P_\nu^2 \rangle$  is the expectation value of the quartic angular momentum operator  $P_\mu^2 P_\nu^2$ .

These six centrifugal distortion constants are not independent and indeterminacies arise when trying to obtain them from the rotational spectrum. Using a higher order analogue of the familiar  $A = \frac{B \cdot C}{B - C}$  planarity assumption, Dowling<sup>14</sup> obtained the following relations;

$$\tau_{cccc} = \frac{C^4}{B^4} \cdot \tau_{bbbb} + \frac{C^4}{A^4} \cdot \tau_{aaaa} + \frac{2C^4}{A^2 B^2} \cdot \tau_{bbaa}$$

$$\tau_{aacc} = \frac{C^2}{B^2} \cdot \tau_{bbaa} + \frac{C^2}{A^2} \cdot \tau_{aaaa}$$

$$\tau_{bbcc} = \frac{C^2}{B^2} \cdot \tau_{bbbb} + \frac{C^2}{A^2} \cdot \tau_{aabb}$$

$$\tau_{acac} = \tau_{bcbc} = 0. \quad (2.6)$$

It is convenient to use the  $\tau$ -constants in units of  $\hbar^4$ . They then become equivalent to the  $\tau'$  with one exception;

$$\tau'_{aabb} = \tau_{aabb} + 2\tau_{abab} \quad (2.7)$$

Combining (2.5), (2.6) and (2.7) gives the following expression for the energy correction;

$$\begin{aligned} \Delta E = & \frac{1}{4} \left[ \tau_{aaaa} (\langle P_a^4 \rangle + \frac{C^2}{A^2} \langle P_c^2 P_a^2 \rangle + \frac{C^4}{A^4} \langle P_c^4 \rangle) \right. \\ & + \tau_{bbbb} (\langle P_b^4 \rangle + \frac{C^2}{B^2} \langle P_b^2 P_c^2 \rangle + \frac{C^4}{B^4} \langle P_c^4 \rangle) \\ & + \tau_{aabb} (\langle P_a^2 P_b^2 \rangle + \frac{C^2}{B^2} \langle P_c^2 P_a^2 \rangle + \frac{C^2}{A^2} \langle P_b^2 P_c^2 \rangle + \frac{2C^4}{A^2 B^2} \langle P_c^4 \rangle) \\ & \left. + \frac{1}{2} \tau_{abab} \langle P_a^2 P_b^2 \rangle \right] \end{aligned}$$

These four  $\tau$ -constants can be obtained with A', B', and C' from a least squares fit. The 'rigid rotor' rotational constants are then given by;

$$A = A' + \frac{1}{2}\tau_{abab}$$

$$B = B' + \frac{1}{2}\tau_{abab}$$

$$C = C' - \frac{3}{4}\tau_{abab}.$$

The problem of indeterminacy in the non-planar asymmetric rotor was resolved by Watson<sup>15</sup> who applied a unitary transformation to the Hamiltonian to obtain a reduced Hamiltonian containing one fewer quartic term. The general asymmetric rotor energies are usually solved in terms of Nielsen's<sup>16</sup> distortion constants,  $D_J$ ,  $D_{JK}$ ,  $D_K$ ,  $\delta_J$ ,  $R_5$  and  $R_6$ . The relationships between these and the  $\tau$ -constants are given in the appendix of reference 12.

Asymmetric rotor least squares fit programs, Asfip and Asfit, by Wenger and Bauder<sup>17</sup> were used to fit the spectrum of normal nitrosyl cyanide. These programs use the theory of Kivelson and Wilson, and Watson, respectively. The results of these fits are shown in tables 2.7 and 2.8. Uncertainties shown are one standard deviation.

As expected, the fit by program Asfit is not as precise, since it uses theory strictly applicable to the non-planar case. One of the distortion constants,  $\delta_K$ , is not well determined. Values of Nielsen's distortion constants,  $D_J$  etc., calculated from the  $\tau$ -constants, are within one standard deviation of those from Asfit which agree with the values from Folo's expressions within experimental error. (Table 2.9) Since systematic errors often

Table 2.7.

Rotational Constants of NO.CN, (MHz), from Program Asfip.

A	81216.23 ± 0.06
B	5384.533 ± 0.004
C	5040.682 ± 0.005
$\tau_{aaaa}$	-62.79 ± 0.10
$\tau_{bbbb}$	-0.01602 ± 0.00009
$\tau_{aabb}$	0.742 ± 0.006
$\tau_{abab}$	-0.129 ± 0.006

Table 2.8.

Rotational Constants of NO.CN, (MHz), from Program Asfit.

A	81216.16 ± 0.07
B	5384.56 ± 0.03
C	5040.68 ± 0.03
$D_J$	0.00297 ± 0.00002
$D_{JK}$	-0.2294 ± 0.0002
$D_K$	15.92 ± 0.04
$\delta_J$	0.000487 ± 0.000003
$\delta_K$	0.04 ± 0.02

arise in fitting procedures of this kind,<sup>18</sup> a reasonable estimate of the uncertainty in each parameter is given by three standard deviations.

Table 2.9.

Comparison of Rotational Constants (MHz) from Asfit, Polo's Expressions and those calculated from the Asfip Constants.

	<u>Asfit</u>	<u>Polo</u>	<u>Asfip</u>
A	81216.16	81216.2	81216.23
B	5384.56	5384.55	5384.533
C	5040.68	5040.66	5040.682
D <sub>J</sub>	0.00297	0.0030	0.00297
D <sub>JK</sub>	-0.2294	-0.2292	-0.2290
δ <sub>J</sub>	0.000487	0.000487	0.000487
δ <sub>K</sub>	0.04	—	0.04
D <sub>K</sub>	15.92	15.86	15.92

#### 4. Structure.

The structure of nitrosyl cyanide was determined using the direct substitution method<sup>8,19</sup> for all coordinates except the small b-coordinates of the nitrile group atoms. The latter were fixed by the first moment,  $\sum ma = 0$ , and product moment conditions.

The moments of inertia of each species were calculated from the rotational constants in table 2.1. The <sup>12</sup>C mass scale was used, giving  $\frac{h}{8\pi^2} = 505376 \text{ MHz amu } \text{Å}^2$  and  $(I_c - I_b)$  was used for  $I_a$ . This is permissible since errors arising from assumption of zero inertial defect are commensurate with those caused by using ground state, rather than equilibrium, rotational constants.

For a planar molecule, coordinates of an isotopically substituted nucleus can be obtained from;<sup>19</sup>

$$a^2 = \frac{\Delta I_b}{\mu} \left[ 1 + \frac{\Delta I_a}{I_a - I_b} \right]$$

and

$$b^2 = \frac{\Delta I_a}{\mu} \left[ 1 + \frac{\Delta I_b}{I_b - I_a} \right]$$

where  $\mu$  is the reduced mass =  $\frac{M \Delta m}{M + \Delta m}$

These expressions are unsatisfactory for calculation of a coordinate smaller than about 0.15 Å due to the small change in the appropriate moment. Costain<sup>9</sup> recommended that such coordinates are best determined by first moment and product moment fits. Structures obtained by Costain's method are termed substitution ( $r_s$ ) structures and are usually good approximations to the equilibrium structures.

Nuclear coordinates of nitrosyl cyanide are given in table 2.10 and the molecular structure is shown in figure 2.5. As all the coordinates were calculated from Kraitchman's equations they can be tested by the first moment relation. It is found that  $\sum ma = 0.063$  amu Å, corresponding to an average error of  $\sim 0.001$  Å, or, if all the discrepancy arises from one coordinate, about 0.004 Å. The uncertainty in the internuclear distances is about 0.005 Å. The angles CNO and NCN are determined to  $\sim 1^\circ$  and  $\sim 3^\circ$  respectively, the error on the latter being larger as it is fixed by the small b-coordinates in the nitrile group.

An important objective in obtaining the structure was the assessment of the contribution of the valence bond mesomer  $O=\overset{\ominus}{N}=\overset{\ominus}{C}=\overset{\oplus}{N}$ . It is useful to compare the structural

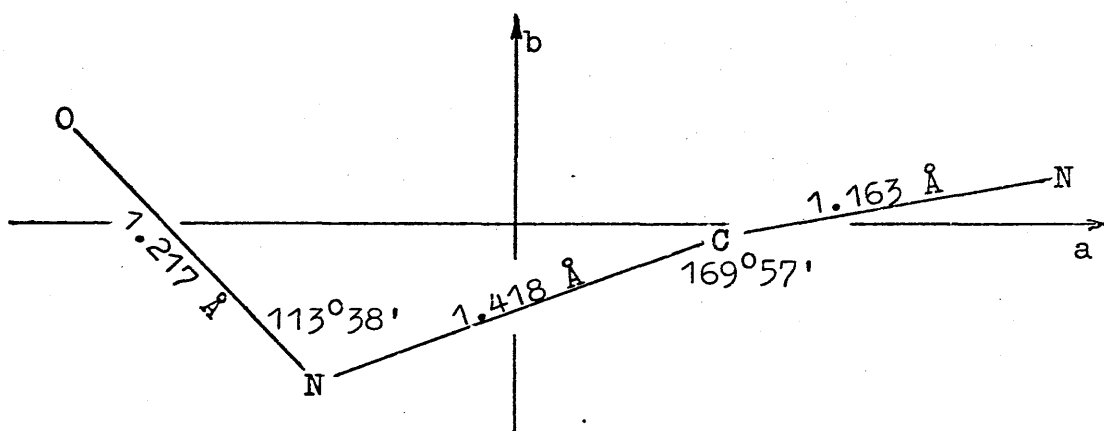
Table 2.10.

Nuclear Coordinates, NO.CN, (Å).

	O	N	C	N
a	-1.501	-0.666	0.667	1.813
b	0.357	-0.528	-0.043	0.157

Figure 2.5.

The Structure of Nitrosyl Cyanide.



parameters with those of other molecules. If the contribution is significant, the central bond will be shorter and the terminal bonds longer than is generally found. The CNO angle would be larger than if there were no  $\pi$ -bonding in the central bond.

The N=O bond is longer than that of nitrosyl chloride, (1.139 Å),<sup>20</sup> but similar to that of CH<sub>3</sub>NO. (1.213 Å)<sup>21</sup>. The C≡N bond is slightly larger than was found for a range of cyanogen halides, (all ~1.159 Å)<sup>22</sup>. However the parameters most sensitive to any contribution from the mesomeric form are the central C-N internuclear distance and the CNO angle. As expected, the central C-N bond (1.418 Å) is considerably shorter than the single

bond values found in  $\text{CH}_3\text{NO}$  (1.48 Å)<sup>21</sup> and  $\text{CH}_3\text{NH}_2$  (1.47 Å)<sup>23</sup>. The shortening is rather less pronounced than that in  $\text{NF}_2\text{CN}$  (1.39 Å)<sup>24</sup> and much less so than that found in  $\text{NH}_2\text{CN}$  (1.346 Å)<sup>25</sup> in which there is thought to be a considerable contribution from the canonical form  $\text{H}_2\overset{\oplus}{\text{N}}=\overset{\ominus}{\text{C}}=\overset{\ominus}{\text{N}}$ . The short central bond in  $\text{NF}_2\text{CN}$  compared with  $\text{CH}_3\text{NH}_2$  was attributed<sup>24</sup> to a difference in repulsive interactions depending on the hybridisation of the central atoms and to some  $\pi$ -bonding between them. The CNO angle is very close to that found for  $\text{CH}_3\text{NO}$  (113.2°).<sup>21</sup> It appears from these considerations that there is a small contribution from the linear mesomeric form.

Perhaps the most interesting structural feature is the distinct bend at the carbon. Similar distortions are found in  $\text{NF}_2\text{CN}$  (171°)<sup>24</sup> and  $\text{PF}_2\text{CN}$  (171.5°),<sup>26</sup> and to a much smaller extent in vinylacetylene (177.9°),<sup>27</sup> acrylonitrile (178.2°)<sup>28</sup> and propynal (178.6°).<sup>10</sup> The bend is probably due to repulsion between the N=O and C≡N  $\pi$ -electron systems in each case. The effect is most pronounced in molecules where there is a lone pair of electrons on one of the central atoms. In the case of  $\text{NF}_2\text{CN}$ <sup>24</sup> it was explained as being partly due to bonding n- $\pi$  interactions, but if it is present at all, the effect must be small, as a greater difference in the NCN angles in  $\text{NF}_2\text{CN}$  and  $\text{PF}_2\text{CN}$  would be expected. Repulsion between the  $\pi$ -electrons of the N=O and C≡N groups would tend to make the molecule non-planar if there were no energy compensation for a planar configuration. This adds further weight to the conclusion that there is a small but significant amount of  $\pi$ -character in the

central N-C bond.

### 5. Stark Effect and Dipole Moment.

Perturbations to rotational energy levels arising from interaction of the dipole moment of an asymmetric rotor with a static electric field have been described by Golden and Wilson.<sup>29</sup>

In the presence of an electric field, the  $(2J+1)$ -fold spatial degeneracy of the rotational energy levels is lifted. The total angular momentum,  $\underline{J}$ , can assume  $(2J+1)$  orientations with respect to the field direction. These are defined by the quantum number  $M$ , which can take the values  $J, J-1, \dots, -J$ . If Stark effects in an asymmetric rotor are small compared with separations between energy levels, they can be accurately described by second order perturbation theory. The second order correction to the energy of a rotational level may be written in terms of the transition strengths as follows;

$$\Delta E^{(2)} = \sum_g \frac{\mu_g^2 E^2}{2J+1} \sum_{\tau} \left[ \frac{J^2 - M^2}{J(2J-1)} \cdot \frac{\mathcal{S}_{J_{\tau}, J-1_{\tau'}}}{E_{J_{\tau}} - E_{J-1_{\tau'}}} + \frac{M^2}{J(J+1)} \cdot \frac{\mathcal{S}_{J_{\tau}, J_{\tau'}}}{E_{J_{\tau}} - E_{J_{\tau'}}} + \frac{(J+1)^2 - M^2}{(J+1)(2J+3)} \cdot \frac{\mathcal{S}_{J_{\tau}, J+1_{\tau'}}}{E_{J_{\tau}} - E_{J+1_{\tau'}}} \right] \quad (2.8)$$

where  $\mu_g$  is a dipole moment component,  $g = a, b, c$ ,

$E$  is the applied field,

$E_{J_{\tau}}$  is the unperturbed energy of the level  $J_{\tau}$ , etc.,

and  $\mathcal{S}_{J_{\tau}, J_{\tau'}}$  is the transition strength between levels  $J_{\tau}$

and  $J_{\tau'}$ , etc., connected by dipole component  $\mu_g$ .

Transition strengths are derived from dipole matrix ele-

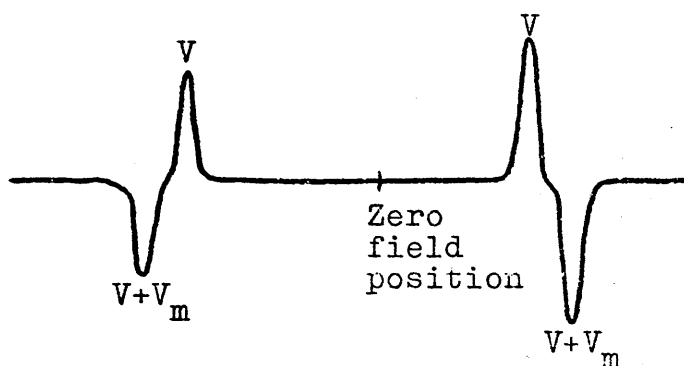
ments and are available in tabulated form<sup>30</sup> at 0.001 intervals of  $\kappa$ .

Stark effects in nitrosyl cyanide were calculated by second order perturbation theory as outlined above. The calculations are simplified somewhat by the fact that  $\mu_c = 0$ .

An accurate positive D.C. voltage from a Fluke 415B supply was applied to the Stark cell septum, with just sufficient modulation voltage,  $V_m$ , based on the D.C. level, to fully resolve a line as illustrated in figure 2.6 for carbonyl sulphide,  $J = 1-2$ . Stark components were measured over a

Figure 2.6.

Stark Effect OCS,  $J=1-2$ .



range of applied voltages. After a set of measurements had been taken the cell was calibrated using the  $J = 1-2$  transition of OCS. Since the dipole moment of OCS is known accurately, ( $\mu = 0.71521$  D),<sup>31</sup> the proportionality constant between the field strength,  $E$ , and the applied voltage,  $V$ , can be determined. The experimental gradients  $\Delta\nu/V^2$ , divided by the cell constant,  $c$ , are shown in table 2.11 with Stark coefficients from equation 2.6.

Table 2.11.

Stark Effects in Nitrosyl Cyanide.

Transition	M	$\frac{\Delta V}{cV^2} \times 10^5$	$\mu_a^2$ Coefft. $\times 10^5$	$\mu_b^2$ Coefft. $\times 10^5$
$2_{02}-3_{03}$	0	-0.3862	-0.24361	-0.04977
	1	-0.1102	-0.06851	-0.01299
	2	0.7308	0.45678	0.09737
$2_{21}-3_{22}$	0	0.7023	0.45668	-0.00689
$2_{20}-3_{21}$	0	0.7021	0.45667	-0.00755
$1_{01}-2_{02}$	0	-2.2724	-1.46164	-0.07603
	1	1.8795	1.18760	0.14012
$1_{11}-2_{12}$	0	1.8325	1.20744	-0.07934

Each expression was represented as a linear plot of  $\mu_a^2$  against  $\mu_b^2$ , (figure 2.7.). In the expanded scale of this plot, the area of intersection is large, and consequently it is difficult to select optimum values of  $\mu_a^2$  and  $\mu_b^2$ . A least squares fit was carried out for  $\mu_a^2$  and  $\mu_b^2$ , using initial values from the figure of 1.54 and 0.30  $D^2$  respectively. Convergence was reached in one cycle giving;  $\mu_a^2 = 1.540 D^2$ ,  $\mu_b^2 = 0.324 D^2$ , and hence  $\mu^2 = 1.864 D^2$ . The uncertainties in these results were estimated by taking account of the worst reasonable values from figure 2.7. The dipole moment components of nitrosyl cyanide are as follows;

$$\mu_a = 1.241 \pm 0.003 D,$$

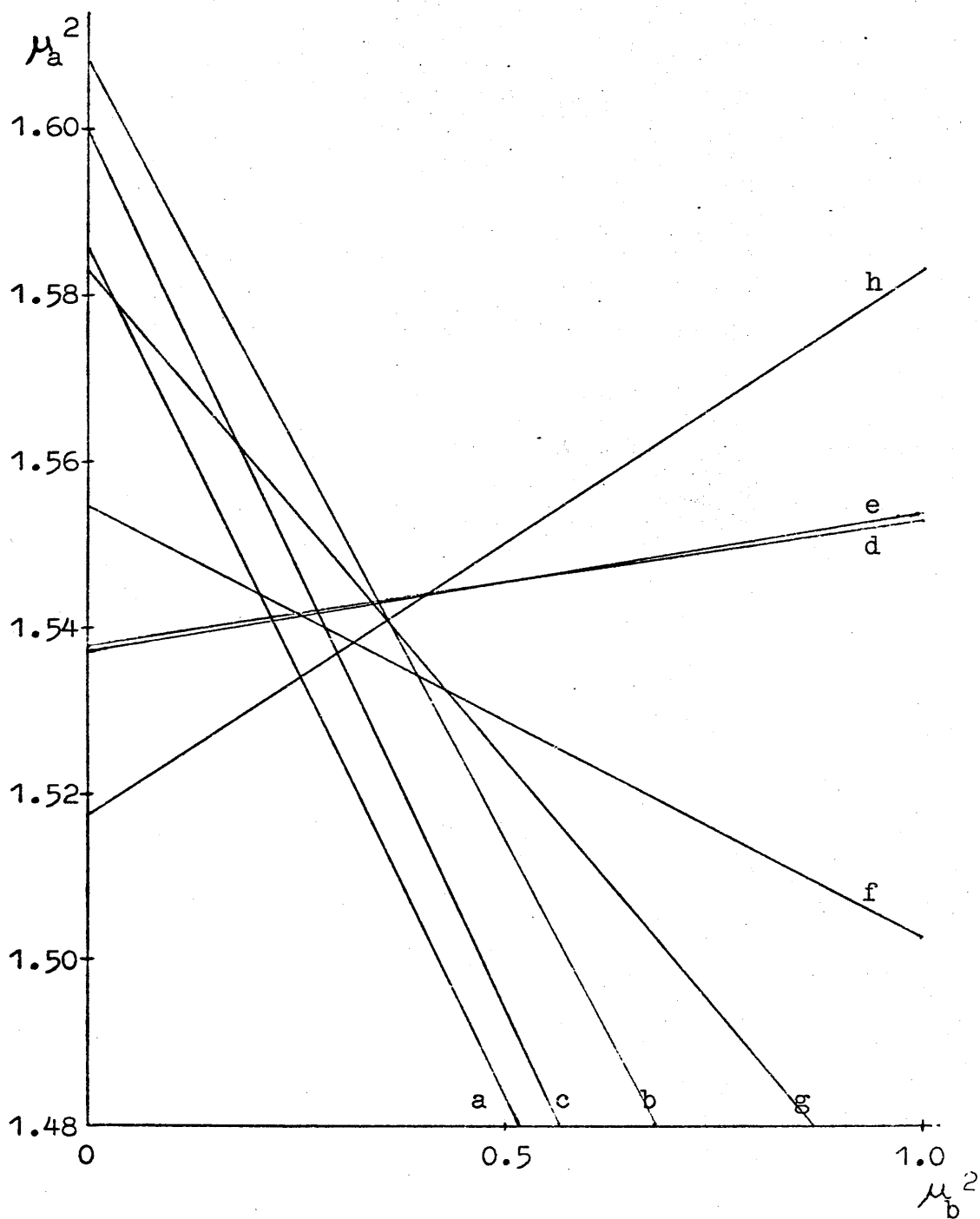
$$\mu_b = 0.57 \pm 0.08 D,$$

$$\mu = 1.365 \pm 0.03 D.$$

The dipole orientation is not obtainable from the above procedure, but it is probably as shown in figure 2.8. It is directed towards the nitrile group, almost parallel to

Figure 2.7.

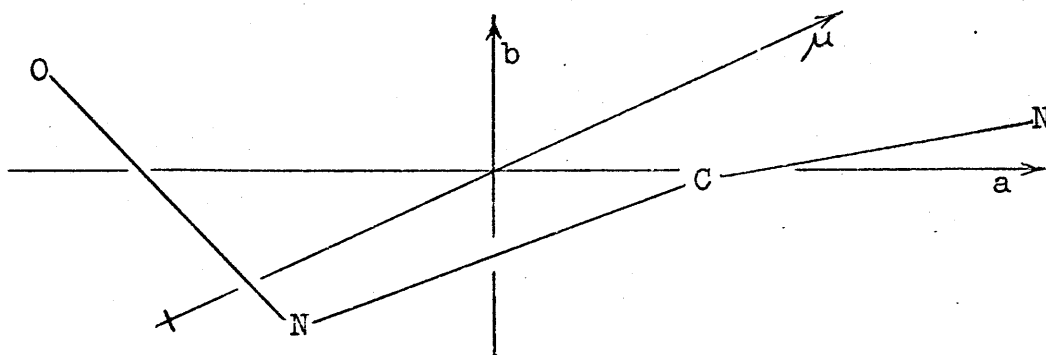
Stark Effect Plots, NO.CN.



	Transition	M		Transition	M
a	$2_{02}-3_{03}$	0	e	$2_{20}-3_{21}$	0
b	$2_{02}-3_{03}$	1	f	$1_{01}-2_{02}$	0
c	$2_{02}-3_{03}$	2	g	$1_{01}-2_{02}$	1
d	$2_{21}-3_{22}$	0	h	$1_{11}-2_{12}$	0

Figure 2.8.

Orientation of the Dipole Moment of Nitrosyl Cyanide.



the central N-C bond. This orientation is similar to that proposed<sup>24</sup> for  $\text{NF}_2\cdot\text{CN}$  which has  $\mu = 1.10$  D. Further evidence for the direction of the dipole moment is obtained from the dipoles of  $\text{NO}\cdot\text{Cl}$ <sup>32</sup> and  $\text{CN}\cdot\text{Cl}$ <sup>33</sup> which are 1.9 and 2.80 D respectively.

6. Quadrupole Coupling in Nitrosyl Cyanide.

<sup>14</sup>N-quadrupole hyperfine structure has been resolved in the spectra of normal  $\text{NO}\cdot\text{CN}$ , <sup>15</sup> $\text{NO}\cdot\text{CN}$  and  $\text{NO}\cdot\text{C}^{15}\text{N}$  and nuclear quadrupole coupling constants derived. This section comprises an account of the method of evaluation of these constants and a brief discussion of the electronic configuration of the molecule.

The spin angular momentum,  $\underline{I}$ , of a nucleus is related to the integer or half-integer quantum number,  $I$ , by  $\underline{I} = \sqrt{I(I+1)}\hbar$ , there being  $(2I+1)$  possible spin states for the nucleus. A nucleus with  $I > \frac{1}{2}$  has an electric quadrupole moment,  $Q$ , which allows its spin angular momentum to couple with the rotational angular momentum. The coupling takes place through the electric field gradient of the molecule effective at the nucleus. The resultant total

angular momentum,  $\underline{F}$ , where  $\underline{F} = \underline{J} + \underline{I}$ , has a value  $\underline{F} = \sqrt{F(F+1)} \hbar$ , where  $F = J+I, J+I-1, \dots |J-I|$ . When more than one nucleus with a non-zero quadrupole moment are present in a molecule, the individual moments may couple via the molecular rotation.

The energy of interaction for a single nucleus coupling in an asymmetric rotor is given by an expression derived by Golden and Bragg;<sup>34</sup>

$$E(F) = eQ \left\{ \frac{\delta^2 V}{\delta a^2} \left[ J(J+1) + E(\kappa) - (\kappa+1) \frac{\delta E(\kappa)}{\delta \kappa} \right] + 2 \frac{\delta^2 V}{\delta b^2} \cdot \frac{\delta E(\kappa)}{\delta \kappa} + \frac{\delta^2 V}{\delta c^2} \left[ J(J+1) - E(\kappa) + (\kappa-1) \frac{\delta E(\kappa)}{\delta \kappa} \right] \right\} \frac{Y(F)}{J(J+1)} \quad (2.9)$$

where  $Q$  is the electric quadrupole moment,

$\frac{\delta^2 V}{\delta a^2}$  is the electric field gradient at the nucleus relative to the a-axis,

$$\text{and } Y(F) = \frac{\frac{3}{2}C(C+1) - I(I+1)J(J+1)}{2I(2I-1)(2J-1)(2J+3)} \quad (\text{Casimir's function})$$

where  $C = F(F+1) - I(I+1) - J(J+1)$ .

Casimir's function is tabulated for a range of  $F, I$ , and  $J$  in reference 35.

Equation 2.9 may be simplified using Laplace's equation,  $\nabla^2 V = 0$ , which will hold since only charges outside the nucleus contribute to the potential.

$$E(F) = \left\{ 2 \chi_{aa} \left[ E(\kappa) - \kappa \frac{\delta E(\kappa)}{\delta \kappa} \right] + \chi_{bb} \left[ E(\kappa) - J(J+1) - (\kappa-3) \frac{\delta E(\kappa)}{\delta \kappa} \right] \right\} \frac{Y(F)}{J(J+1)} \quad (2.10)$$

where  $\chi_{aa} = eQ \frac{\delta^2 V}{\delta a^2}$  etc.

Calculation of the hyperfine interaction in a molecule containing two quadrupolar nuclei depends on the relative magnitudes of the coupling. If one nucleus is coupled much more strongly then it provides the main contribution to the hyperfine splittings, and the weaker coupling can be treated as a perturbation on these. However in the case of two nitrogen nuclei, this treatment is generally unsatisfactory. The quadrupole coupling energies were calculated using a program by Macdonald,<sup>36</sup> based on the theory of Bardeen and Townes,<sup>37</sup> a summary of which is given below.

The Hamiltonian for the two nuclear interactions may be written;-

$$H = H_1(I_1, J) + H_2(I_2, J) \quad (2.11)$$

where the labels 1 and 2 refer to the different nuclei. The total angular momentum is still denoted by  $\underline{F}$  and  $\underline{F}_1$  and  $\underline{F}_2$  are the vector sums of  $\underline{J}$  with  $\underline{I}_1$  and  $\underline{I}_2$  respectively. Wave functions for the combined system may be obtained by first fixing  $F_1$ ,

$$\underline{F}_1 = \underline{J} + \underline{I}_1 ,$$

$$F_1 = (I_1 + J) \dots \dots \dots |I_1 - J| ,$$

and then combining  $\underline{I}_2$  with  $\underline{F}_1$  to obtain

$$\underline{F} = \underline{F}_1 + \underline{I}_2 ,$$

$$F = (F_1 + I_2) \dots \dots \dots |F_1 - I_2| .$$

Let  $\Psi_1 (F_1, F)$  be the wave functions for the state

defined by  $F_1$  and  $F$ . Alternatively, it is possible to fix  $F_2$  by first combining  $\underline{J}$  and  $\underline{I}_2$  which generates a similar set of wave functions  $\Psi_2(F_2, F)$  where  $\underline{F}_2 = \underline{J} + \underline{I}_2$ , and  $\underline{F} = \underline{F}_2 + \underline{I}_1$ . The number of different wave functions is the same as before and the two sets of wave functions are related;

$$\Psi_1(F_1, F) = \sum_{F_2} c(F_1, F_2) \Psi_2(F_2, F)$$

$$\text{and } \Psi_2(F_2, F) = \sum_{F_1} c(F_1, F_2) \Psi_1(F_1, F)$$

The transformation coefficients,  $c(F_1, F_2)$ , have been evaluated by Bardeen and Townes for a range of  $I_1$  for the special cases  $I_2 = 1, 3/2$ .

Where both couplings are appreciable, the wave functions are given by appropriate linear combinations of either set;

$$\Psi(F) = \sum_i a_i(F_1) \Psi_1(F_1, F) \quad (2.12)$$

Using (2.11), the fact that  $\Psi_1$  and  $\Psi_2$  are eigenfunctions of  $H_1$  and  $H_2$  respectively, and that the  $\Psi_1(F_1, F)$  are orthogonal, it can be shown that;

$$\left[ A(F_1, F_2) + E(F_1) - E \right] a(F_1) + \sum_{F_1' \neq F_1} A(F_1, F_1') a(F_1') = 0. \quad (2.13)$$

$$\text{where } A(F_1, F_2) = \sum_{F_2} c(F_1, F_2) c(F_1', F_2) E(F_2)$$

for each value of  $F_1$  and  $F_2$  associated with the same  $F$ . For non-trivial solutions of (2.13), the determinants of the coefficients must be zero. The  $E(F_i)$  are simply the single nucleus coupling energies from (2.10).

In calculation of hyperfine splitting patterns, the intensities of the components are required. Exact intensities

could, in principle, be obtained by solution of (2.13) for the  $a(F)$ 's and using these in calculation of dipole matrix elements.<sup>38</sup> A much simpler, but approximate approach is to use the tables in reference 35 for  $J$  and the more strongly coupling nucleus angular momentum quantum number, say  $I_1$ . The intensities of the finer splitting components are then obtained by replacing  $J$  by  $F_1$  and  $I_1$  by  $I_2$ . Where the nuclei are coupling to an approximately equal extent, the intensities can be found by interpolation. This method was used in calculation of hyperfine structures.

It is useful in analysis of hyperfine patterns to estimate the magnitude of the coupling constants using the approach of Townes and Dailey.<sup>39</sup> From consideration of the structure of nitrosyl cyanide, the contribution from the linear valence bond mesomer was estimated to be low. To the degree of approximation in this method, it may be neglected. Assuming a coupling of 10 MHz for an imbalance of one p-electron on nitrogen, the following estimates of the coupling constants, in MHz, are obtained;

	N(1)	N(2)
$\chi_{aa}$	-5.0	3.0
$\chi_{bb}$	2.5	-6.7

Here N(1) and N(2) refer to the nitrile and nitrosyl group nitrogens. These labels are used in the remainder of this section.

It was hoped originally that a full quadrupole analysis could be performed on the hyperfine splittings of the normal species. However, it quickly became apparent that this was not possible because of the different magnitudes

of the coupling constants of the two nuclei. The first transition studied was  $0_{00}-1_{01}$  as there is no  $\chi_{bb}$  dependence in the hyperfine splittings. Under high resolution, this line appears to be a normal cyanide pattern with a little fine structure on the two lower frequency peaks. An approximate value of  $\chi_{aa}(1)$  was determined as  $-4.1 \pm 0.2$  MHz but it was not possible to obtain  $\chi_{aa}(2)$ . It is evident from the Townes and Dailey predictions that the same problem arises when the  $\chi_{bb}$  are dominant, as the main contribution will come from the nitrosyl nitrogen, and  $\chi_{bb}(1)$  will not be obtainable. It was decided to measure hyperfine structure in the single quadrupolar nucleus species.

Splittings were measured for some low J R-branch, and some higher J, ( $10 \leq J \leq 13$ ), Q-branch lines. Errors arising from sample deterioration were minimised by photographing the oscilloscope trace with a superimposed marker chain of spacing 1.70 MHz (figure 2.9(a)). For each single nucleus case,  $\chi_{aa}$  was obtained from the  $0_{00}-1_{01}$  transition and  $\chi_{bb}$  was found from the series  $J_{1J}-J_1(J-1)$  for which equation 2.10 gives 2:1 doublets of splitting  $(\chi_{aa} + 2\chi_{bb})\Delta Y(F)$  for high J. The fact that this splitting was observed in the spectrum of  $^{15}\text{NO.CN}$  provides an immediate indication that the electronic configuration about the nitrile nitrogen is not cylindrically symmetric. The more intense component of each Q-branch line is to low frequency in both spectra, showing both  $(\chi_{aa} + 2\chi_{bb})$  to be negative.

Analysis of hyperfine splitting in normal nitrosyl cyanide

was hindered by difficulty in relating calculated patterns to those observed. Use of weighted means of components or triangular line shapes gave poor correlation with observed splittings. Calculated splittings were obtained by computer simulation of the transition concerned using Lorentzian functions,

$$I = \frac{\Delta\nu}{(\nu - \nu_0)^2 + \Delta\nu^2}$$

Frequencies of components were calculated as detailed above. Intensities for the two nuclei case were found by the method of Townes and Schawlow,<sup>35</sup> the cyanide nitrogen providing the main quadrupole perturbation for the  $K_{-1} = 0$ , R-branch transitions, and the nitrosyl nitrogen for the  $K_{-1} = 1$ , Q-branch and R-branch transitions. The line shapes produced this way were in good agreement with those observed, except for the Q-branch lines, where the absence of the partly-resolved Stark lobes results in a slightly different appearance. When one set of hyperfine components appears as a shoulder on another, the calculated separation is strongly dependent on the half-height half-width,  $\Delta\nu$ . This is adjusted with the coupling constants until the best correlation between calculated and observed patterns is obtained.

This method of analysis effected an improvement in the coupling constants of the single nucleus cases. Values of these constants, in MHz, are as follows;

	$\chi_{aa}$	$\chi_{bb}$
N(1)	$-3.92 \pm 0.05$	$1.08 \pm 0.10$
N(2)	$1.52 \pm 0.05$	$-5.68 \pm 0.10$

The higher degree of uncertainty in the  $\chi_{bb}$  values results

from difficulty in resolving the high-field Stark lobes in the Q-branch transitions.

Quadrupole coupling in normal nitrosyl cyanide was studied in the  $0_{00}-1_{01}$ ,  $1_{01}-2_{02}$ ,  $1_{11}-2_{12}$ ,  $10_{110}-10_{19}$ , and  $11_{111}-11_{110}$  transitions. Calculated patterns were obtained from Macdonald's program described previously, using full secular determinants.<sup>36</sup>

The hyperfine splittings were analysed taking the coupling constants of the nitrosyl nitrogen to be those for  $\text{NO.C}^{15}\text{N}$  and varying the N(1) constants to fit the observed patterns. The N(2), rather than N(1) constants were fixed because the swing of the inertial axes on  $^{15}\text{N}$  substitution at the cyanide end is smaller than that for substitution of the nitroso group nitrogen,  $\sim 11^\circ$  and  $\sim 14^\circ$ , respectively. Conversely, it could be argued that the greater asymmetry of the electronic environment about N(2) renders the N(2) constants more sensitive to any axis rotation. However it was found that the spectrum could be fitted by fixing the N(2) constants. The  $0_{00}-1_{01}$  transition was used to determine  $\chi_{aa}(1)$ , taking  $\chi_{aa}(2)$  as 1.52 MHz as before. The observed and calculated patterns are shown in figure 2.9. The value of  $\chi_{aa}(1)$  obtained is significantly different from the single nucleus case.

Measurement of the small splitting in the Q-branch lines due to N(1) is difficult, as it appears as fine structure on the more widely spaced components due to N(2) coupling, and  $\chi_{bb}(1)$  cannot be determined directly. However, since  $\chi_{aa}(1)$  is known, and  $\chi_{cc}$  coupling constants are invariant with respect to in-plane swing of axes,  $\chi_{bb}(1)$  can be

**FIGURE 2.9.**

**$^{14}\text{N}$ -QUADRUPOLE HYPERFINE SPLITTING, NORMAL NO.CN.**

$$0_{00} \rightarrow 1_{01}$$

**(a) OBSERVED. MARKER SPACING = 1.70 MHz.**



**(b) CALCULATED.**

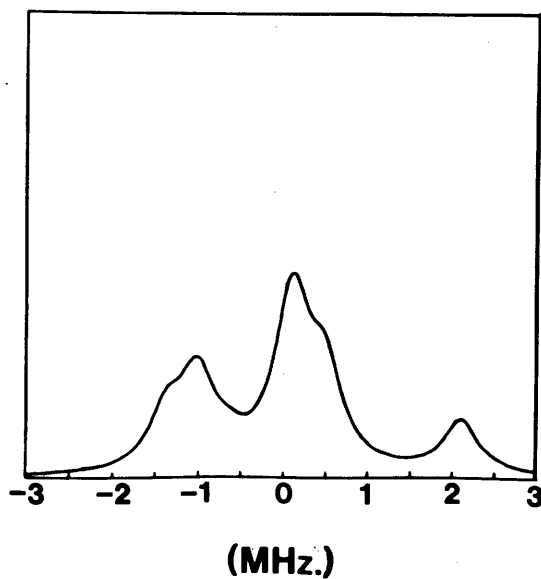


**FIGURE 2.10.**

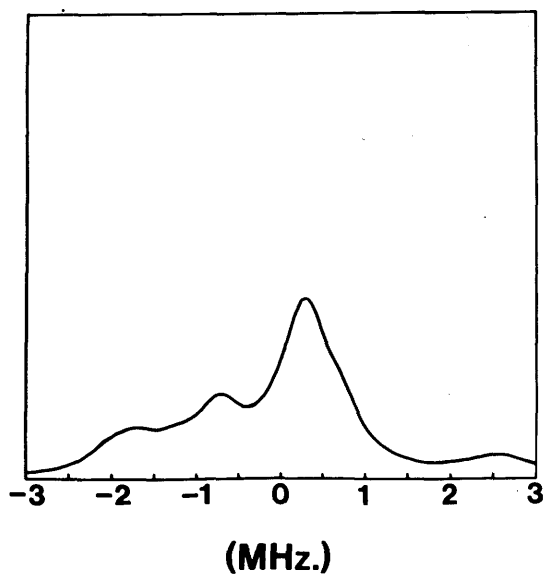
**<sup>14</sup>N-QUADRUPOLE HYPERFINE SPLITTING, NORMAL NO.CN.**

$$1_{11} \rightarrow 2_{12}$$

**(a) OBSERVED. MARKER SPACING = 5.1 MHz.**



**(b) CALCULATED.**



found from  $\chi_{bb}(1) = -\chi_{aa}(1) - \chi_{cc}(1)$ . This gives the following coupling constants (in MHz) for the normal species;

	$\chi_{aa}$	$\chi_{bb}$
N(1)	$-4.10 \pm 0.10$	$1.26 \pm 0.15$
N(2)	$1.52 \pm 0.10$	$-5.68 \pm 0.15$

The larger error estimates arise from greater complication of the hyperfine structures and uncertainty from assuming the N(2) constants invariant under N(1) substitution.

Figure 2.10 allows comparison of the observed hyperfine pattern of the largely  $\chi_{bb}$ -dependent  $1_{11}-2_{12}$  transition of normal NO.CN with that calculated from the above constants. Tables 2.12-14 show measured and calculated hyperfine splittings for nitrosyl cyanide.

Table 2.12.

<u><math>^{14}\text{N}</math>-Quadrupole Splittings in NO.C<math>^{15}\text{N}</math>.</u>			
Transition	$\chi_{aa} = 1.52 \text{ MHz}$	$\chi_{bb} = -5.68 \text{ MHz}$	
	Principal Components F-F'	$\Delta\nu_{\text{obs}}$	$\Delta\nu_{\text{calc}}$ (MHz)
$0_{00}-1_{01}$	1-0	0.67	0.68
	1-2	0.47	0.46
	1-1		
$11_{111}-11_{110}$	10-10,12-12	3.75	3.69
	11-11		
$12_{112}-12_{111}$	11-11,13-13	3.66	3.69
	12-12		
$13_{113}-13_{112}$	12-12,14-14	3.64	3.68
	13-13		

Table 2.13.

 $^{14}\text{N}$ -Quadrupole Splittings in  $^{15}\text{NO.CN}$ .

$\chi_{aa} = -3.92 \text{ MHz}$

$\chi_{bb} = 1.08 \text{ MHz}$

Transition	Principal Components F-F'	$\Delta\nu_{\text{obs}}$	$\Delta\nu_{\text{calc}}$ (MHz)
$0_{00}-1_{01}$	1-1	1.17	1.18
	1-2	1.78	1.76
	1-0		
$1_{01}-2_{02}$	2-2,0-1	1.08	1.09
	1-2,2-3	1.94	1.90
	1-1		
$1_{11}-2_{12}$	1-2,2-2	1.24	1.23
	2-3,1-1	0.85	0.92
	0-1		
$1_{10}-2_{11}$	1-2	1.09	1.14
	2-2,2-3,2-1	1.50	1.49
	0-1		
$10_{110}-10_{19}$	9-9,11-11	0.66	0.66
	10-10		
$11_{111}-11_{110}$	10-10,12-12	0.65	0.66
	11-11		
$12_{112}-12_{111}$	11-11,13-13	0.68	0.66
	12-12		

Table 2.14.

$^{14}\text{N}$ -Quadrupole Splittings in Normal NO.CN.

Transition	$\chi_{aa}$	$\chi_{bb}$	$\Delta\nu_{\text{obs}}$ (MHz)	$\Delta\nu_{\text{calc}}$
N(1)	-4.10 MHz	1.26 MHz		
N(2)	1.52 MHz	-5.68 MHz		
	Principal Components $F_1, F-F_1, F_1'$			
0 <sub>00</sub> -1 <sub>01</sub>	1,2-1,2		1.19	1.19
	1,2-2,1 1,2-2,3		1.93	1.96
	1,2-0,1			
1 <sub>01</sub> -2 <sub>02</sub>	0,1-1,2 0,1-1,1 2,3-2,3		1.14	1.18
	2,3-3,4 2,2-3,3 1,2-2,3 2,1-3,2		1.94	1.96
	1,2-1,2 1,2-1,1			
	$F_2, F-F_2, F_1'$			
1 <sub>11</sub> -2 <sub>12</sub>	0,1-1,2		0.88	0.96
	2,2-3,3		0.99	1.00
	1,1-2,2 1,0-2,1 1,2-2,3 2,3-3,4		2.22	2.30
	1,2-1,2			

cotd.

Table 2.14, contd.

$^{14}\text{N}$ -Quadrupole Splittings in Normal NO.CN.

Transition	Principal Components $F_2, F-F_2, F_1$	$\Delta\nu_{\text{obs}}$ (MHz)	$\Delta\nu_{\text{calc}}$
$10_{110}-10_{19}$	9, 8-9, 8 9, 10-9, 10 11, 10-11, 10 11, 12-11, 12	0.66	0.66
	9, 9-9, 9 11, 11-11, 11	2.95	2.85
	10, 9-10, 9 10, 11-10, 11		
$11_{111}-11_{110}$	10, 9-10, 9 10, 11-10, 11 12, 11-12, 11 12, 13-12, 13	3.62	3.57
	11, 10-11, 10 11, 12-11, 12		

The asymmetry of the electronic configuration about the nitrile nitrogen and the angle of  $10^{\circ}8'$  between the  $C\equiv N$  bond and the a-axis will tend to lower the value of  $\chi_{aa}(1)$  relative to the prediction. It may be compared with the  $\chi$ -values of HCN ( $-4.58 \pm 0.05$  MHz),<sup>40</sup> HCCCN ( $-4.28 \pm 0.05$  MHz),<sup>22</sup> and ClCN ( $-3.63 \pm 0.1$  MHz).<sup>41</sup> These illustrate increasingly larger degrees of  $\pi$ -electron delocalisation. The observed value of  $\chi_{aa}(1) = -4.10$  MHz confirms earlier conclusions that the contribution from  $O=\overset{\oplus}{N}=\overset{\ominus}{C}=\overset{\ominus}{N}$  is small.

Further confirmation is obtained from the value of  $\chi_{bb}(2)$ . The angle between the N=O bond and the a-axis in NO.CN ( $43^{\circ}22'$ ) is very close to that found for nitrosyl fluoride ( $44^{\circ}23'$ ), allowing direct comparison of the coupling constants. The small value of  $-4.83 \pm 0.05$  MHz<sup>42</sup> for  $\chi_{bb}$  in FNO was explained by a 10% contribution from  $\overset{\oplus}{F}=\overset{\ominus}{N}=\overset{\ominus}{O}$ . There is certainly less delocalisation of the  $\pi$ -electrons in NO.CN, the contribution from the mesomeric form probably being smaller than 5%.

## 7. The Vibrational Spectrum.

The vapour phase infra-red<sup>43,44</sup> and far infra-red<sup>44</sup> spectra of nitrosyl cyanide have been reported. These are briefly discussed here in the general context of the molecule. Some discrepancies between the two references are resolved.

Table 2.15 lists the assigned fundamental vibration frequencies from both studies. The  $\nu_4$  and  $\nu_6$  fundamentals, which were observed in the far infra-red by Campbell, were calculated by Dorko and Buelow from their normal coordin-

Table 2.15.

Fundamental Vibration Frequencies of NO.CN.

Normal Mode	Principal Component	$\bar{\nu}(\text{cm}^{-1})$ Dorko & Buelow	$\bar{\nu}(\text{cm}^{-1})$ Campbell
$\nu_1$	C $\equiv$ N stretch	2177.5	2175
$\nu_2$	N=O stretch	1484.3	1500
$\nu_3$	N-C stretch	820.0	821
$\nu_4$	C-N=O bend	(103.2)	270
$\nu_5$	N-C $\equiv$ N bend	583.3	600
$\nu_6$	Out of plane wag	(54.4)	240

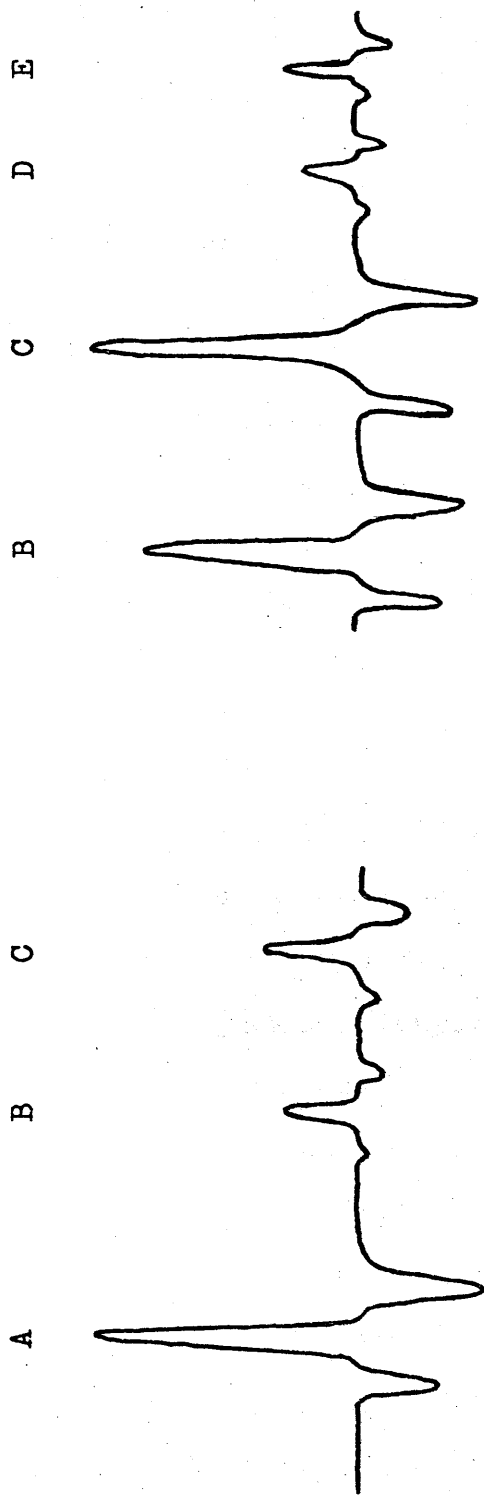
-ate analysis. The frequency of the  $\nu_5$  vibration was not accurately measured by Campbell as the  $\nu_2$  fundamental of NO.Cl is in the same region, and no sample of greater than ~60% purity was observed.

It is evident from the microwave spectrum that the calculated frequencies of Dorko and Buelow are wrong, as there are no vibrational satellites of sufficient intensity. The  $1_{01}-2_{02}$  transition of normal NO.CN and its vibrational satellites were recorded at  $-78^\circ\text{C}$ . The observed spectrum is shown in figure 2.11, A being the ground-state line. The observed frequencies and intensities are presented in table 2.16, along with vibrational energies calculated from the Boltzmann distribution.

The assignments in the table are derived from the frequency shifts from the ground state line in the microwave spectrum and the vibrational energies. The line corresponding to the second quantum of  $\nu_4$  was observed but it was not possible to measure its intensity as it is very close to line C. The vibrational energy levels are determined only

Figure 2.11.

Vibrational Satellites  $\nu_{01-202}$  NO.CN.



to approximately  $10 \text{ cm}^{-1}$  by this method due to uncertainty in the exact temperature of the Stark cell and difficulty in obtaining accurate estimates of intensities. These results are in good agreement with the far infra-red measurements.

Table 2.16.

<u>Vibrational Satellites <math>1_{01}-2_{02}</math> NO.CN.</u>				
Line	Frequency (MHz)	Relative Intensity	$E_{\text{vib}} - E_{\text{gs}}$ ( $\text{cm}^{-1}$ )	Assignment
A	20849.14	100	0	
B	20894.93	13.1	275	$\nu_4$
C	20928.09	18.5	229	$\nu_6$
D	20974.15	3.24	465	$\nu_4 + \nu_6$
E	21004.12	3.72	446	$2\nu_6$

Although it is not strictly permissible to assign a mode of vibration to a particular localised deformation, it is a good approximation for the  $\text{C}\equiv\text{N}$  and  $\text{N}=\text{O}$  stretches since their energies are well removed from those of the other modes. Generally, in organic molecules, these vibrations are in the regions  $2210-2260 \text{ cm}^{-1}$  and  $1500-1600 \text{ cm}^{-1}$  respectively. The  $\text{C}\equiv\text{N}$  stretching frequency in NO.CN is similar to those observed in cyanogen bromide, (2198.3) and cyanogen iodide, (2176.0), both of which exhibit competing resonance and inductive effects. The  $\text{N}=\text{O}$  frequency is lower than generally found, due to the fact that inductive and resonance effects will both tend to weaken this bond. Thus there is some evidence of  $\pi$ -electron delocalisation from the infra-red spectrum. The central  $\text{N}-\text{C}$  stretch and the in-plane bending modes are strongly coupled and cannot be compared directly with

similar molecules.

## 8. Theoretical Calculations.

Molecular properties of nitrosyl cyanide have been calculated using a standard INDO program and the Atmol2 package, which is an ab initio SCF program. There were two main objectives in this work, the first of which was to examine the degree of accuracy with which experimentally determined quantities, such as the dipole moment and quadrupole coupling constants, could be reproduced. The second region of interest was in calculation of the potential function for variation of the NCN angle, fixing the other structural parameters to their experimental values. The preferred conformations from these calculations can then be compared with the experimental value.

In the INDO calculations, minimum basis sets were used throughout. The Atmol calculations used a slightly extended basis set, (minimum basis + 3s orbitals on all nuclei), to determine the dipole moment, quadrupole coupling constants, and the preferred conformation of the NCN fragment. The dipole moment was calculated on Atmol adding 3d orbitals at each nucleus. An error in the properties program precluded calculation of quadrupole coupling constants on this basis. Slater type orbitals, (STO's), were used in the Atmol calculations with 4 gaussian functions making up each STO for all orbitals except the 1s and 3d which were comprised of 6 and 3 gaussians respectively.

The observed and calculated components of the dipole moment are shown in table 2.17, in which Atmol(+) denotes inclusion of the 3d orbitals. Note that the signs of the

Table 2.17.

Observed and Calculated Dipole Moment Components, (D).

	Experimental	INDO	Atmol	Atmol(+)
$\mu_a$	+1.241	+0.713	+1.380	+1.646
$\mu_b$	+0.57	+0.132	-0.184	+0.160
$\mu$	1.365	0.725	1.392	1.654

observed values are postulated rather than determined. The theoretical calculations confirm that the negative pole is at the cyanide end of the molecule, but give little indication as to whether it lies above or below the a-axis. The orientation shown in figure 2.8 still seems most reasonable.

Table 2.18 shows experimental and calculated values of the quadrupole coupling constants. The INDO results were calculated from the p-electron densities, assuming a coupling of 10 MHz for an imbalance of one p-electron on nitrogen. The Atmol figures were calculated directly from the electric field gradients. Agreement between observed and

Table 2.18.

Quadrupole Coupling Constants, (MHz).

Coupling Constant	Observed	INDO	Atmol
$\chi_{aa}(1)$	-4.10	-1.96	-1.45
$\chi_{bb}(1)$	+1.26	+0.12	+0.06
$\chi_{aa}(2)$	+1.52	+0.89	+3.61
$\chi_{bb}(2)$	-5.68	-3.81	-4.12

calculated coupling constants is poor. Only the signs of the constants are consistent. This is largely due to

approximations in the theoretical calculations which break down near the nucleus. It is well known, for example, that Slater type orbitals do not give a good description of electrons near the nucleus.

Molecular energies of NO.CN for a range of NCN angles were computed by INDO and Atmol. Figures 2.12 and 2.13 show the plots of energy against NCN angle. The minimum energy in each case shows a deviation from linearity. The preferred conformation from INDO and Atmol is angle NCN =  $178^\circ$  and  $173.2^\circ$  respectively, the experimental value being  $169^\circ 57'$ . Thus the bend at the carbon could have been predicted from theoretical calculations. The Atmol calculation gives reasonable agreement with the observed angle.

Leibovici<sup>45</sup> has calculated the preferred conformation of the cyanide group in  $\text{NF}_2\text{.CN}$  and  $\text{PF}_2\text{.CN}$  by CNDO/2 and extended Huckel (EHT) calculations. The results of his calculations are compared with the observed values in table 2.19. The good agreement for the simple extended

Table 2.19.

Observed and Calculated XCN Angles in  $\text{NF}_2\text{.CN}$  and  $\text{PF}_2\text{.CN}$ .

	Observed <sup>24,26</sup>	CNDO/2	EHT
$\text{NF}_2\text{.CN}$	$173.9^\circ$	$180^\circ$	$171.4^\circ$
$\text{PF}_2\text{.CN}$	$171.2^\circ$	$180^\circ$	$170.6^\circ$

Huckel treatment seems to be largely fortuitous. No conclusions on the origin of the tilt of the cyano group in these molecules could be made on the basis of these results. Study of the overlap integrals from the Atmol calculations shows repulsion between the  $\text{C}\equiv\text{N}$  and  $\text{N}=\text{O}$   $\pi$ -systems to be a major cause of the bend at the carbon.

Figure 2.12.

Potential Function for Variation of NCN Angle; INDO.

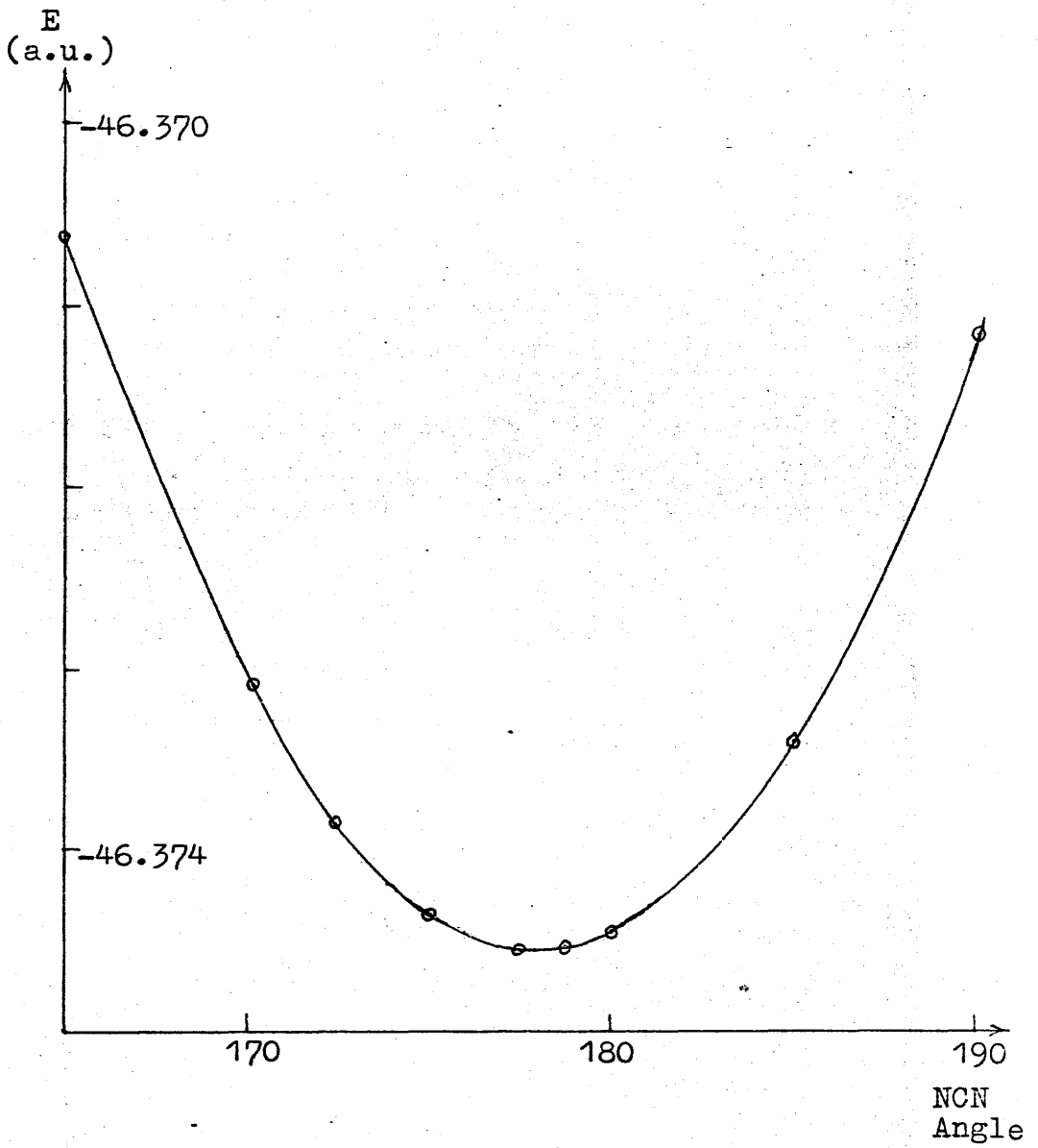
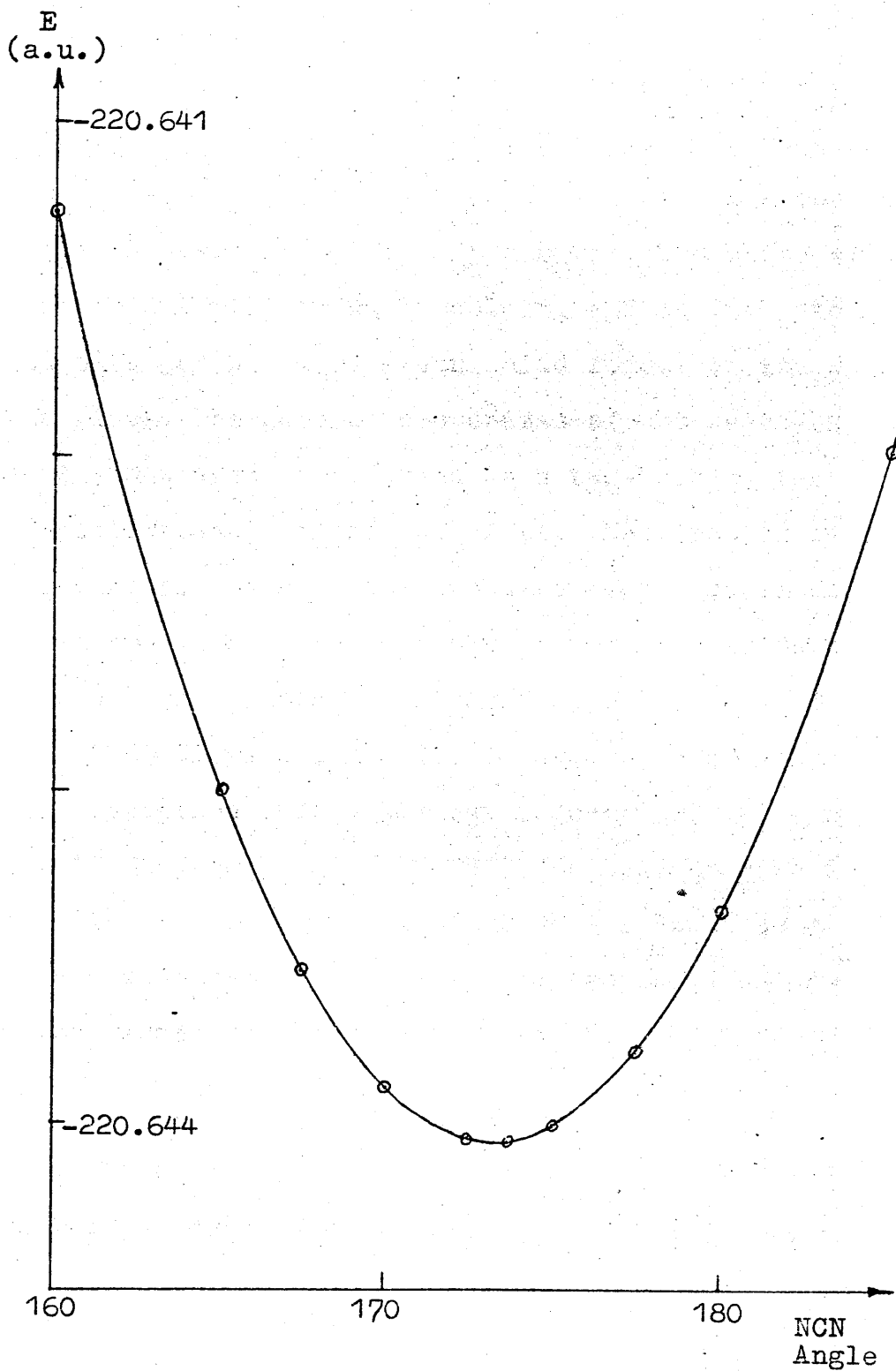


Figure 2.13.

Potential Function for Variation of NCN Angle; Atmol.



## 9. Preparation of NO.CN and Isotopically Substituted Species.

Nitrosyl cyanide was prepared by reaction of nitrosyl chloride and silver cyanide at  $-50^{\circ}\text{C}$ .

NO.Cl gas was condensed onto AgCN at  $-196^{\circ}\text{C}$  on the vacuum line connected to the Stark cell. The reaction vessel was brought to  $-50^{\circ}\text{C}$  by immersion in a dry ice / acetone bath and allowed to react for ca. 15 minutes. The white silver cyanide became pale brown in colour, and on immersion in liquid nitrogen a bright green solid formed on the walls of the flask. The gaseous components of the reaction mixture at  $-50^{\circ}\text{C}$  were transferred to a two-bulb system where fractionation was carried out. After the first or second fractionation, the constituents were recognisable as yellow nitrosyl chloride and blue nitrosyl cyanide. The NO.Cl was never completely separated, but ratios of ca. 4:1 NO.CN:NO.Cl were achieved. On admission of a sample to the absorption cell, this ratio decreased quite rapidly as the NO.CN decomposed. At  $-78^{\circ}\text{C}$  the maximum time for observation of the spectrum of NO.CN was about 30 minutes. The brown colouration of the AgCN disappeared as the reaction vessel was allowed to warm up to room temperature,  $\text{NO}_2$  being given off.

Although NO.CN decomposes rapidly in the Stark cell it may be stored 5-6 days at room temperature, and for several months at  $-20^{\circ}\text{C}$ , in a glass vessel.

Nitrosyl chloride was prepared by careful addition of aqueous sodium nitrite solution ( $\sim 0.5\text{g/ml}$ ) to concentrated

HCl under nitrogen at room temperature.<sup>46</sup> The nitrosyl chloride was flushed from the reaction vessel by the nitrogen stream, dried over anhydrous calcium chloride, and condensed as a cherry-red liquid in a dry ice/acetone bath. The reaction vessel was warmed to  $\sim 80^{\circ}\text{C}$  to outgas dissolved  $\text{NO}\cdot\text{Cl}$  and also to distill a little HCl into the cold trap to react with the small amount of  $\text{NO}_2$  formed initially. The  $\text{NO}\cdot\text{Cl}$  was finally purified by distillation on the vacuum line. Silver cyanide was prepared by addition of  $\text{AgNO}_3$  to KCN in aqueous solution, the precipitated  $\text{AgCN}$  being collected by filtration and dried under vacuum.

Isotopically-substituted species of  $\text{NO}\cdot\text{CN}$  were prepared from suitably enriched  $\text{NO}\cdot\text{Cl}$  or  $\text{AgCN}$ .

#### $\text{Ag}^{13}\text{CN}$ and $\text{AgC}^{15}\text{N}$ .

These were obtained using commercial samples of 61.5%  $^{13}\text{C}$ -enriched KCN and 96%  $^{15}\text{N}$ -KCN respectively.

#### $^{15}\text{NO}\cdot\text{Cl}$ .

$^{15}\text{NO}\cdot\text{Cl}$  was prepared from reaction of 97.8%  $^{15}\text{N}$ - $\text{NaNO}_2$  with HCl as detailed previously.

#### $\text{N}^{18}\text{O}\cdot\text{Cl}$ .

$^{18}\text{O}$ -enriched  $\text{NaNO}_2$  was prepared by equilibration of normal  $\text{NaNO}_2$  in  $\text{H}_2^{18}\text{O}$  containing a trace of nitric acid.<sup>47</sup> A solution of 0.1 g  $\text{NaNO}_2$  in 0.2 ml 62.5%  $^{18}\text{O}$ -enriched water with a trace (one drop) of nitric acid was allowed to equilibrate for three days. This solution was then reacted with 0.6 ml  $\text{H}_2^{18}\text{O}$  saturated with HCl to give  $^{18}\text{O}$ -enriched  $\text{NO}\cdot\text{Cl}$ .

## REFERENCES.

1. R.G.W. Norrish and F.F.R. Smith, *Trans. Far. Soc.*, 1928, 24, 620; N. Basco, J.E. Nicholas, R.G.W. Norrish and W.H.J. Vickers, *Proc. Roy. Soc.*, 1963, A272, 147; N. Basco and R.G.W. Norrish, *Proc. Roy. Soc.*, 1965, A283, 291.
2. J.P. Galvin and N.O. Pritchard, *J. Phys. Chem.*, 1964, 68, 1035.
3. F. Horsewood and G.W. Kirby, *Chem. Comm.*, 1971, 1139.
4. P. Horsewood and G.W. Kirby, Unpublished work.
5. K.W. Bentley, P. Horsewood, G.W. Kirby and Serjinder Singh, *Chem. Comm.*, 1969, 1411.
6. (a) R. Dickinson, G.W. Kirby, J.G. Sweeny and J.K. Tyler, *J. Chem. Soc. Chem. Comm.*, 1973, 241.  
(b) R. Dickinson, B.Sc. Thesis, University of Glasgow, 1973.
7. S.R. Polo, *Canad. J. Phys.*, 1957, 35, 880.
8. C.C. Costain, *J. Chem. Phys.*, 1958, 29, 864.
9. T. Oka and Y. Morino, *J. Mol. Spectroscopy*, 1963, 11, 349.
10. M. Sugie, T. Fukuyama and K. Kuchitsu, *J. Mol. Structure*, 1972, 14, 333.
11. D.R. Herschbach and V.W. Laurie, *J. Chem. Phys.*, 1964, 40, 3142.
12. D. Kivelson and E.B. Wilson, Jr., *J. Chem. Phys.*, 1952, 20, 1575.
13. E.B. Wilson, Jr. and J.B. Howard, *J. Chem. Phys.*, 1936, 4, 260.
14. J.M. Dowling, *J. Mol. Spectroscopy*, 1961, 6, 550.
15. J.K.G. Watson, *J. Chem. Phys.*, 1967, 46, 1935.
16. H.H. Nielsen, *Revs. Mod. Phys.*, 1951, 23, 90.
17. H. Wenger and A. Bauder, Unpublished work.
18. W.H. Kirchhoff, *J. Mol. Spectroscopy*, 1972, 41, 333.
19. J. Kraitchman, *Am. J. Phys.*, 1953, 21, 17.
20. D.J. Millen and J. Pannell, *J. Chem. Soc.*, 1961, 1322.
21. A.P. Cox, Unpublished work.
22. J.K. Tyler and J. Sheridan, *Trans. Far. Soc.*, 1963, 59, 2663.

23. D.R. Lide, Jr., J. Chem. Phys., 1957, 27, 343.
24. P.L. Lee, K. Cohn and R.H. Schwendeman, Inorg. Chem., 1972, 11, 1920.
25. J.K. Tyler, J. Sheridan and C.C. Costain, J. Mol. Spectroscopy, 1972, 43, 248.
26. P.L. Lee, K. Cohn and R.H. Schwendeman, Inorg. Chem., 1972, 11, 1917.
27. T. Fukuyama, K. Kuchitsu and Y. Morino, Bull. Chem. Soc. Japan, 1969, 42, 379.
28. T. Fukuyama and K. Kuchitsu, J. Mol. Structure, 1970, 5, 131.
29. S. Golden and E.B. Wilson, Jr., J. Chem. Phys., 1948, 16, 669.
30. P.F. Wacker and M.R. Pratto, "Microwave Spectral Tables, Line Strengths of Asymmetric Rotors", National Bureau of Standards, Washington, 1964.
31. J.S. Muentzer, J. Chem. Phys., 1968, 48, 4544.
32. E.L. Beeson, Q. Williams and T.C. Weatherly, Bull. Am. Phys. Soc., 1959, 4, 291.
33. R.G. Schulman, B.P. Dailey and C.H. Townes, Phys. Rev., 1950, 78, 145.
34. S. Golden and J.K. Bragg, Phys. Rev., 1949, 75, 735.
35. C.H. Townes and A.L. Schawlow, "Microwave Spectroscopy", McGraw-Hill Book Co. Inc., 1955.
36. J.N. Macdonald, Ph.D. Thesis, University of Glasgow, 1969.
37. J. Bardeen and C.H. Townes, Phys. Rev., 1948, 73, 97.
38. E.U. Condon and G.H. Shortley, "The Theory of Atomic Spectroscopy", The Macmillan Co., New York, 1935.
39. C.H. Townes and B.P. Dailey, J. Chem. Phys., 1949, 17, 782.
40. J.W. Simmons, W.E. Anderson and W. Gordy, Phys. Rev., 1950, 70, 77; errata, 1952, 86, 1055.
41. C.H. Townes, A.N. Holden, J. Bardeen and F.R. Merrit, Phys. Rev., 1947, 71, 644L, erratum, 1947, 71, 829L; C.H. Townes, A.N. Holden and F.R. Merrit, Phys. Rev., 1948, 74, 1113.
42. K.S. Buckton, A.C. Legon and D.J. Millen, Trans. Far. Soc., 1969, 65, 1975.

43. E.A. Dorko and L. Buelow, J. Chem. Phys., 1975, 62, 1869.
44. J.A. Campbell, B.Sc. Thesis, University of Glasgow, 1974.
45. C. Leibovici, J. Mol. Structure, 1973, 18, 343.
46. J.R. Morton and H.W. Wilcox, Inorg. Synth., 1953, 4, 48.
47. C.A. Bunton, D.R. Llewellyn and G.J. Stedman, J. Chem. Soc., 1959, 568.

## CHAPTER 3.

### THE MICROWAVE SPECTRUM OF MALEIMIDE.

#### 1. Introduction.

There has been much interest in the conformation of amide groups; in particular, whether or not the N-hydrogens are coplanar with the N-C=O fragment. The amide group is planar in the resonance form  $\text{H}_2\overset{\oplus}{\text{N}}=\text{C}=\overset{\ominus}{\text{O}}$  which would be expected to make a large contribution to the electronic configurations of these molecules. Many molecules of this type, once thought to be planar, have been shown to be non-planar from the presence of inversion effects in their microwave spectra. These include urea,<sup>1</sup> and the related molecules, cyanamide,<sup>2,3</sup> and nitramide.<sup>4</sup> There is still some controversy over the conformation of formamide, the most recent suggestion being that this molecule is planar.<sup>5-7</sup>

Maleimide, 1H-pyrrole-2,5-dione, is an interesting example of this type of problem. With two equivalent resonance forms,  $\overset{\oplus}{\text{N}}=\overset{\ominus}{\text{C}}-\overset{\ominus}{\text{O}}$ , and inductive effects of the two carbonyl groups adjacent to the nitrogen, this molecule would be expected to be planar or very near planar. The object of this work was to determine the conformation at the nitrogen atom by analysis of the microwave spectrum. A previous attempt to assign and analyse the spectrum was unsuccessful,<sup>8</sup> as it is complicated, with a large number of lines. The vibrational spectra of maleimide and N-deutero-maleimide have been successfully analysed on the basis of a  $\text{C}_{2v}$  (planar) structure,<sup>9</sup> but this was not claimed to be conclusive evidence for planarity.

The ground vibrational state microwave spectra of maleimide and N-deutero-maleimide have been assigned and rotational constants obtained. These are discussed with respect to the conformation at the nitrogen. The dipole moment of maleimide has been determined as  $1.65 \pm 0.03$  D from Stark effect measurements.

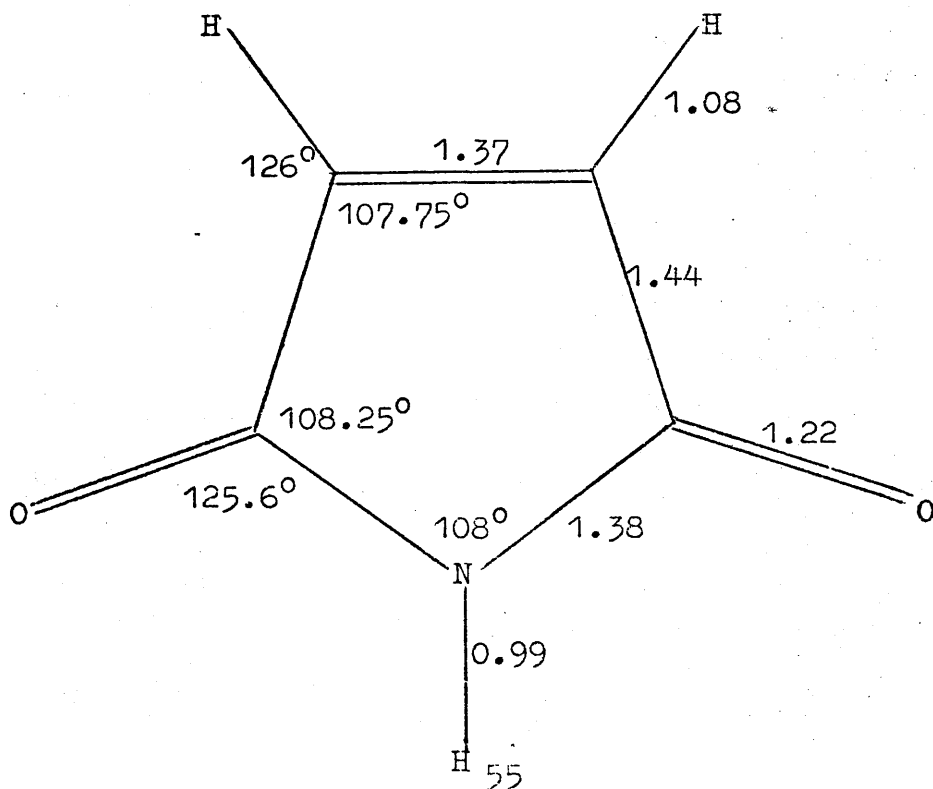
## 2. Observation and Analysis of the Spectrum.

A commercial sample of maleimide was used without further purification. At room temperature it is a waxy solid with just sufficient vapour pressure for microwave work. The sample vapour was drawn through the Stark cell at  $35^{\circ}\text{C}$ , the pressure in the cell being approximately 0.05 Torr.

The spectrum was predicted from a planar model, parameters being derived largely from the structures of pyrrole<sup>10</sup> and maleic anhydride.<sup>11</sup> The model is shown in figure 3.1. The

Figure 3.1.

Planar Model of Maleimide, Distances in Å.



moments of inertia were calculated from this model as;  $I_a = 71.15 \text{ amu } \text{\AA}^2$ ,  $I_b = 210.16 \text{ amu } \text{\AA}^2$ ,  $I_c = 281.31 \text{ amu } \text{\AA}^2$ , giving the following values for the rotational constants;  $A = 7103 \text{ MHz}$ ,  $B = 2405 \text{ MHz}$ , and  $C = 1797 \text{ MHz}$  with  $\kappa = -0.7708$ . The b-axis in this model corresponds to the  $C_2$  axis. Spectra were predicted using program Asrot by H. Wenger and A. Bauder, which calculates transition frequencies and intensities from rotational constants. A large number of Q- and R-branch lines were predicted in the 18-40 GHz region.

In an initial attempt to assign the spectrum, a line diagram of the stronger predicted lines in K-band was compared with the observed spectrum. However, no obvious correlation was observed. The strongest series in this region are the  $J_2(J-2) \rightarrow J_3(J-3)$ , ( $8 \leq J \leq 15$ ), and  $J_3(J-3) \rightarrow J_4(J-4)$ , ( $13 \leq J \leq 17$ ), Q-branch lines. Frequencies of these lines are given by;

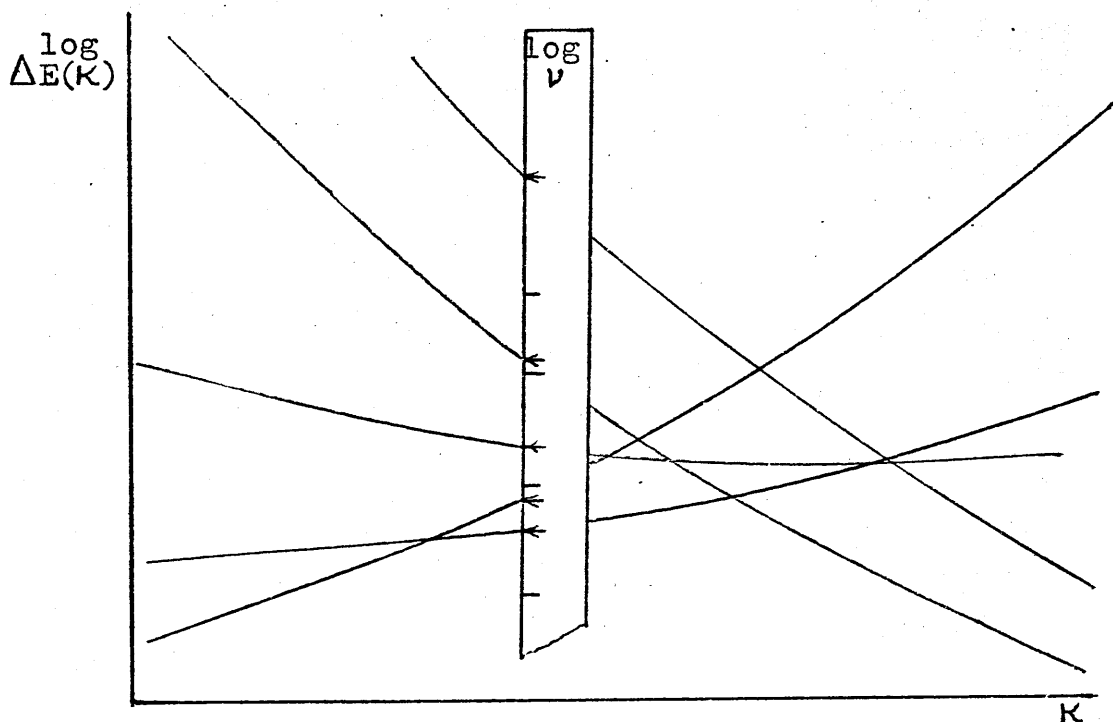
$$\nu = \frac{A-C}{2} \Delta E(\kappa)$$

and hence  $\log \nu = \log \frac{A-C}{2} + \log \Delta E(\kappa)$ .

These Q-branch series were plotted as two sets of curves of  $\log \Delta E(\kappa)$  against  $\kappa$  between -0.80 and -0.74. Approximate frequencies of observed transitions, thought to correspond to these series were plotted as  $\log \nu$  on the same scale on a strip of graph paper. Keeping the  $\log \Delta E(\kappa)$  and  $\log \nu$  axes parallel, the strip is displaced horizontally and vertically until the transitions fall on the Q-branch curves.<sup>12</sup> This procedure is illustrated schematically in figure 3.2.

For both Q-branch series a fit was obtained for  $\kappa = -0.760$ ,

Figure 3.2.  
Q-branch Curves.

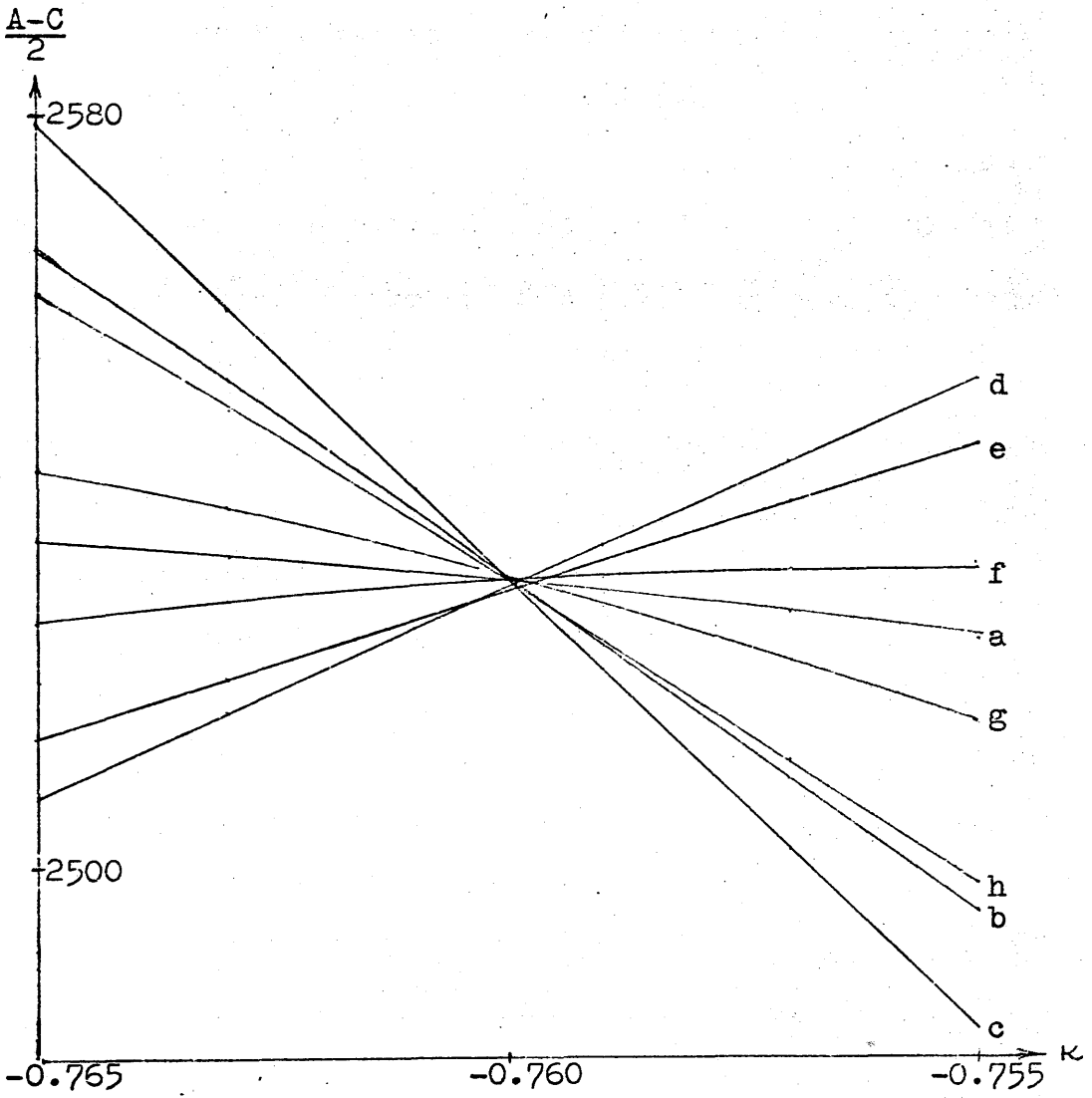


corresponding to  $\frac{A-C}{2}$  of 2531 MHz. Determination of these parameters allowed prediction and assignment of a large number of Q-branch lines which were then measured. A Q-branch plot of  $\frac{A-C}{2}$  versus  $\kappa$  was drawn for some of these lines. (figure 3.3) The area of intersection is small, giving improved values of  $\kappa = -0.75995$  and  $\frac{A-C}{2} = 2530.4$  MHz.

Intensity fluctuations arising from nuclear statistical effects are expected in the spectrum, whether or not the molecule is planar. If the molecule is non-planar to a small extent, inversion will occur at the nitrogen. The separate vibrational levels associated with this inversion transform according to the  $C_{2v}$  point group, and the same intensity effects will be observed as in the planar case.<sup>2</sup> One pair of fermions, the olefinic protons, are exchanged

Figure 3.3.

Q-Branch Plot, Maleimide.



a  $11_{29} - 11_{38}$

b  $13_{211} - 13_{310}$

c  $14_{212} - 14_{311}$

d  $13_{310} - 13_{49}$

e  $14_{311} - 14_{410}$

f  $15_{312} - 15_{411}$

g  $16_{313} - 16_{412}$

h  $17_{314} - 17_{413}$

on rotation of  $180^\circ$  about the  $C_2$  axis. The ratio of symmetric to antisymmetric nuclear spin states is  $(I+1):I = 3:1$ . According to Fermi-Dirac statistics the total wave function must be antisymmetric with respect to  $180^\circ$  rotation about the b-axis. Thus the ratio of symmetric to antisymmetric rotational energy level populations is  $1:3$ . The  $11_{38}-11_{47}$  transition is expected to be approximately three times more intense than the  $10_{37}-10_{46}$ . This is observed, eliminating the small possibility of a rigid tetrahedral conformation at the nitrogen.

For the purpose of prediction of R-branch lines it was necessary to assume planarity. The rotational constants were calculated as;

$A = 6816$  MHz,  $B = 2362$  MHz, and  $C = 1754$  MHz.

If the molecule is planar, or very near planar, these constants are determined to approximately 15 MHz. The  $1_{10}-2_{21}$  transition, which was assigned on the basis of its Stark effect, was found within 2 MHz of its predicted frequency. Since the frequency of this line is given by  $(3A+C)$ , the rotational constants were now obtained independent of the planarity assumption as;

$A = 6815.3 \pm 1$  MHz,  $B = 2361.9 \pm 1$  MHz,  $C = 1754.5 \pm 1$  MHz.

Good agreement, (within 2 MHz), was found between R-branch frequencies predicted from these constants and those observed.

It was then a simple matter to predict, assign and measure the remainder of the ground state spectrum. A large number of lines were not assigned. Some of these were of comparable intensity to the stronger ground state lines. There

was no obvious relationship between the positions of these lines and the assigned ground state spectrum. The possible origins of these lines, which remain unassigned, are discussed in section 3.

Rotational and centrifugal distortion constants of the ground state spectrum of maleimide were obtained by least squares, using the programs Asfip and Asfit by Wenger and Bauder, described in Chapter 2. Tables 3.1 and 3.2 show the constants obtained from these programs and table 3.3 gives observed and calculated line frequencies. The value of the inertial defect ( $-0.05138 \text{ amu } \text{\AA}^2$ ) confirms that the molecule is, or is nearly, planar. In an attempt to clarify further the conformation at the nitrogen, it was decided to observe the spectrum of N-deutero maleimide.

N-deutero maleimide was prepared by repeated treatment of maleimide with  $\text{D}_2\text{O}$  at ca.  $70^\circ\text{C}$  with successive evaporation of the liquid. At higher temperatures, hydrolysis took place. Deuteration was effected to ca. 45%, sufficient for study of the microwave spectrum.

Approximate moments of inertia of the deuterated species were obtained by calculating the change in the moments of the model on deuteration using;

$$\Delta I_a = \Delta I_c = \frac{M \Delta m}{M + \Delta m} x^2 \quad \text{and} \quad \Delta I_b = 0.$$

where  $x$  is the distance of the N-hydrogen from the centre of mass,

$M$  is the molecular weight of the normal species,

and  $\Delta m$  is the change in mass on deuteration.

These are added to the observed moments of the normal

Table 3.1.

Rotational Constants of Maleimide from Asfip, (MHz).

A	6815.333	±	0.0091
B	2361.8584	±	0.0046
C	1754.3191	±	0.0030
$\tau_{aaaa}$	-0.0112	±	0.0020
$\tau_{bbbb}$	-0.00078	±	0.00010
$\tau_{aabb}$	0.00099	±	0.00057
$\tau_{abab}$	-0.00136	±	0.00026
( $\Delta$	-0.05138	±	0.00072
			amu Å <sup>2</sup> )

Table 3.2.

Rotational Constants of Maleimide from Asfit, (MHz).

A	6815.3340	±	0.0091
B	2361.8583	±	0.0045
C	1754.3171	±	0.0040
$D_J$	0.000104	±	0.000022
$D_{JK}$	0.000327	±	0.000098
$D_K$	0.00209	±	0.00062
$\delta_J$	0.0000427	±	0.0000053
$\delta_K$	0.00025	±	0.00013

Table 3.3.Observed and Calculated Transition Frequencies  
of Maleimide. (MHz).

Transition	$\nu_{\text{obs}}$	$\nu_{\text{calc}}$	$\nu_{\text{obs}} - \nu_{\text{calc}}$
3 <sub>03</sub> -4 <sub>14</sub>	18329.71	18329.88	-0.17
4 <sub>04</sub> -5 <sub>15</sub>	21257.90	21258.00	-0.10
5 <sub>05</sub> -6 <sub>16</sub>	24203.90	24203.86	0.04
7 <sub>07</sub> -8 <sub>18</sub>	30412.42	30412.31	0.11
8 <sub>08</sub> -9 <sub>19</sub>	33690.55	33690.44	0.11
9 <sub>09</sub> -10 <sub>110</sub>	37053.33	37053.17	0.16
1 <sub>10</sub> -2 <sub>21</sub>	22200.34	22200.28	0.06
3 <sub>12</sub> -4 <sub>23</sub>	28906.48	28906.68	-0.20
4 <sub>13</sub> -5 <sub>24</sub>	31805.85	31805.99	-0.14
5 <sub>14</sub> -6 <sub>25</sub>	34435.56	34435.68	-0.12
6 <sub>15</sub> -7 <sub>26</sub>	36848.12	36848.21	-0.09
7 <sub>16</sub> -8 <sub>27</sub>	39124.83	39124.92	-0.09
2 <sub>12</sub> -3 <sub>21</sub>	27818.44	27818.16	0.28
3 <sub>13</sub> -4 <sub>22</sub>	33386.11	33385.74	0.37
2 <sub>21</sub> -3 <sub>30</sub>	36172.55	36172.74	-0.19
5 <sub>15</sub> -6 <sub>06</sub>	21366.82	21356.79	0.03
6 <sub>16</sub> -7 <sub>07</sub>	25402.09	25402.04	0.05
7 <sub>17</sub> -8 <sub>08</sub>	29267.15	29267.15	0.00
8 <sub>18</sub> -9 <sub>09</sub>	33003.91	33003.92	-0.01
9 <sub>19</sub> -10 <sub>010</sub>	36652.68	36652.51	0.17
6 <sub>25</sub> -7 <sub>16</sub>	21484.59	21484.55	0.04
8 <sub>27</sub> -9 <sub>18</sub>	32142.81	32142.86	-0.05
9 <sub>28</sub> -10 <sub>19</sub>	37071.52	37071.66	-0.14
8 <sub>36</sub> -9 <sub>27</sub>	21653.22	21653.20	0.02
10 <sub>38</sub> -11 <sub>29</sub>	34454.73	34454.82	-0.09

contd.

Table 3.3, contd.

Transition	$\nu_{\text{obs}}$	$\nu_{\text{calc}}$	$\nu_{\text{obs}} - \nu_{\text{calc}}$
$12_{49} - 13_{310}$	32666.33	32666.37	-0.04
$11_{011} - 11_{110}$	32971.63	32971.58	0.05
$13_{112} - 13_{211}$	30576.20	30576.27	-0.07
$6_{16} - 6_{25}$	20954.95	20954.75	0.20
$9_{19} - 9_{28}$	28542.38	28542.29	0.09
$7_{25} - 7_{34}$	20436.09	20436.14	-0.05
$9_{27} - 9_{36}$	18433.08	18433.01	0.07
$11_{29} - 11_{38}$	18187.92	18187.96	-0.04
$12_{210} - 12_{39}$	19139.16	19139.26	-0.10
$13_{211} - 13_{310}$	20927.40	20927.49	-0.09
$14_{212} - 14_{311}$	23569.30	23569.35	-0.05
$15_{213} - 15_{312}$	27001.23	27001.21	0.02
$6_{25} - 6_{34}$	24756.67	24756.63	0.04
$10_{29} - 10_{38}$	29524.14	29524.18	-0.04
$8_{35} - 8_{44}$	31814.97	31815.06	-0.09
$9_{36} - 9_{45}$	30848.61	30848.61	0.00
$10_{37} - 10_{46}$	29559.35	29559.35	0.00
$11_{38} - 11_{47}$	28031.82	28031.92	-0.10
$12_{39} - 12_{48}$	26443.93	26443.85	0.08
$13_{310} - 13_{49}$	25034.87	25034.82	0.05
$14_{311} - 14_{410}$	24058.16	24058.15	0.01
$15_{312} - 15_{411}$	23735.85	23735.86	-0.01
$16_{313} - 16_{412}$	24233.53	24233.61	-0.09
$17_{314} - 17_{413}$	25654.35	25654.36	-0.01
$18_{315} - 18_{414}$	28033.67	28033.71	-0.04
$19_{316} - 19_{415}$	31326.62	31326.49	0.13
$10_{38} - 10_{47}$	33657.49	33657.64	-0.15
$13_{49} - 13_{58}$	39088.42	39088.34	0.08

Table 3.3, contd.

Transition	$\nu_{\text{obs}}$	$\nu_{\text{calc}}$	$\nu_{\text{obs}} - \nu_{\text{calc}}$
$14_{410} - 14_{59}$	37519.85	37519.83	0.02
$15_{411} - 15_{510}$	35655.18	35655.14	0.04
$16_{412} - 16_{511}$	33655.53	33655.51	0.02
$17_{413} - 17_{512}$	31762.30	31762.12	0.18
$18_{414} - 18_{513}$	30251.34	30251.57	-0.23
$19_{415} - 19_{514}$	29384.66	29384.69	-0.03
$20_{416} - 20_{515}$	29368.80	29368.80	0.00
$21_{417} - 21_{516}$	30341.53	30341.47	0.06

Table 3.4.

Rotational Constants of N-D Maleimide from Asfip, (MHz).

A	6493.809	±	0.011
B	2361.911	±	0.006
C	1732.336	±	0.006
$\tau_{aaaa}$	-0.0069	±	0.0019
$\tau_{bbbb}$	-0.00075	±	0.00013
$\tau_{aabb}$	0.00005	±	0.0008
$\tau_{abab}$	-0.0009	±	0.0003
( $\Delta$	-0.0625	±	0.0010
			amu Å <sup>2</sup> )

Table 3.5.

Rotational Constants of N-D Maleimide from Asfit, (MHz).

A	6493.807	±	0.011
B	2361.910	±	0.006
C	1732.333	±	0.006
$D_J$	0.000105	±	0.000033
$D_{JK}$	0.00038	±	0.00011
$D_K$	0.00094	±	0.00069
$\delta_J$	0.000035	±	0.000004
$\delta_K$	0.00023	±	0.00011

Table 3.6.

Observed and Calculated Transition Frequencies,N-D Maleimide, (MHz).

Transition	$\nu_{\text{obs}}$	$\nu_{\text{calc}}$	$\nu_{\text{obs}} - \nu_{\text{calc}}$
4 <sub>04</sub> -5 <sub>15</sub>	20740.26	20740.39	-0.13
5 <sub>05</sub> -6 <sub>06</sub>	23676.97	23676.94	0.03
8 <sub>08</sub> -9 <sub>19</sub>	33177.08	33176.87	0.21
9 <sub>09</sub> -10 <sub>110</sub>	36528.86	36528.89	-0.03
1 <sub>10</sub> -2 <sub>21</sub>	21213.71	21213.73	-0.02
5 <sub>15</sub> -6 <sub>06</sub>	21347.92	21347.95	-0.03
6 <sub>16</sub> -7 <sub>07</sub>	25270.99	25271.00	-0.01
7 <sub>17</sub> -8 <sub>08</sub>	29032.12	29032.17	-0.05
8 <sub>18</sub> -9 <sub>09</sub>	32678.27	32678.30	-0.03
9 <sub>19</sub> -10 <sub>010</sub>	36249.62	36249.50	0.12
10 <sub>110</sub> -11 <sub>011</sub>	39774.62	39774.64	-0.02
6 <sub>25</sub> -7 <sub>16</sub>	22300.14	22300.08	0.06
8 <sub>27</sub> -9 <sub>18</sub>	32646.49	32646.58	-0.09
8 <sub>36</sub> -9 <sub>27</sub>	23541.41	23541.38	0.03
10 <sub>38</sub> -11 <sub>29</sub>	36183.64	36183.73	-0.09
11 <sub>110</sub> -11 <sub>29</sub>	23043.67	23043.53	0.14
13 <sub>112</sub> -13 <sub>211</sub>	31497.08	31496.93	0.15
7 <sub>25</sub> -7 <sub>34</sub>	18671.45	18671.42	0.03
12 <sub>210</sub> -12 <sub>39</sub>	18863.37	18863.37	0.00
13 <sub>211</sub> -13 <sub>310</sub>	21195.41	21195.37	0.04
15 <sub>213</sub> -15 <sub>312</sub>	28265.14	28265.09	0.05
16 <sub>214</sub> -16 <sub>313</sub>	32641.54	32641.40	0.14
17 <sub>215</sub> -17 <sub>314</sub>	37250.81	37250.82	-0.01
12 <sub>211</sub> -12 <sub>310</sub>	33208.18	33208.08	0.10
11 <sub>38</sub> -11 <sub>47</sub>	25291.32	25291.34	-0.02
12 <sub>39</sub> -12 <sub>48</sub>	23806.47	23806.34	0.13

Table 3.6, contd.

Transition	$v_{\text{obs}}$	$v_{\text{calc}}$	$v_{\text{obs}} - v_{\text{calc}}$
13 <sub>310</sub> -13 <sub>49</sub>	22678.59	22678.52	0.07
14 <sub>311</sub> -14 <sub>410</sub>	22165.08	22165.07	0.01
15 <sub>312</sub> -15 <sub>411</sub>	22464.65	22464.67	-0.02
16 <sub>313</sub> -16 <sub>412</sub>	23704.86	23704.96	-0.10
17 <sub>314</sub> -17 <sub>413</sub>	25938.02	25938.02	0.00
19 <sub>316</sub> -19 <sub>415</sub>	33126.59	33126.62	-0.03
14 <sub>312</sub> -14 <sub>411</sub>	36332.64	36332.59	0.05
15 <sub>313</sub> -15 <sub>412</sub>	38355.75	38356.30	-0.55
12 <sub>48</sub> -12 <sub>57</sub>	36958.98	36959.04	-0.06
13 <sub>49</sub> -13 <sub>58</sub>	35527.73	35527.74	-0.01
15 <sub>411</sub> -15 <sub>510</sub>	31800.82	31800.78	0.04
17 <sub>413</sub> -17 <sub>512</sub>	28351.43	28351.37	0.06
19 <sub>415</sub> -19 <sub>514</sub>	27418.32	27418.42	-0.10
20 <sub>416</sub> -20 <sub>515</sub>	28414.35	28414.38	-0.03
21 <sub>417</sub> -21 <sub>516</sub>	30500.99	30501.07	-0.08
23 <sub>419</sub> -23 <sub>518</sub>	37713.60	37713.64	-0.04
19 <sub>514</sub> -19 <sub>613</sub>	38258.87	38258.85	0.02
21 <sub>516</sub> -21 <sub>615</sub>	34011.71	34011.69	0.02
22 <sub>517</sub> -22 <sub>616</sub>	32711.93	32711.88	0.05
23 <sub>518</sub> -23 <sub>617</sub>	32330.13	32330.12	0.01
25 <sub>520</sub> -25 <sub>619</sub>	34940.65	34940.68	-0.03
26 <sub>521</sub> -26 <sub>620</sub>	37998.07	37997.94	0.13
26 <sub>620</sub> -26 <sub>719</sub>	37988.75	37988.74	0.01

species. Rotational constants from these were used to predict the spectra to an accuracy of ca. 20 MHz. This allowed assignment of the Q-branch lines. The values of the rotational constants were refined in a similar manner to those of the normal species. Final values of the rotational constants are shown in tables 3.4 and 3.5. Observed and calculated transition frequencies are shown in table 3.6.

### 3. Structure.

On the basis of the comparatively little inertial information obtained on maleimide, it is possible to make only qualitative conclusions concerning the molecular structure.

Maleimide is clearly a borderline case of planarity. The best known example of this is formamide. In the first microwave investigations of this molecule, it was concluded to be planar.<sup>5</sup> In a more detailed study by Costain and Dowling<sup>6</sup> it was suggested that the equilibrium positions of the amino hydrogens are about 0.15 Å out of the plane defined by the remainder of the molecule. The basis of their argument was the behaviour of the inertial defect on replacement of an N-hydrogen by deuterium. In addition, each line in the spectrum of every isotopic species studied was accompanied by a vibrational satellite of anomalously high intensity. These satellites were assigned to the first excited state of the NH<sub>2</sub> wagging vibration. The anharmonicity of this vibration was taken as a strong indication that the molecule is non-planar. More recently, Hirota et al<sup>7</sup> carried out a full structure determination on formamide and proposed a planar conformation on the

basis of assignment and analysis of vibrational spectra and vibrational satellites in the microwave spectrum. The minimum of the potential function used to fit the observed spectra corresponded to the planar structure. However it remains uncertain whether or not formamide is indeed planar.

If maleimide is non-planar, the N-H out of plane bending vibration will be anharmonic, and the effects of this will be observable in the microwave spectrum. The frequency of this vibration was reported<sup>9</sup> as  $721 \text{ cm}^{-1}$  but if it is indeed strongly anharmonic, it is possible that the measured transition terminates on the  $V=2$  level. The lowest frequency vibrational transitions measured are the carbonyl out of plane bending modes, which occur at  $175 \text{ cm}^{-1}$  and  $300 \text{ cm}^{-1}$ . The lower of these two modes will give rise to lines in the microwave spectrum of just less than half the intensity, neglecting nuclear statistics, of the ground state lines. This is not sufficiently intense to account for some of the unassigned lines in the microwave spectrum. It cannot be assumed, however, that these lines arise from inversion effects. To summarise, no effects of inversion at the nitrogen have been positively identified in the rotational or vibrational spectra of maleimide.

The most direct indication of planarity in a molecule is provided by the inertial defect. However the fact that the inertial defect is small or positive does not establish planarity. Oka and Morino<sup>13</sup> have shown that the planarity of a molecule is most rigourously established

if the observed inertial defect agrees with that calculated from vibrational parameters assuming planarity. Such a calculation for maleimide would be complex. In addition to this, the published fit of out of plane vibration frequencies calculated from force constants to those observed was poor. The out of plane vibrations are particularly important in ring compounds. For these reasons, no calculation of the inertial defect of maleimide was undertaken. However, some evidence on whether or not the molecule is planar can be obtained by comparison with related molecules.

In general for a planar molecule, the inertial defect for the ground vibrational state is expected to be positive, unless one or more out of plane vibrations are of very low frequency. Planar ring molecules have several low frequency out of plane modes which counteract the contribution from the in-plane modes. These molecules usually have rather small, positive inertial defects.<sup>14</sup> Inertial defects of some planar ring molecules are presented in table 3.7. With the exceptions of maleic anhydride and maleimide, the negative inertial defects are caused by low frequency, large amplitude, torsional vibrations of aryl substituents. In p-fluorostyrene for example,<sup>25</sup> correction for the torsion mode gave an inertial defect of +0.01 amu Å<sup>2</sup>. The negative value for maleic anhydride arises from the low frequency ( 173, 275 cm<sup>-1</sup> )<sup>26</sup> carbonyl out of plane bending modes. These vibrations contribute to the negative inertial defect of maleimide also, but to a slightly smaller extent, since they occur at higher frequencies, ( 175, 301 cm<sup>-1</sup> ).<sup>9</sup>

Table 3.7.

Inertial Defects of some Planar Ring Molecules.

<u>Molecule</u>	<u><math>\Delta(\text{amu } \text{Å}^2)</math></u>	<u>Reference</u>
Benzonitrile	+0.093 <sup>1</sup>	15
Phenyl Isocyanide	+0.0777	16
1,2,4 Triazole	+0.040	17
Pyridine	+0.032	18
Pyrazole	+0.03159	19
Pyrrole	+0.015	20
Maleic Anhydride	-0.019	21
Phenol	-0.0299	22
Maleimide	-0.0514	This work
Benzaldehyde	-0.128	23
Nitrosobenzene	-0.15	24
p-Fluorostyrene	-0.775	25

It appears that an additional factor is required to explain the magnitude of the inertial defect of maleimide. While the presence of inversion would produce this kind of effect, this cannot be taken as a firm indication of non-planarity.

The change in the inertial defect on deuteration has been used as test for planarity.<sup>6</sup> This is generally small and positive (ca. +0.005 amu Å<sup>2</sup>) for planar ring molecules. The inertial defects of maleimide and N-deutero maleimide are -0.0514 and -0.0625 amu Å<sup>2</sup> respectively, a difference of -0.0111 amu Å<sup>2</sup>. Following the reasoning of Costain and Dowling,<sup>6</sup> this would be taken to suggest a non-planar structure. However, several instances of negative changes in the inertial defects of planar ring molecules of this

order of magnitude have been recorded. For example, deuteration at the 4-position in benzonitrile<sup>15</sup> and phenol<sup>22</sup> produces changes from +0.093 to +0.047 amu Å<sup>2</sup> and -0.0299 to -0.0355 amu Å<sup>2</sup> respectively.

Thus, in spite of accurate determination of inertial defects of the normal and N-deutero species, no definite conclusions can be made regarding planarity. The similarities in the rotational and vibrational spectra of maleimide and maleic anhydride favour the planar structure. Alternatively, the differences in the inertial defects of maleimide and maleic anhydride, and the change in  $\Delta$  on N-deuteration support a non-planar structure. Further investigation may resolve this problem. This would include the assignment and analysis of the remainder of the microwave spectrum.

#### 4. Dipole Moment.

Determination of the dipole moment of maleimide presented some difficulty. The low J, R-branch lines which would generally be used, are very weak in this spectrum and the strong Q-branch lines have complex Stark effects.

Two lines were found which, although of fairly high J, exhibited '0-1' type Stark effects. These are the  $7_{07}-8_{18}$  and  $9_{36}-9_{45}$  transitions. Whether the molecule is planar or not, the  $\mu_c$  Stark effect connections are zero, in the first instance because  $\mu_c$  is zero, and in the second because of inversion tunneling effects. Thus only  $\mu_b$  connections are considered. The Stark coefficients were calculated as detailed in Chapter 2. It was found for

both transitions that the calculated Stark effect was more diffuse than that observed. This discrepancy was traced to non-linearity of the  ${}^8S_{\tau J \tau' J'}$  terms in equation 2.8. with  $\kappa$ . Interpolation in the tables<sup>27</sup> at this value of  $\kappa$  introduced a large degree of error. A subroutine was written for program Asrot which computes second order Stark coefficients directly from the dipole matrix elements. The Stark effect patterns predicted from these calculations showed good agreement with those observed. Table 3.8 lists the  $\mu_b^2 \xi^2$  coefficients and relative intensities for the Stark components of both lines.

Table 3.8.

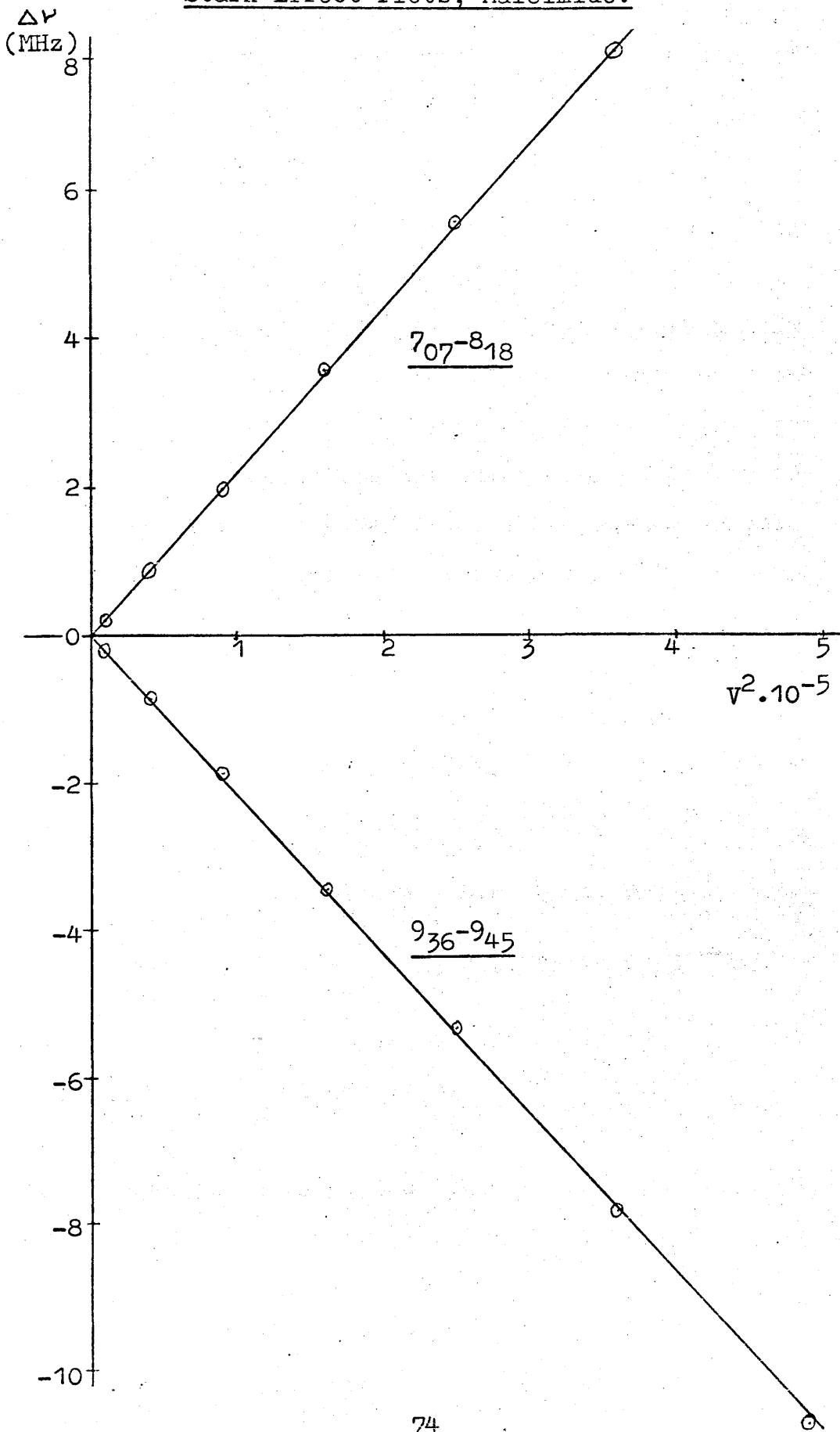
Stark Coefficients, Maleimide.

M	<u>7<sub>07</sub>-8<sub>18</sub></u>		<u>9<sub>36</sub>-9<sub>45</sub></u>	
	$\mu_b^2 \xi^2$ Coefft.	Relative Intensity	$\mu_b^2 \xi^2$ Coefft.	Relative Intensity
0	0.74784.10 <sup>-5</sup>	64	-0.77641.10 <sup>-5</sup>	0
1	0.75095.10 <sup>-5</sup>	63	-0.77602.10 <sup>-5</sup>	1
2	0.76027.10 <sup>-5</sup>	60	-0.77485.10 <sup>-5</sup>	4
3	0.77581.10 <sup>-5</sup>	55	-0.77289.10 <sup>-5</sup>	9
4	0.79756.10 <sup>-5</sup>	48	-0.77017.10 <sup>-5</sup>	16
5	0.82553.10 <sup>-5</sup>	39	-0.76666.10 <sup>-5</sup>	25
6	0.85971.10 <sup>-5</sup>	28	-0.76237.10 <sup>-5</sup>	36
7	0.90011.10 <sup>-5</sup>	15	-0.75730.10 <sup>-5</sup>	49
8	-		-0.75145.10 <sup>-5</sup>	64
9	-		-0.74482.10 <sup>-5</sup>	81
Wtd. Mean	0.78363.10 <sup>-5</sup>		-0.75542.10 <sup>-5</sup>	

The Stark effects were measured as before, the cell being calibrated using the J = 1-2 transition of OCS ( $\mu = 0.71521$  D).<sup>28</sup> Figure 3.4 shows the experimental Stark

Figure 3.4.

Stark Effect Plots, Maleimide.



effect plots for maleimide. The values of  $\mu_b$  obtained from the  $7_{07}-8_{18}$  and  $9_{36}-9_{45}$  transitions are 1.649 and 1.653 D respectively. The uncertainty in these figures may be estimated from the Stark effect plots giving;-

$$\mu_b = 1.65 \pm 0.03 \text{ D.}$$

This value may be compared with that of maleic anhydride, 3.85 D.<sup>21</sup> In both cases the dipole is directed with the negative pole towards the hetero ring atom, due mainly to the carbonyl groups. The difference in magnitude of the dipoles (2.20 D) may be explained by the H-N moment being oppositely directed to the molecular dipole, and by the greater tendency of the N-H fragment to assume a small positive charge. A similar difference (2.50 D) is found between the dipoles of furan, 0.66 D,<sup>29</sup> and pyrrole, 1.84 D,<sup>30</sup> oppositely directed.

#### REFERENCES.

1. R.D. Brown, P.D. Godfrey and J. Storey, J. Mol. Spectroscopy, 1975, 58, 445.
2. D.J. Millen, G. Topping and D.R. Lide, Jr., J. Mol. Spectroscopy, 1962, 8, 153.
3. J.K. Tyler, J. Sheridan and C.C. Costain, J. Mol. Spectroscopy, 1972, 43, 248.
4. J.K. Tyler, J. Mol. Spectroscopy, 1963, 11, 39.
5. R.J. Kurland, J. Chem. Phys., 1955, 23, 2202; R.J. Kurland and E.B. Wilson, Jr., J. Chem. Phys., 1957, 27, 585.
6. C.C. Costain and J.M. Dowling, J. Chem. Phys., 1960, 32, 158.
7. E. Hirota, R. Sugisaki, C.J. Nielsen and G.O. Sorensen, J. Mol. Spectroscopy, 1974, 49, 251.
8. A. Wardley, Unpublished work.
9. T. Woldbaek, P. Klaboer and C.J. Nielsen, J. Mol. Structure, 1975, 27, 283.

10. B. Bak, D. Christensen, L. Hansen and J. Rastrup-Andersen, *J. Chem. Phys.*, 1956, 24, 720.
11. R.L. Hilderbrandt and E.M.A. Peixoto, *J. Mol. Structure*, 1972, 12, 31.
12. J. Wollrab, *Rotational Spectra and Molecular Structure*, Academic Press, London, 1967.
13. T. Oka and Y. Morino, *J. Mol. Spectroscopy*, 1963, 11, 349.
14. D.R. Herschbach and V.W. Laurie, *J. Chem. Phys.*, 1964, 40, 3142.
15. B. Bak, D. Christensen, W.B. Dixon, L. Hansen-Nygaard and J. Rastrup-Andersen, *J. Chem. Phys.*, 1962, 37, 2027.
16. B. Bak, B.P. Van Eijck and C. Kierkegaard, *J. Mol. Structure*, 1973, 18, 429.
17. G.L. Blackman, R.D. Brown, F.R. Burden and A. Mishra, *J. Mol. Spectroscopy*, 1975, 57, 294.
18. B. Bak, L. Hansen-Nygaard and J. Rastrup-Andersen, *J. Mol. Spectroscopy*, 1958, 2, 361.
19. L. Nygaard, D. Christen, J.T. Nielsen, E.J. Pedersen, O. Snerling, E. Vestergaard and G.O. Sorensen, *J. Mol. Structure*, 1974, 22, 401.
20. B. Bak, D. Christensen, L. Hansen-Nygaard and J. Rastrup-Andersen, *J. Chem. Phys.*, 1956, 24, 720.
21. V. Williams, Ph.D. Thesis, University College of North Wales, Bangor, 1969.
22. T. Pedersen, N.W. Larsen and L. Nygaard, *J. Mol. Structure*, 1969, 4, 59.
23. R.K. Kakar, E.A. Rinehart, C.R. Quade and T. Kojima, *J. Chem. Phys.*, 1970, 52, 3803.
24. Y. Hanyu and J.E. Boggs, *J. Chem. Phys.*, 1965, 43, 3454.
25. W.M. Ralowski, P.J. Mjoberg and S.O. Ljungren, *J. Mol. Structure*, 1976, 30, 1.
26. H. Baranska, D.H. Christensen, F.M. Nicolaisen, O.F. Nielsen and P. Klaboe, *Acta Chem. Scand.*, 1971, 25, 2364.
27. *Microwave Spectral Tables, Line Strengths of Asymmetric Rotors*, National Bureau of Standards, Monograph 70, Vol. 2.
28. J.S. Muentzer, *J. Chem. Phys.*, 1968, 48, 4544.

29. M.H. Sirvetz, J. Chem. Phys., 1951, 19, 1609.
30. A.D. Buckingham, B. Harris and R.J.W. LeFevre, J. Chem. Soc., 1953, 1626.

## CHAPTER 4.

# THE EFFECT OF p-HALOGEN SUBSTITUENTS ON THE AMINE GROUP GEOMETRY OF ANILINE; THE MICROWAVE SPECTRUM OF ND<sub>2</sub>-p-FLUOROANILINE.

### 1. Introduction.

Aniline<sup>1</sup> and its p-fluoro<sup>2-5</sup> and p-chloro<sup>6</sup> derivatives have been shown to be non-planar from the large negative values of their inertial defects, the changes in these on N-deuteration, and the presence of strong vibrational satellites in their microwave spectra attributable to the first excited inversion state.

The out of plane angle,  $\phi$ , between the HNH and aryl group planes, has been found to be in the region 33-43° for these molecules, considerably smaller than the tetrahedral value, 54°44'. This is due to participation of the nitrogen lone pair in the molecular  $\pi$ -system. The magnitude of this involvement, and hence of the out of plane angle, is affected by ring substituents via the aryl  $\pi$ -system. Thus determination of  $\phi$  for a series of related molecules allows comparison of the bonding of the various substituents.

The spectra of NH<sub>2</sub>-, NHD- and ND<sub>2</sub>-aniline<sup>1</sup> and p-chloro-aniline,<sup>6</sup> and NH<sub>2</sub>- and NHD-p-fluoroaniline<sup>2-5</sup> have been studied. The spectrum of normal p-fluoroaniline was analysed by MacNeil<sup>2</sup> and the NHD-species by Hastie.<sup>3</sup> Assuming an N-H bond length of 1.00 Å, the out of plane angle was obtained<sup>4</sup> as 46°22'. However, the spectrum of the monodeuterated species was re-examined<sup>5</sup> in view of what appeared to be an anomalously high value of the

ground state inertial defect, ( $-0.718 \text{ amu \AA}^2$ ). Resolution of the ground state and  $V=1$  lines was achieved for some of the rotational transitions, and improved rotational constants were obtained, giving  $\theta=41^\circ 36'$ , which is much closer to the values reported for aniline ( $37^\circ 39'$ )<sup>1</sup> and p-chloroaniline ( $33^\circ 22'$ ).<sup>6</sup>

The present work on the spectrum of  $\text{ND}_2$ -p-fluoroaniline was undertaken in order to complete the data for this series of molecules, thus enabling closer comparison of the amine group geometries.

## 2. Analysis of the Spectrum of $\text{ND}_2$ -p-Fluoroaniline.

The rotational constants of normal p-fluoroaniline<sup>2</sup> and the amino-hydrogen coordinates<sup>5</sup> were used to calculate the rotational constants of the  $\text{ND}_2$ -species. These are as follows;  $A = 5495.0 \text{ MHz}$ ,  $B = 1364.1 \text{ MHz}$  and  $C = 1094.9 \text{ MHz}$ .  $\mu_a$ , R-branch transitions in the 18-26 GHz region were calculated from these constants. Lines expected in this region include the 7-8, 8-9 and 9-10 transitions.

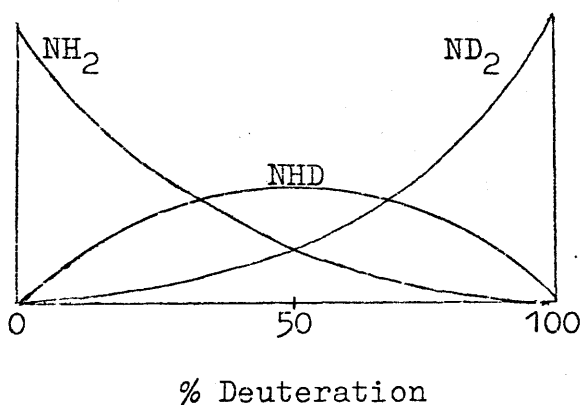
A solution of commercial normal p-fluoroaniline in ether (ca. 1:7 by volume) was treated with dry HCl gas and the hydrochloride thus formed was filtered and dried. 1g of this salt was dissolved in 6 ml of  $\text{D}_2\text{O}$  and, after allowing time to equilibrate, NaOD was added to liberate the free deuterated base. This was extracted into ether, dried over  $\text{MgSO}_4$  and distilled on the vacuum line.

After first allowing a pressure of approximately 0.1 torr to stand in the cell for ca. 15 minutes to fill any active sites for adsorption, the sample vapour was drawn through

the cell. Initial observation of the spectrum showed the predominant species to be the NHD-p-fluoroaniline, indicating that deuteration had not proceeded to the required extent. Generally all three species will be present as shown in figure 4.1. The extent of deuteration in this case was estimated as about 55%. This was found to be just sufficient for observation of the ND<sub>2</sub>-species.

Figure 4.1.

Concentrations of NH<sub>2</sub>-, NHD- and ND<sub>2</sub>-p-Fluoroaniline with respect to Extent of Deuteration.

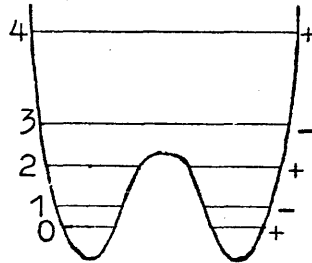


The spectrum was readily assigned, with all lines being found within 6 MHz of prediction. Each transition appeared as a doublet, the components of which correspond to the ground and first excited inversion states. There are two stable configurations which may be assumed by the amino-hydrogens, one on each side of the plane of the benzene ring. The potential energy function of the inversion vibration consists of a well, at the bottom of which there is a barrier. Inversion can occur by a 'tunneling' process through the barrier. If the barrier to inversion is considered to be infinitely high, then the lower energy levels are doubly degenerate. However, for intermediate barriers this degeneracy is lifted, the

splitting increasing as the barrier decreases. As may be seen from figure 4.2, this vibration is strongly anharmonic.

Figure 4.2.

Potential Function for Intermediate Barrier.



The separation in energy between the ground and first excited inversion states is comparatively small and consequently differences in intensity between rotational transitions of these levels due to the Boltzmann distribution is small also. The relative intensities of the two components of a doublet will largely depend on nuclear spin statistical weight effects. There are two pairs of equivalent hydrogen nuclei and one pair of equivalent deuterium nuclei in the molecule. Hence Bose-Einstein statistics apply, the total wave function being symmetric with respect to  $180^\circ$  rotation about the a-axis. The total wave function may be written as a product of electronic, vibrational, rotational and nuclear spin wave functions thus;

$$\Psi_{\text{tot}} = \Psi_e \cdot \Psi_v \cdot \Psi_r \cdot \Psi_n \quad (4.1)$$

For n pairs of equivalent nuclei, the ratio of symmetric to antisymmetric nuclear spin wave functions is given by;

$$n_s : n_a = \left[ \prod_{i=1}^n (2I_i + 1) + 1 \right] : \left[ \prod_{i=1}^n (2I_i + 1) - 1 \right] \quad (4.2)$$

Applying (4.2) to ND<sub>2</sub>-p-fluoroaniline gives  $n_g:n_a = 13:11$ . Thus from (4.1) and (4.2) the following ratios are obtained. For rotational lines with

$$K_{-1} \text{ even, } (V=0):(V=1) = 13:11$$

$$\text{and } K_{-1} \text{ odd, } (V=0):(V=1) = 11:13.$$

It is possible then, to assign components of a doublet by their relative intensities.

All transitions in the observed region of the rotational spectrum could then be assigned and measured. Observed frequencies were fitted by least squares using program Asfit described in Chapter 2. It was found that values for the centrifugal distortion constants were all smaller than their respective standard deviations. The spectrum was accurately described by rigid rotor theory as was found for p-chloroaniline.<sup>6</sup> Table 4.1 gives the measured and calculated transition frequencies for the ground and first excited inversion states, and table 4.2 the respective rotational constants and moments of inertia.

### 3. Calculation of the NH<sub>2</sub>-Group Geometry.

The inertial defect of ND<sub>2</sub>-p-fluoroaniline is consistent with a non-planar configuration at the nitrogen. Since the moments of inertia of the normal, NHD- and ND<sub>2</sub>-species are now known it is possible to carry out calculations of the geometry of the NH<sub>2</sub>-group.

To ensure consistency in the moments of inertia of the three species, the ground state rotational constants of the NH<sub>2</sub>- and NHD-species were calculated from the same fitting procedure used for the ND<sub>2</sub>. These constants and moments of inertia, shown in table 4.3 with those of the

Table 4.1.

Observed and Calculated Transition Frequencies  
of ND<sub>2</sub>-p-Fluoroaniline (MHz).

Transition	<u>V = 0.</u>		<u>V = 1.</u>	
	$\nu_{\text{obs}}$	$\nu_{\text{calc}}$	$\nu_{\text{obs}}$	$\nu_{\text{calc}}$
7 <sub>07</sub> -8 <sub>08</sub>	18787.05	18786.78	18788.50	18788.53
7 <sub>17</sub> -8 <sub>18</sub>	18390.63	18390.47	18392.10	18392.12
7 <sub>16</sub> -8 <sub>17</sub>			20453.25	20453.30
7 <sub>26</sub> -8 <sub>27</sub>	19523.69	19523.60		
7 <sub>25</sub> -8 <sub>26</sub>	20412.36	20411.93		
7 <sub>34</sub> -8 <sub>35</sub>	19878.76	19878.90	19880.14	19880.07
7 <sub>53</sub> -8 <sub>54</sub>	19740.43	19740.44	19741.76	19741.71
7 <sub>52</sub> -8 <sub>53</sub>		19740.49		19741.76
7 <sub>62</sub> -8 <sub>63</sub>				
7 <sub>61</sub> -8 <sub>62</sub>	19726.62	19726.20		
8 <sub>08</sub> -9 <sub>09</sub>	20965.71	20965.56	20967.30	20967.56
8 <sub>18</sub> -9 <sub>19</sub>	20637.01	20636.98	20638.91	20638.86
8 <sub>17</sub> -9 <sub>18</sub>	22893.85	22894.71	22896.29	22896.24
8 <sub>27</sub> -9 <sub>28</sub>	21911.52	21911.51		
8 <sub>26</sub> -9 <sub>27</sub>	23076.68	23076.62	23077.62	23077.71
8 <sub>36</sub> -9 <sub>37</sub>	22272.22	22272.12	22273.51	22273.54
8 <sub>35</sub> -9 <sub>36</sub>	22436.70	22436.83	22438.10	22438.10
8 <sub>45</sub> -9 <sub>46</sub>	22257.10	22257.16		
8 <sub>44</sub> -9 <sub>45</sub>	22264.02	22264.38		
8 <sub>54</sub> -9 <sub>55</sub>	22221.62	22221.54	22223.02	22222.97
8 <sub>53</sub> -9 <sub>54</sub>		22221.69		22223.11
8 <sub>63</sub> -9 <sub>64</sub>	22201.32	22201.27		
8 <sub>62</sub> -9 <sub>63</sub>				
9 <sub>09</sub> -10 <sub>10</sub>	23131.92	23131.76	23133.93	23134.00

Table 4.1 contd.

Transition	<u>V = 0.</u>		<u>V = 1.</u>	
	$\nu_{\text{obs}}$	$\nu_{\text{calc}}$	$\nu_{\text{obs}}$	$\nu_{\text{calc}}$
$9_{19}-10_{110}$	22871.90	22872.07	22874.27	22874.18
$9_{18}-10_{19}$	25290.22	25289.84	25291.71	25291.63
$9_{28}-10_{29}$	24282.07	24281.98	24283.84	24283.80
$9_{37}-10_{38}$		24754.26		24755.85
	24754.29		24755.72	
$9_{46}-10_{47}$		24753.93		24755.48
$9_{36}-10_{37}$	25027.83	25027.86	25029.08	25029.19
$9_{45}-10_{46}$	24769.27	24769.43		
$9_{55}-10_{56}$		24707.40		24708.97
	24707.63		24709.25	
$9_{54}-10_{55}$		24707.81		24709.38
$9_{64}-10_{65}$	24679.80	24679.63	24681.15	24681.22
$9_{63}-10_{64}$				
$9_{82}-10_{83}$	24652.54	24652.62		
$9_{81}-10_{82}$				
$9_{91}-10_{92}$	24645.01	24645.45		
$9_{90}-10_{91}$				
$10_{010}-11_{011}$	25294.61	25294.60	25297.18	25297.06
$10_{110}-11_{111}$	25096.83	25097.20	25099.52	25099.54

Table 4.2.

Rotational Constants (MHz), and Moments of Inertia  
(amu Å<sup>2</sup>), of ND<sub>2</sub>-p-Fluoroaniline.

	<u>V = 0.</u>	<u>V = 1.</u>
A	5494.14 ± 0.93	5494.99 ± 0.39
B	1364.471 ± 0.011	1364.544 ± 0.005
C	1095.294 ± 0.010	1095.404 ± 0.004
I <sub>a</sub>	91.984	91.9703
I <sub>b</sub>	370.3824	370.3680
I <sub>c</sub>	461.4067	461.3604
Δ	-0.9602	-0.9779

Table 4.3.

Rotational Constants (MHz), and Moments of Inertia  
(amu Å<sup>2</sup>) of NH<sub>2</sub>-, NHD- and ND<sub>2</sub>-p-Fluoroaniline.

	p-Fluoroaniline	NHD-p-F-aniline	ND <sub>2</sub> -p-F-aniline
A	5594.20	5546.79	5494.14
B	1449.124	1405.033	1364.471
C	1152.162	1122.731	1095.294
I <sub>a</sub>	90.3393	91.1114	91.9846
I <sub>b</sub>	348.7459	359.6898	370.3824
I <sub>c</sub>	438.6328	450.1310	461.4067
Δ	-0.4524	-0.6702	-0.9602

ND<sub>2</sub>-species, are in good agreement with the previous values.<sup>2,5</sup> The magnitude of the inertial defect and its behaviour on deuteration are indicative of a planar FC<sub>6</sub>H<sub>4</sub>N fragment with the two amino-hydrogens out of the plane.

From the moments of inertia of the NH<sub>2</sub>- and NHD-species, the amino-hydrogen coordinates are located by Kraitchman's equations for a non-planar molecule;

$$a^2 = \frac{1}{2\mu} (\Delta I_b + \Delta I_c - \Delta I_a) \left[ 1 + \frac{\Delta I_a + \Delta I_b - \Delta I_c}{2(I_a - I_c)} \right] \left[ 1 + \frac{\Delta I_c + \Delta I_a - \Delta I_b}{2(I_a - I_b)} \right] \quad \dots(4.3)$$

The corresponding expressions for b<sup>2</sup> and c<sup>2</sup> are obtained by cyclic permutation of the subscripts. These coordinates can also be derived from the moments of inertia of normal and ND<sub>2</sub>-p-fluoroaniline. The a and c coordinates are obtained by using the parameters Δ'I<sub>a</sub> and Δ'I<sub>c</sub> (defined below) in Kraitchman's equations for a planar asymmetric rotor, where b is found from the relation;

$$b^2 = \frac{1}{4\Delta m} (\Delta I_a + \Delta I_c - \Delta I_b).$$

$$\Delta' I_a = \Delta I_a - 2\Delta m b^2$$

$$\Delta' I_c = \Delta I_c - 2\Delta m b^2$$

where Δm = m<sub>D</sub> - m<sub>H</sub>.

Coordinates of the amino-hydrogen atoms from the two methods are shown in table 4.4. The a- and b-coordinates

Table 4.4.

Amino-Hydrogen Coordinates, p-Fluoroaniline (Å).

	<u>a</u>	<u>b</u>	<u>c</u>
NH <sub>2</sub> /NHD	3.2913	±0.8315	0.3380
NH <sub>2</sub> /ND <sub>2</sub>	3.2876	±0.8317	0.3696

show the expected variation arising from zero-point vibrational effects. However the error in the c-coordinate, and consequently the out of plane angle, is much larger. This results from the fact that the  $(\Delta I_a + \Delta I_b - \Delta I_c)$  term in equations 4.3 is very small, ca.  $0.2 \text{ amu } \text{\AA}^2$ .

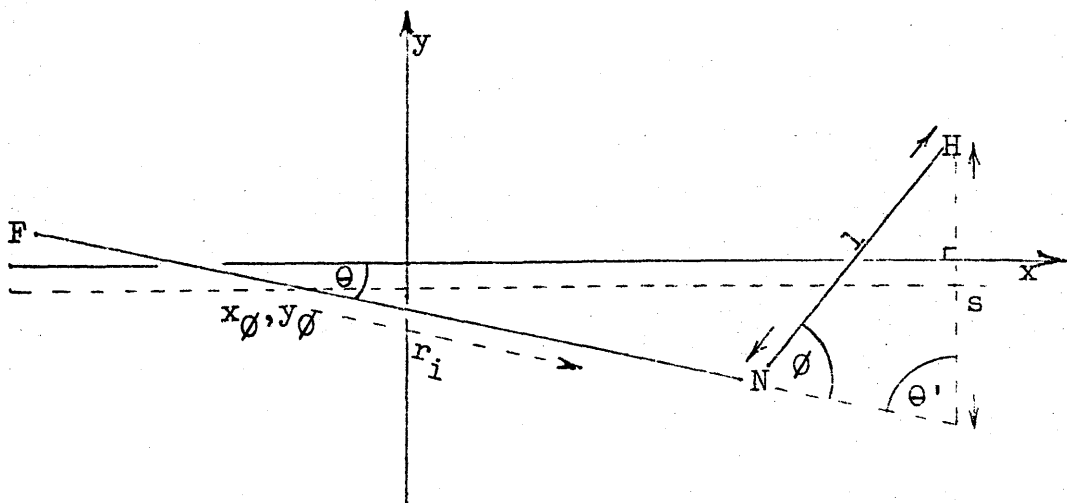
The c-coordinate may be calculated from the inertial defects of the  $\text{NH}_2$ - and  $\text{ND}_2$ -species, taking the a- and b-coordinates from Kraitchman's equations. The inertial defect of a planar ring compound is generally about  $+ 0.05 \text{ amu } \text{\AA}^2$ , the effects of the in-plane and out of plane vibrations almost cancelling. For examples of this see table 3.7. Although there will be a significant negative contribution from the inversion vibration, the inertial defect may be written, to a first approximation as;

$$\Delta = 2 \sum_i m_i y_i^2 + 4m_{\text{H}} y_{\text{H}}^2 \quad (4.4)$$

The notation for equation 4.4 and the following argument is defined in figure 4.3. The angle between the plane of

Figure 4.3.

$\text{NH}_2$ -Group Geometry.



the ring and the x-axis,  $\theta$ , can be expressed as;

$$\theta = \sin^{-1} \frac{2m_H x_H y_H (1 + \frac{2m_H}{M_\emptyset})}{I_b'} \quad (4.5)$$

where  $m_H$  is the mass of the H (or D) atom,

$x_H, y_H$  are coordinates of the amino-hydrogens relative to the a- and c-axes respectively,

$M_\emptyset$  is the mass of the  $FC_6H_4N$  fragment,  $x_\emptyset, y_\emptyset$  being the coordinates of its centre of gravity,

and  $I_b' = I_b + \mu(x_H^2 + y_H^2)$  where  $\mu = \frac{M(-2m_H)}{M-2m_H}$

The y-coordinate of any atom in the plane is given by;

$$y_i = y_\emptyset - r_i \sin\theta.$$

Squaring both sides and summing over the respective nuclear masses, one obtains;

$$\sum_i m_i y_i^2 = M_\emptyset y_\emptyset^2 + I_b' \sin^2\theta \quad (4.6)$$

Combining 4.5 and 4.6,

$$\sum_i m_i y_i^2 = 4m_H y_H^2 \left[ \frac{1}{M_\emptyset} + \frac{x_H^2 (1 + \frac{2m_H}{M_\emptyset})^2}{I_b'} \right] \quad (4.7)$$

Thus the c-coordinate ( $y_H$ ) can be found by solution of equations 4.4 and 4.7.

The out of plane angle,  $\emptyset$ , and the HNH angle may be obtained if the N-H bond length is taken to be 1.00 Å. This should be a good estimate as this parameter in aniline was reported<sup>1</sup> as 1.001 Å. The length of the HNH bisector,  $l$  in figure 4.3, and the HNH angle are then easily calculated from the b-coordinate. The distance  $s$  may be expressed as;

$$s = (y_H - y_\emptyset) + (x_H - x_\emptyset) \tan\theta,$$

which allows  $\emptyset$  to be calculated from;

$$\sin \emptyset = \frac{s \cdot \sin\theta'}{l}.$$

Since good agreement was found for the a- and b-coordinates from the  $\text{NH}_2/\text{NHD}$  and the  $\text{NH}_2/\text{ND}_2$  Kraitchman calculations, selection of which to use in evaluation of the c-coordinate is unimportant. The  $\text{NH}_2/\text{ND}_2$  coordinates were used throughout. The c-coordinates and amino-group geometries from the  $\text{NH}_2$ - and  $\text{ND}_2$ -species' inertial defects are presented in table 4.5. These are discussed

Table 4.5.

Amino-Group Geometry, p-Fluorocaniline.

	<u>c</u>	<u>∅</u>	<u>HNH</u>
From $\text{NH}_2$	0.3213	$38^\circ 59'$	$112^\circ 30'$
From $\text{ND}_2$	0.3184	$42^\circ 21'$	$112^\circ 30'$

in relation to the corresponding parameters in aniline and p-chloroaniline in the next section. The inertial defect of the  $\text{FC}_6\text{H}_4\text{N}$  fragment was calculated from the  $\text{ND}_2$  coordinates as  $0.0006 \text{ amu } \text{\AA}^2$ , which is good evidence for its planarity.

4. The Configuration of the Amine Group in Aniline and its p-Fluoro- and p-Chloro-Derivatives.

The object of comparison of the amino-group geometries in these molecules was to examine the effects of halogen substituents on the electronic configuration of the aryl and amine groups. The spectra of aniline, p-chloroaniline and their deuterated species were analysed as described in section 2 to maintain consistency and to resolve the apparent discrepancy between the reported out of plane angles from  $\text{NH}_2$ - and  $\text{ND}_2$ -p-chloroaniline,  $33^\circ 22'$  and  $39^\circ 12'$  respectively.<sup>6</sup> The recalculated rotational constants (table 4.6) are in good agreement with the pre-

Table 4.6.

Rotational Constants (MHz) and Inertial Defects (amu Å<sup>2</sup>)  
of Aniline and p-Chloroaniline.

		<u>A</u>	<u>B</u>	<u>C</u>	<u>Δ</u>
$C_6H_5-NH_2$	V=0	5617.4	2593.83	1777.04	-0.4119
	V=1	5615.6	2592.24	1776.73	-0.5106
-NHD	V=0	5572.0	2493.60	1726.10	-0.5836
	V=1	5569.2	2492.90	1726.28	-0.7166
-ND <sub>2</sub>	V=0,1	5519.7	2403.75	1679.04	-0.8124
$ClC_6H_4-NH_2$	V=0	5600.4	975.327	831.250	-0.4287
	V=1	5598.8	975.131	831.202	-0.5235
-NHD	V=0	5554.7	949.464	811.618	-0.5796
	V=1	5551.3	949.409	811.689	-0.6714
-ND <sub>2</sub>	V=0	5503.5	925.387	793.213	-0.8268
	V=1	5502.1	925.448	793.310	-0.8921

viously reported values.

Nuclear coordinates from Kraitchman's equations are shown in table 4.7 and amino-group geometries from the NH<sub>2</sub>- and ND<sub>2</sub>-species' inertial defects in table 4.8. The differences in the c-coordinates of the NH<sub>2</sub>- and ND<sub>2</sub>-species of each molecule calculated from the inertial defects are partly due to the fact that they refer to different axis systems. The angles may be compared directly, as they are independent of the location of the centre of mass.

The out of plane angles of aniline and its p-fluoro- and p-chloro-derivatives show a marked difference from the tetrahedral value, indicating significant involvement of the nitrogen lone pair in the π-electron system of each molecule. The fluorine derivative has a slightly larger

Table 4.7.

Nuclear Coordinates of Aniline, p-Fluoro-  
and p-Chloroaniline by Kraitchman's Method (Å).

		<u>a</u>	<u>b</u>	<u>c</u>
Aniline	NH <sub>2</sub> /NHD	2.7800	±0.8355	0.3013
	NH <sub>2</sub> /ND <sub>2</sub>	2.7770	±0.8317	0.3307
p-Fluoroaniline	NH <sub>2</sub> /NHD	3.2913	±0.8315	0.3380
	NH <sub>2</sub> /ND <sub>2</sub>	3.2876	±0.8317	0.3696
p-Chloroaniline	NH <sub>2</sub> /NHD	3.7467	±0.8302	0.2793
	NH <sub>2</sub> /ND <sub>2</sub>	3.7428	±0.8309	0.3252

Table 4.8.

Amino-Group Geometries, Aniline, p-Fluoro- & p-Chloro-  
Aniline from Inertial Defects.

	<u>c(Å)</u>	<u>∅</u>	HNH
C <sub>6</sub> H <sub>5</sub> -NH <sub>2</sub>	0.3028	37°23'	112°34'
-ND <sub>2</sub>	0.2865	39°16'	
FC <sub>6</sub> H <sub>4</sub> -NH <sub>2</sub>	0.3213	38°59'	112°30'
-ND <sub>2</sub>	0.3184	42°21'	
ClC <sub>6</sub> H <sub>4</sub> -NH <sub>2</sub>	0.3144	37°26'	112°24'
-ND <sub>2</sub>	0.2985	38°09'	

out of plane angle than the other two molecules, which are equal within experimental error. The uncertainty in  $\phi$  was estimated as  $\pm 2^\circ$  from the scatter in the values of the c-coordinates. However, this may be an over-estimate of the precision of these angles. For molecules in which large amplitude vibrations occur, rigid rotor theory, and in particular, application of ground state moments of inertia to solution of structures, may lead to erroneous results.<sup>7</sup> Interaction between the inversion vibration and the molecular rotation makes an appreciable contribution to the effective rotational constants. Zero-point effects in this vibration account for the observed differences between the  $\text{NH}_2$  and  $\text{ND}_2$  determinations of  $\phi$ . Information on the inversion potential function is required before detailed comparison can be made.

Changes in out of plane angles of substituted anilines due to ring substituents may be rationalised in terms of competing mesomeric and inductive effects. The geometry of the amine group in anilines is dependent on the extent of participation of the nitrogen lone pair in the molecular  $\pi$ -system. Consequently the amino-group configuration will be most affected by the mesomeric interaction of a ring substituent. Apparently the small mesomeric interaction of the chlorine, which will tend to increase  $\phi$ , is counterbalanced by the considerably larger inductive effect which will tend to facilitate electron donation from the nitrogen with resultant decrease in  $\phi$ . In p-fluoroaniline the mesomeric interaction is slightly larger, accounting for the higher value of  $\phi$ .

## REFERENCES.

1. D.G. Lister, Ph.D. Thesis, University of Glasgow, 1968.
2. R.L. MacNeil, B.Sc. Thesis, University of Glasgow, 1968.
3. A. Hastie, B.Sc. Thesis, University of Glasgow, 1969.
4. A. Hastie, D.G. Lister, R.L. MacNeil and J.K. Tyler, J. Chem. Soc., D, 1970, 108.
5. C.I. Carle, B.Sc. Thesis, University of Glasgow, 1972.
6. S.A. Mackay, Ph.D. Thesis, University of Glasgow, 1971.
7. D.R. Lide, Jr., J. Mol. Spectroscopy, 1962, 8, 142.

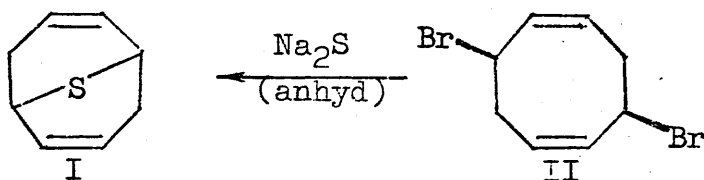
## CHAPTER 5.

### THE MICROWAVE SPECTRUM OF

### 9-THIABICYCLO [3,3,1] NONA-2,6-DIENE.

#### 1. Introduction.

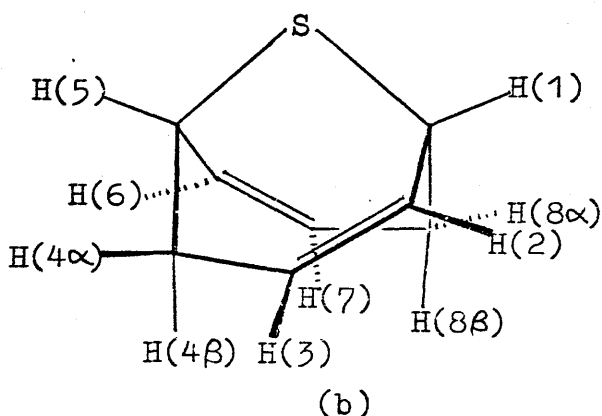
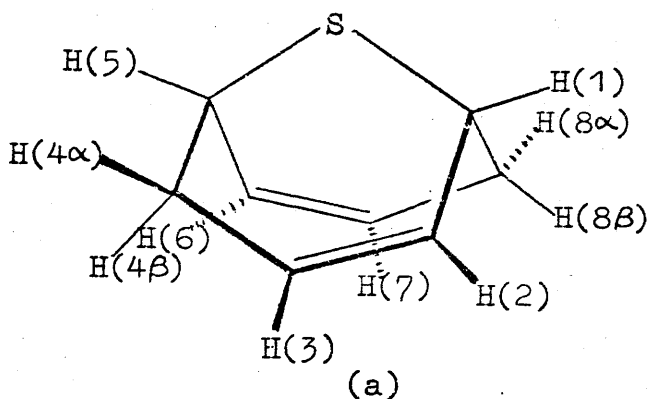
9-Thiabicyclo [3,3,1] nona-2,6-diene (I) was prepared from reaction of (Z,Z)-cis-3,7-dibromocyclo-octa-1,5-diene (II) and anhydrous sodium sulphide, as one of a series of [3,3,1] bicyclic compounds, most of which contained a hetero-atom bridge.



The structure I was assigned to the product of this reaction on the basis of its reduction to the known 9-thiabicyclo [3,3,1] non-2-ene, formation of a single sulphoxide, and its mass spectrum. In addition, a detailed computer analysis of the high resolution n.m.r. spectrum has been carried out.<sup>2</sup> Consideration of Dreiding models led to the conclusion that the molecule was likely to exist in a boat conformation in which facile ring flexing could occur. Dihedral angles for various pairs of protons were calculated from observed coupling constants using a Karplus-type relationship ( $J_{vic} = a + b\cos\theta + c\cos 2\theta$ ). These were compared with angles estimated from models of two possible conformations, one extreme and one intermediate position in the ring twisting vibration. These conformations are illustrated in figure 5.1. The observed coupling constant for H(3), H(4 $\alpha$ ) is +2.0 Hz, giving an

Figure 5.1.

Conformation of 9-Thiabicyclo[3,3,1] nona-2,6-diene.



approximate dihedral angle of  $65^\circ$  or  $110^\circ$  from the Karplus relation, which is then compared with estimated angles of  $65^\circ$  and  $30^\circ$  from models (a) and (b) respectively. The other coupling constants are consistent with this finding that (a) is the predominant conformation in solution.<sup>2</sup>

This microwave investigation of 9-thiabicyclo[3,3,1] nona-2,6-diene was undertaken to supplement the information from the n.m.r. analysis. The rotational spectrum has been analysed and an approximate determination of the ring flexing vibration frequency has been made from intensity comparisons of excited state lines. A more detailed study, including measurement of the dipole moment was precluded by the weakness of the spectrum.

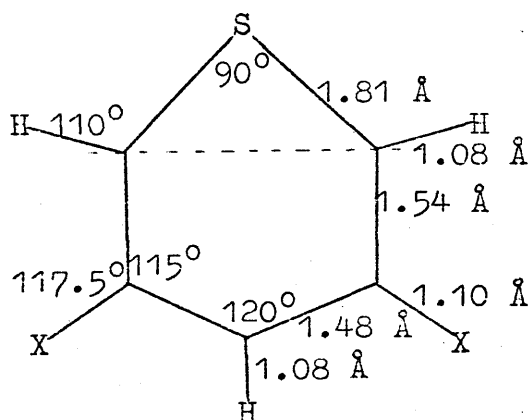
## 2. Observation and Analysis of the Spectrum.

9-Thiabicyclo[3,3,1]nona-2,6-diene is a pale yellow waxy solid at room temperature, with easily sufficient vapour pressure for observation by microwave spectroscopy. The pure compound is stable and crystallises in prisms (m.p. 41-41.5°C).<sup>1</sup> A pressure of approximately 0.2 torr was allowed to stand in the cell for a few minutes to deactivate sites for adsorption, before admitting doses from the vacuum line.

The spectrum was predicted from the  $C_{2v}$  model shown in figure 5.2, in which X refers to a hypothetical species

Figure 5.2.

### Model for Prediction of Spectrum.



of mass 1.5 amu, introduced to give a plane of symmetry to the model. All nuclei, except H(1), H(5) and S, occupy two planes, the angle between which is  $110^\circ$ . The moments of inertia and rotational constants obtained are as follows;  $I_a = 282.0$ ,  $I_b = 322.7$ , and  $I_c = 335.7$  amu  $\text{\AA}^2$ , and  $A = 1792$ ,  $B = 1566$  and  $C = 1505$  MHz. ( $\kappa = -0.58$ ). The a-axis is that principal axis which, in the model, runs parallel to a line connecting C(3) and C(7). In the molecule this axis is slightly removed from this position

due to the absence of the plane of symmetry. It is not, however, readily ascertained which of the b- and c-axes corresponds to the  $C_2$  axis, along which must lie the dipole moment. The model predicts this to be the c-axis, but due to its inherent approximations, it cannot safely be used to discriminate between two moments which are different by only ca. 4%. Consequently, it is necessary to predict the spectrum for both possible cases.

Both  $\mu_b$ - and  $\mu_c$ -type spectra were predicted from the rigid rotor expression;

$$\nu = (J + 1)(A + C) + \frac{A-C}{2} \Delta E(\kappa). \quad (5.1)$$

The spectra are similar, with most of the  $J = 8-9$  transitions being predicted in the 29-32 GHz region in each case. Figure 5.3 shows the  $\mu_b$ - and  $\mu_c$ -,  $J = 8-9$  transitions as  $\Delta E(\kappa)$ , taking  $\kappa$  as  $-0.60$ . The principal difference between the two predictions is that there are rather more lines in the  $\mu_b$ -type spectrum, particularly to low frequency.

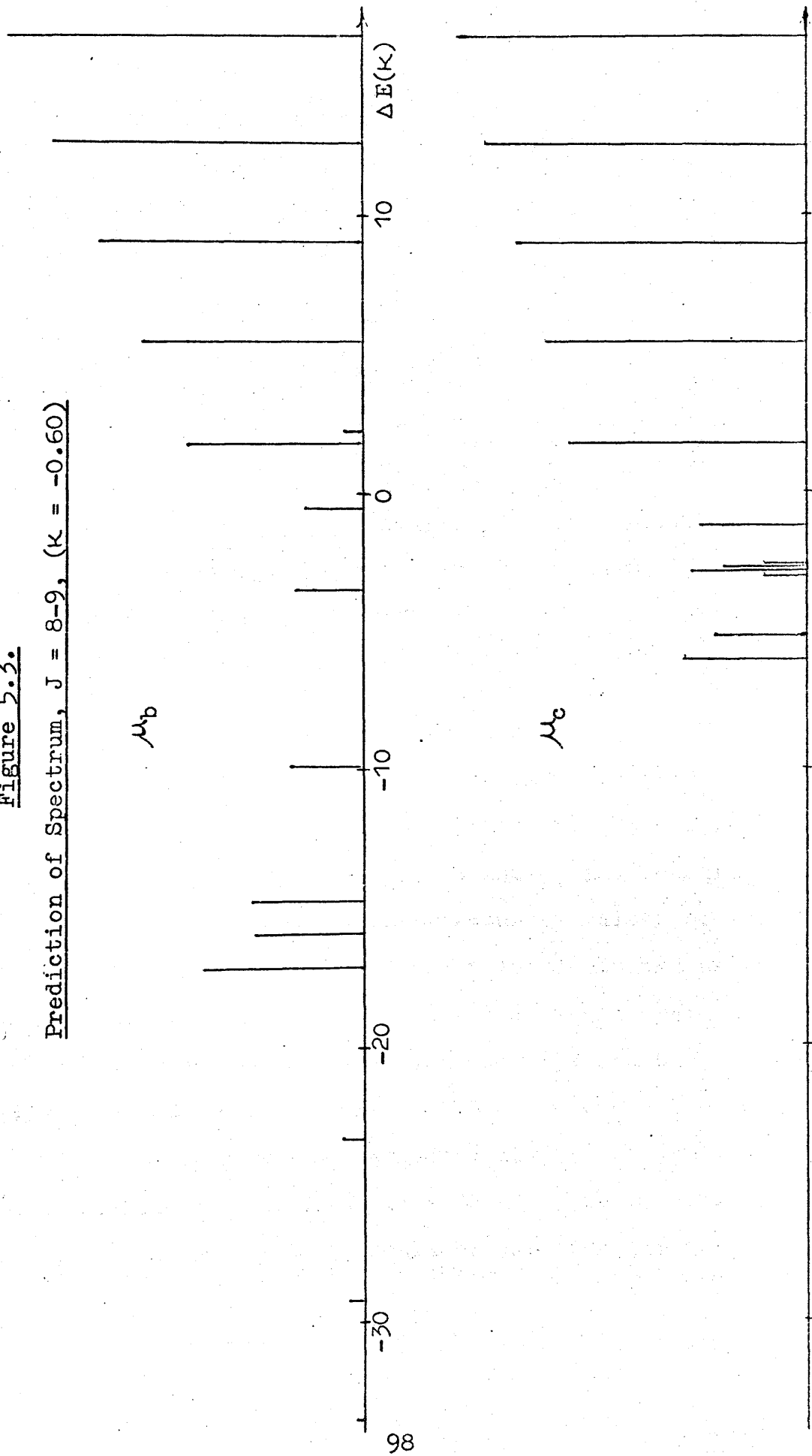
Good correlation was found between the observed, and  $\mu_c$ -predicted patterns. The  $\mu_b$  case was eliminated as several of its predicted lines were not found in the observed spectrum. It was possible to assign some lines from their  $\mu_c$  predictions. To verify these assignments and to improve the rotational constants, an R-branch plot was constructed. From (5.1) the difference in frequency between two R-branch lines of the same  $J$  is given by;

$$\Delta\nu = \frac{A-C}{2} \Delta(\Delta E(\kappa)).$$

Using the measured frequencies of assigned lines, values of  $\frac{A-C}{2}$  may be derived for each pair of lines over sev-

Figure 5.3.

Prediction of Spectrum,  $J = 8-9$ , ( $\kappa = -0.60$ )



eral different values of  $\kappa$ . Provided the assignments are correct, plots of  $\frac{A-C}{2}$  against  $\Delta(\Delta E(\kappa))$  for various pairs of transitions will intersect at one point. The R-branch plot is presented in figure 5.4, the notation for each line in the plot being explained in table 5.1.

Table 5.1.

Notation for R-branch Plot.

Line	Transitions	Frequency Difference
a	(8 <sub>80</sub> -9 <sub>90</sub> ) - (8 <sub>71</sub> -9 <sub>81</sub> )	568.07 MHz
b	(8 <sub>71</sub> -9 <sub>81</sub> ) - (8 <sub>62</sub> -9 <sub>72</sub> )	568.69 "
c	(8 <sub>45</sub> -9 <sub>55</sub> ) - (8 <sub>36</sub> -9 <sub>46</sub> )	495.70 "
d	(8 <sub>54</sub> -9 <sub>64</sub> ) - (8 <sub>36</sub> -9 <sub>46</sub> )	1061.51 "
e	(8 <sub>36</sub> -9 <sub>46</sub> ) - (8 <sub>35</sub> -9 <sub>45</sub> )	224.84 "
f	(8 <sub>27</sub> -9 <sub>37</sub> ) - (8 <sub>26</sub> -9 <sub>36</sub> )	513.11 "

The good intersection of the R-branch plot verifies that the dipole moment is on the c-axis. Improved values of  $\frac{A-C}{2}$  and  $\kappa$  were obtained as 157.45 MHz and -0.6262 respectively. It was then possible to assign and measure a large number of R-branch lines. Accurate values of the rotational constants were found by least squares using program Asfit, described in Chapter 2. These are;  $A = 1848.357 \pm 0.008$ ,  $B = 1592.288 \pm 0.011$  and  $C = 1533.427 \pm 0.019$  MHz with  $\kappa = -0.626139$ , where the uncertainties shown are one standard deviation. Centrifugal distortion constants were found to be very small and poorly determined, as would be expected for this type of molecule. Table 5.2 gives measured and calculated transition frequencies of 9-thiabicyclo[3,3,1]nona-2,6-diene.

Figure 5.4.

R-Branch Plot.

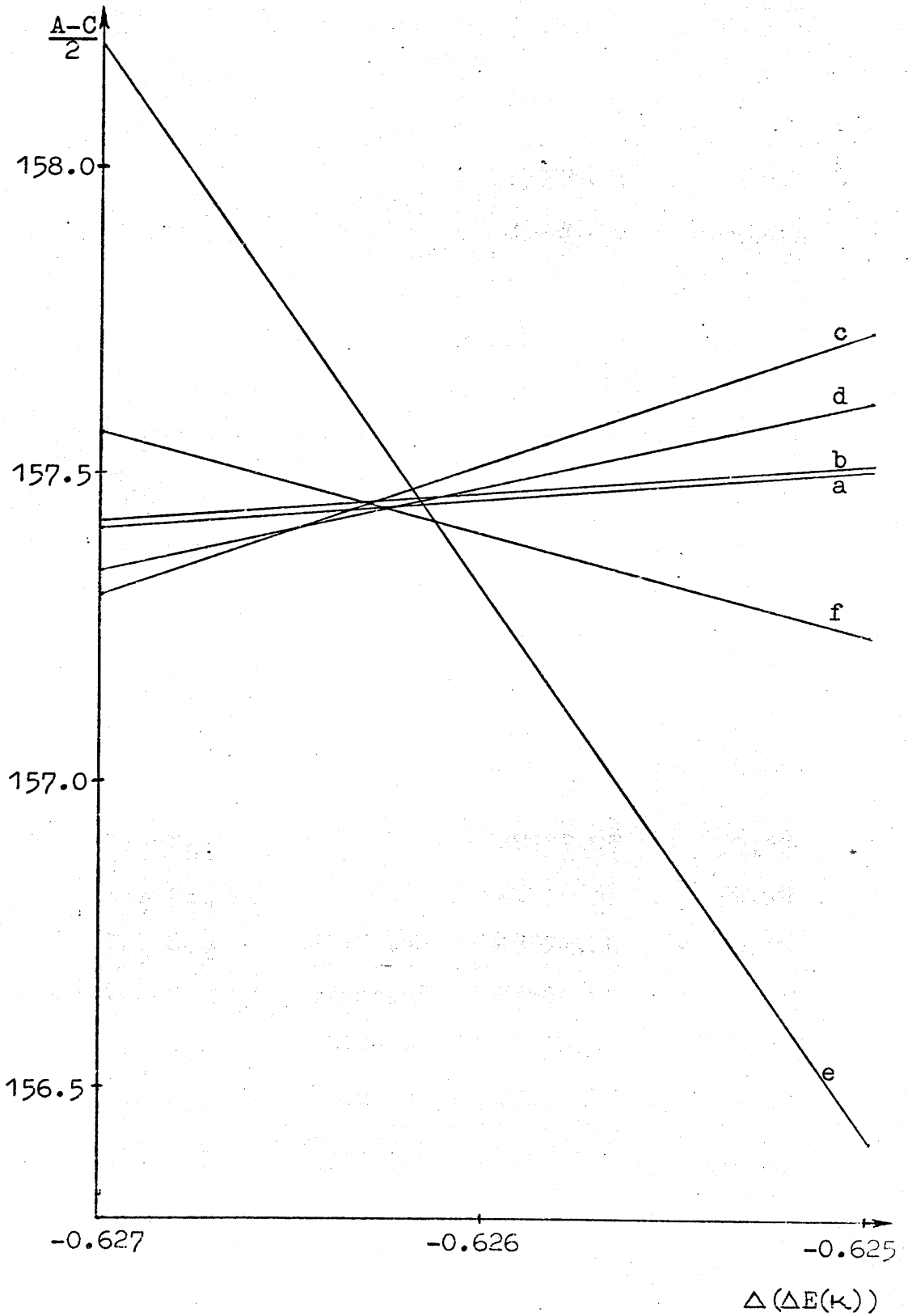


Table 5.2.

Observed and Calculated Transition Frequencies  
of 9-Thiabicyclo [3,3,1] nona-2,6-diene, (MHz).

Transition	$\nu_{\text{obs}}$	$\nu_{\text{calc}}$	$\nu_{\text{obs}} - \nu_{\text{calc}}$
$6_{60} - 7_{70}$	25592.78	25592.83	-0.05
$6_{61} - 7_{71}$			
$6_{51} - 7_{61}$	25024.57	25024.53	0.04
$6_{52} - 7_{62}$		25024.58	-0.01
$6_{42} - 7_{52}$	24453.18	24453.21	-0.03
$6_{43} - 7_{53}$	24455.98	24455.98	0.00
$6_{33} - 7_{43}$	23848.02	23848.08	-0.06
$6_{34} - 7_{44}$	23904.28	23904.36	-0.08
$6_{24} - 7_{34}$	23171.77	23171.70	0.07
$6_{25} - 7_{35}$	23479.31	23479.42	-0.11
$6_{15} - 7_{25}$	22878.01	22877.98	0.03
$7_{70} - 8_{80}$	29289.57	29289.48	0.09
$7_{71} - 8_{81}$			
$7_{61} - 8_{71}$	28721.35	28721.31	0.04
$7_{62} - 8_{72}$			
$7_{52} - 8_{62}$	28152.16	28152.05	0.11
$7_{53} - 8_{63}$		28152.35	-0.19
$7_{43} - 8_{53}$	27574.42	27574.26	0.15
$7_{44} - 8_{54}$	27583.95	27583.94	0.01
$7_{34} - 8_{44}$	26929.98	26930.00	-0.02
$7_{35} - 8_{45}$	27053.34	27053.27	0.07
$7_{25} - 8_{35}$	26282.55	26282.61	-0.06
$7_{26} - 8_{36}$	26702.07	26702.06	0.01
$7_{16} - 8_{26}$	26168.12	26168.03	0.09

contd.

Table 5.2, contd.

Transition	$\nu_{\text{obs}}$	$\nu_{\text{calc}}$	$\nu_{\text{obs}} - \nu_{\text{calc}}$
$8_{80} - 9_{90}$	32986.05	32986.09	-0.04
$8_{81} - 9_{91}$			
$8_{71} - 9_{81}$	32417.98	32417.99	-0.01
$8_{72} - 9_{82}$			
$8_{62} - 9_{72}$	31849.29	31849.27	0.02
$8_{63} - 9_{73}$		31849.30	-0.01
$8_{53} - 9_{63}$	31277.85	31277.82	0.03
$8_{54} - 9_{64}$	31279.02	31279.09	-0.07
$8_{45} - 9_{55}$	30713.21	30713.17	0.04
$8_{35} - 9_{45}$	29992.67	29992.63	0.04
$8_{36} - 9_{46}$	30217.51	30217.56	-0.05
$8_{26} - 9_{36}$	29437.00	29437.02	-0.02
$8_{27} - 9_{37}$	29950.11	29950.13	-0.02
$8_{17} - 9_{27}$	29509.17	29509.19	-0.02

### 3. General Conclusions.

The microwave spectrum of this molecule is consistent with the structure I. It is difficult to carry out a more detailed investigation in view of the weakness of the spectrum and the size of the molecule. It is not possible to distinguish between the conformational isomers (5.1 a) and (5.1 b) as the two sets of rotational constants will be very similar in magnitude.

The lack of intensity of spectral lines stems from three factors; it is a reasonably heavy molecule for microwave work, with a large number of rotational levels occupied at ambient temperatures; it has a low dipole moment, probably around 0.6 D; there is a low frequency vibration, several excited states of which are significantly populated.

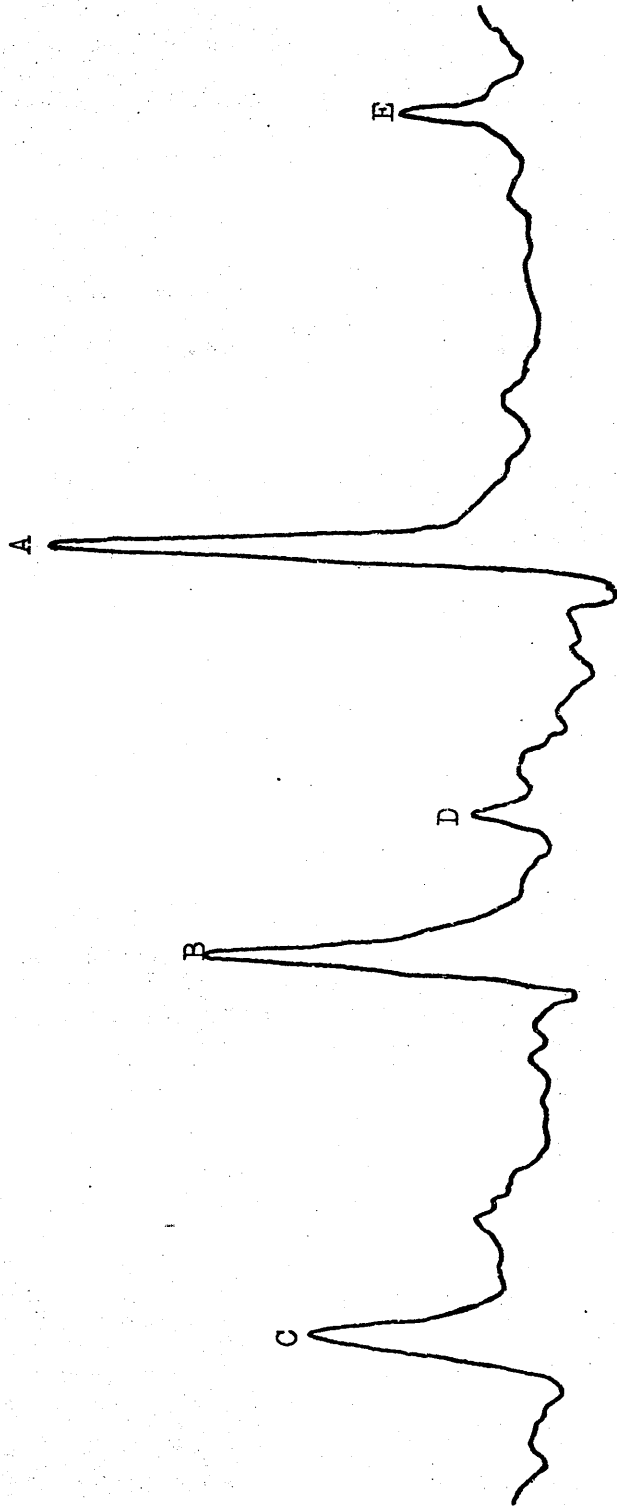
An attempt was made to measure the dipole moment. The problems in measurement of the dipole of maleimide (Chapter 3.4) are encountered again here. Stark effects at J values greater than 5 tend to be complex and diffuse. This problem was resolved in the case of maleimide by measuring '0-1' type Stark effects of two transitions. No lines with Stark effects of this kind were found in this spectrum.

It is evident from the rotational spectrum that there is one vibration of considerably lower energy than the others. This is almost certainly the ring flexing vibration mentioned earlier. Figure 5.5 shows the ground state line due to the coincident  $770-880$  and  $771-881$  transitions, and its vibrational satellites. The differ-

Figure 5.5.

Ground State Line and Vibrational Satellites

of  $(Z_{70-80} + Z_{71-81})$  at 298 K.



ences in energy between the various vibrational levels may be obtained from their relative intensities according to the Boltzmann distribution, e.g.,

$$n_A : n_B = \exp\left(\frac{-\Delta E}{kT}\right).$$

The lowest frequency vibration is determined as 86 and 87  $\text{cm}^{-1}$  from the A:B and B:C ratios, respectively. The other vibrations which have significant excited state populations (peaks D and E) have energies of 308 and 392  $\text{cm}^{-1}$  relative to the ground state. It is difficult to conceive of another assignment for the low energy vibration apart from the ring flexing mode. It seems most likely that the equilibrium conformation of the molecule is that illustrated in figure 5.1(a). The flexing vibration is near-harmonic, and it is unlikely that it will involve amplitudes as large as that suggested by figure 5.1(b).

#### REFERENCES.

1. E. Cuthbertson and D.D. MacNicol, J. Chem. Soc., Perkin I, 1974, 1893.
2. E. Cuthbertson, Ph.D. Thesis, University of Glasgow, 1974.

## CHAPTER 6.

### APPLICATION OF MICROWAVE SPECTROSCOPY TO ANALYSIS OF DEUTEROPROPENE MIXTURES FORMED BY HETEROGENEOUS CATALYSIS.

#### 1. Introduction.

Microwave spectroscopy has an important application in the elucidation of mechanisms of catalytic exchange reactions by locating deuterium atom positions in reaction products. This technique was first applied by Hirota, Hironaka and Hirota<sup>1</sup> to study the exchange of propene with  $D_2O$  on metal catalysts. Use of microwave spectroscopy in investigation of mechanisms of reactions by heterogeneous catalysis has been reviewed by Hirota<sup>2</sup> and Tamaru.<sup>3</sup>

Deuterium has long been utilised as a tracer in mechanistic studies of surface-catalysed reactions.<sup>2</sup> Initially, only the total number of deuterium atoms in a reaction product was obtainable from mass spectrometric analysis. More recently, this technique has been used to locate deuterated positions in molecules, but this procedure is inaccurate due to uncertainties about isotope effects on fragmentation patterns.<sup>4</sup> Infra-red spectroscopy has been applied to analysis of deuterated olefin mixtures in conjunction with mass spectrometry, but this is generally limited to qualitative analysis as there is a high probability of overlap of key bands.<sup>5</sup> Nuclear magnetic resonance has been used in quantitative analysis of catalysis products (e.g., ref. 6) but again, problems of resolution arise, particularly when a large number of isotopically

related molecules are present.

Because of its high sensitivity and resolution, microwave spectroscopy is a powerful technique for the analysis of mixtures of deuterated organic molecules. Microwave spectroscopy has not been widely utilised as an analytical technique due to the requirements of a dipole moment and a vapour pressure of approximately  $10^{-2}$  torr, preferably at ambient or dry ice temperatures. In addition, it is rather specialised, as spectra are often complicated, and integrated microwave spectrometers have only recently become commercially available. However, catalytic exchange reactions are generally carried out on small molecules to simplify analysis. Many of these can be studied by microwave spectroscopy.

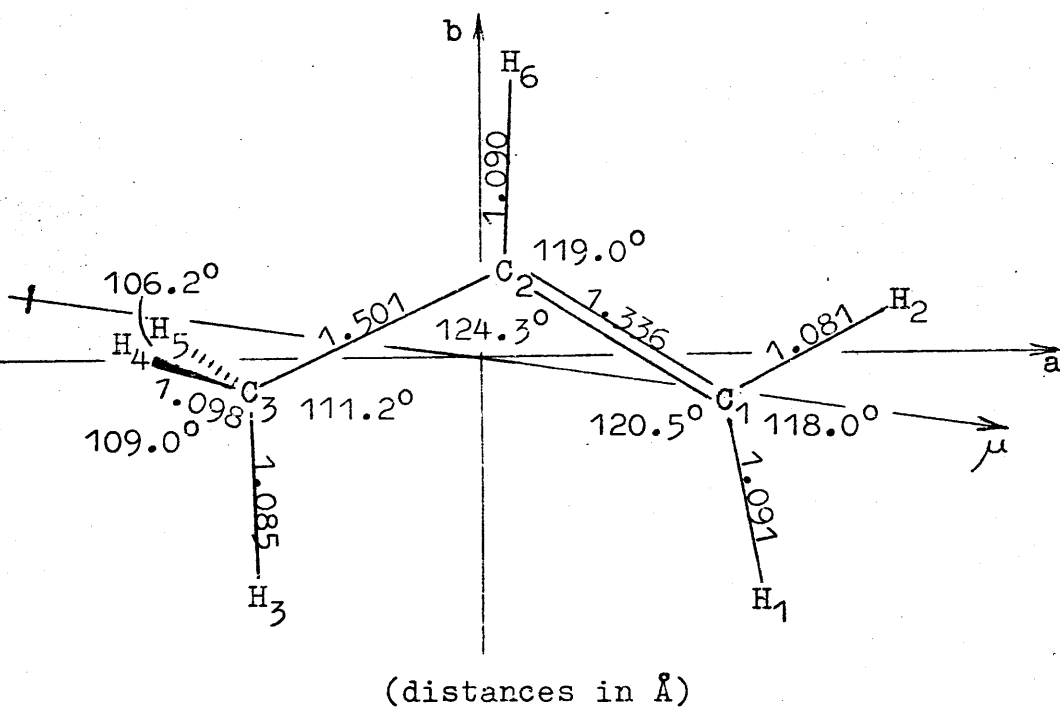
Propene is a suitable molecule for mechanistic studies of catalytic exchange reactions. It is small, which simplifies analysis, and yet may be adsorbed on surfaces as several different species. These include allyl anion, allyl radical, propen-1-yl and propen-2-yl species, and, if there are hydrogen atoms or protons available on the surface, carbonium ion, prop-1-yl and prop-2-yl species. A full analysis of exchanged propenes, locating exactly the positions of the deuterium atoms combined with a qualitative consideration of the catalyst, (e.g. a basic catalyst will favour an allyl anion surface substituent) will give a reasonably precise indication of the reaction mechanism.

Propene has been extensively studied by microwave spectroscopy.<sup>7-11</sup> The molecular structure,<sup>9,11</sup> dipole moment<sup>7,11</sup>

and the potential function for hindered rotation of the methyl group<sup>7,10</sup> have been determined. The structure<sup>9</sup> of propene and the orientation of its dipole moment<sup>11</sup> ( $\mu = 0.364 \pm 0.003$  D) are shown in figure 6.1. Each propene species has three strong lines in Q-band corresponding to the  $J = 1-2$  transitions. Assignment of these spectra is simple, with no significant overlap of lines from the  $d_0-d_3$  species.

Figure 6.1.

The Structure of Propene.



The substance of this chapter concerns the analysis of deuteropropene mixtures formed by heterogeneous catalysis using microwave spectroscopy. The application of microwave spectroscopy to chemical analysis demands consideration of certain theoretical and practical factors. These are discussed in the following sections.

## 2. Factors governing line intensities.<sup>12</sup>

For incident microwave radiation of power  $P_0$ , the transmitted power  $P$ , is given by;

$$P = P_0 \cdot \exp(-\gamma l_{\text{rad}}) \quad (6.1)$$

where  $\gamma$  is the absorption coefficient of the transition and  $l_{\text{rad}}$  is the effective path length of radiation in the cell.

Since  $\gamma l_{\text{rad}} \ll 1$ ,

$$P \approx P_0(1 - \gamma l_{\text{rad}}).$$

In a microwave spectrometer, the change in power is observed. This is given by;

$$\Delta P = P_0 l_{\text{rad}} \gamma. \quad (6.2)$$

Thus for a given spectrometer in which the wavelength is considerably smaller than the cut-off value, the absorbed power is proportional to the absorption coefficient for any transition.

The Van Vleck - Weisskopf expression for the line shape of a narrow, pressure-broadened absorption is;

$$\gamma = \frac{8\pi^2 N f}{3k c T} |\mu_{ij}|^2 \nu^2 \frac{\Delta \nu}{(\nu - \nu_0)^2 + (\Delta \nu)^2} \quad (6.3)$$

where  $N$  is the number of molecules per ml in the cell,

$f$  is the fraction of these molecules in the lower of the two states involved in the transition,

$|\mu_{ij}|^2$  is the square of the dipole matrix element summed over three perpendicular directions in space,

$\nu_0$  is the resonant frequency, or, to a good approximation, the centre frequency of the absorption,

$\Delta \nu$  is the half width of the line at half maximum intensity

and the other terms have their usual meanings.

The peak absorption of the line lies very close to

$\nu = \nu_0$  and is;

$$\chi_{\max} = \frac{8\pi^2 N f |\mu_{ij}|^2 \nu_0^2}{3ckT\Delta\nu} \quad (6.4)$$

This parameter is independent of pressure over a large range, since both  $N$  and  $\Delta\nu$  are proportional to it. In quantitative analytical work, precise ratios of the various  $N$  values are required. These can be obtained by comparison of peak intensities ( $\chi_{\max}$ ) only if corrections are made for the other variables in equation 6.4. These are considered below with respect to analysis of deuterio-propene mixtures.

f. The fraction of molecules occupying the lower level will change upon deuteration. This fraction may be expressed as;

$$f = f_J \cdot f_V \quad (6.5)$$

$$\text{where } f_J = \frac{(2J+1)\exp(-\frac{E_{J\tau}}{kT})}{\sum_J (2J+1)\exp(-\frac{E_{J\tau}}{kT})}$$

$$\text{and } f_V = \exp(-\frac{E_V}{kT}) \prod_n \left[ 1 - \exp(-\frac{h\omega_n}{kT}) \right]^{d_n}$$

which are, respectively, the rotational and vibrational components. If  $\frac{kT}{h} \gg A$ , the rotational part may be written;

$$f_{J\tau} = (2J+1)\exp(-\frac{E_{J\tau}}{kT}) \sqrt{\frac{ABC}{\pi}} \left(\frac{h}{kT}\right)^{\frac{3}{2}} \quad (6.6)$$

This approximation has been reported<sup>13</sup> to be reasonably accurate for  $T > 100$  K. Consequently a ratio of the respective  $(ABC)^{\frac{1}{2}}$  terms for two isotopic species is a good estimate of the correction required for different rota-

tional populations of the  $1_{01}$  level, the exponential term in equation 6.6 being very close to 1 for all isotopic species.

The vibrational component is not so easily taken into account. Most of the excited vibrational states in each isotopic species is populated to only a small extent at 195 K. The first excited states of the methyl group torsion vibration, however, are significantly populated. No measured frequencies of this vibration are available for the various deuterated species. To obtain an indication of the range of ground state populations, the energy of the first excited state relative to the ground state was calculated for normal propene and  $CD_3.CH.CH_2$ . Taking the reported value<sup>7</sup> for  $V_3$  of  $692\text{ cm}^{-1}$ , and using the harmonic oscillator approximation, 210 and  $165\text{ cm}^{-1}$  were obtained respectively. This gives a difference of approximately 10% in ground state populations. Because of the complexity of this calculation for the singly and doubly deuterated methyl group species, no correction has been made for these differences. However, the above results represent the most extreme case, and it is unlikely, even in such a case, that any imbalance introduced by this approximation will exceed 4% of the total mixture.

$|\mu_{ij}|^2$ . The dipole moment matrix element may be written as;

$$|\mu_{ij}|^2 = \frac{\mu_g^2 \cdot S_{J_t J_t'}}{2J+1}$$

where  $\mu_g$  is the appropriate dipole component,  $g = a, b, c$ , and  $S_{J_t J_t'}$  is the transition strength.

The transition strength will change on deuteration due to differences in the rotational constants. This change is small and may be neglected. The change in the dipole component arises from the swing of the inertial axes on deuteration. Since the direction and magnitude of the dipole moment are known,<sup>7,11</sup> this change can be evaluated. The largest change in dipole component relative to the normal species is that of  $d_3(1,4,5)$  propene, the labels referring to the H positions shown in figure 6.1. The angle of rotation of the inertial axes between these is  $2^{\circ}36'$ , which changes the  $\mu_a$  component from 0.360 D to 0.358 D. The change in this component is small because of the small angle subtended by the dipole to the a-axis. As the relative change is within the experimental error, no correction was applied for differences in the dipole moment matrix element.

$\nu_0^2$ . The change in intensity arising from the square of the resonance frequency is easily taken into account. This, in most cases, is the largest correction, sometimes greater than 25% between the  $d_0$  and  $d_3$  species.

$\Delta\nu$ . It is not easy to correct for the half-width at half maximum intensity. Any correction for this, however, would be expected to be small. As  $\Delta\nu$  tends to be small at normal working pressures, ca. 0.4 MHz, it is difficult to measure. A study of several isotopic species in a mixture showed that to within experimental error, the  $\Delta\nu$  values were the same, and so no corrections have been made for this.

Selection of a transition for intensity measurements is very important. The microwave spectrum of propene is complicated by the internal rotation of the methyl group. The  $J = 1-2$ ,  $K_{-1} = 1$ , lines in the spectrum of the normal species are clearly split into two components. This splitting is different in other isotopic species; in particular, it decreases considerably on deuteration in the methyl group. Consequently, these lines are unsuitable for intensity measurements. The splitting in the  $1_{01}-2_{02}$  transition is very small and is not evident at the pressures used here.

Further justification for use of the approximations outlined above is obtained from the consistently good agreement between microwave and mass spectrometric analyses. Table 6.1 shows the correction factors used in the analyses. The observed intensities of the  $1_{01}-2_{02}$  transitions are multiplied by the appropriate correction factor to give the 'true' intensities.

Certain instrumental and practical considerations must also be made. Specialised equipment for analytical work by microwave spectroscopy is generally unnecessary, as the difficulties encountered are the same, although somewhat more critical, as those found in more usual applications.

The Stark spectrometer provides the simplest means of obtaining good sensitivity, but it has some disadvantages in quantitative analysis. Care must be taken that the responses of the signal amplifiers are linear, that reflections in the absorption cell are minimised, and

Table 6.1.

Intensity Correction Factors for  
Analysis of Deuteriopropene Mixtures.

Species	Correction Factor	Species	Correction Factor
$d_0$	1.0000	$d_3(1,2,3)$	1.7841
$d_1(1)$	1.2001	(1,2,4)	1.8769
(2)	1.2712	(1,2,6)	1.7456
(3)	1.2034	(1,3,4)	1.7371
(4)	1.2440	(1,3,6)	1.6265
(6)	1.1646	(1,4,5)	1.8278
$d_2(1,2)$	1.5218	(1,4,6)	1.7161
(1,3)	1.4201	(2,3,4)	1.8508
(1,4)	1.4941	(2,3,6)	1.7379
(1,6)	1.3931	(2,4,5)	1.9298
(2,3)	1.5161	(2,4,6)	1.8155
(2,4)	1.5823	(3,4,5)	1.7699
(2,6)	1.4773	(3,4,6)	1.6759
(3,4)	1.4620	(4,5,6)	1.7513
(3,6)	1.3729		
(4,5)	1.5396		
(4,6)	1.4382		

that the square-wave modulation voltage has a good wave form, the voltage being sufficiently high to completely resolve the Stark components. Other precautions include ensuring that the rate of sweep through a line is slow enough to avoid distortion of the line shape with resultant loss of intensity, and that the microwave power is sufficiently low to avoid power saturation. The spectrometer must be generally stable, as must the temperature of the absorption cell.

Minimisation of reflections in the cell is particularly important, as a 10% variation in the transmitted power with frequency, can produce a 20% variation in the response of the spectrometer to a given transition. Reflections are reduced by; placing a ferrite isolator between the microwave source and the absorption cell; tapering the Stark septum at both ends; and optimising the length of taper from the X-band waveguide of the cell to the Q-band source and detector.

Adsorption of gases on surfaces in the cell presents a serious problem. Because of the small samples used, a very small amount of material adsorbing or outgassing during analysis will have a pronounced effect on the results. There are several means of counteracting this. The cell is designed in such a way as to minimise adsorption on surfaces, teflon being used as an insulator. The cell may be outgassed between analyses by prolonged pumping at an elevated temperature. This, however, is impractical in observation of deuteropropene mixtures at 195 K. In practice, two batches of the sample to be analysed are

allowed into the cell for periods of approximately 15 minutes to permit any exchange with the cell walls, pumping out after each. Another batch is then admitted, this being pumped to a normal working pressure of 0.05 torr. The remainder of the experimental procedure is detailed below.

The catalytic exchange reactions were carried out by Dr. C.S. John in the University of Edinburgh and the product mixtures brought to Glasgow for analysis. A selected sample is frozen in liquid nitrogen and any air pumped out on the vacuum line. It is then admitted to the Stark cell as outlined above.

Recorder pen deflections are maintained in the same order of magnitude using an attenuator of approximately 10 dB, and recorder sensitivity gains of 2 and 5 times. The load on the attenuator varies with the gain setting of the 100 KHz receiver and, as this is generally different for each analysis, the attenuator must be calibrated using a strong  $1_{01}-2_{02}$  transition.

The sweep width for the measurement of each line is constant at approximately 25 MHz. Each region is swept at a rate of 0.4 MHz/s using a bandwidth of 10 Hz. A consistent transmitted microwave power level with detector crystal current of 100  $\mu$ A at the line centre is used. The Stark voltage required to fully resolve the lines is 1200 V. The receiver gain control, recorder sensitivity and attenuation are adjusted for good line shape and almost full scale deflection for the  $1_{01}-2_{02}$  transition of the most abundant component.

The  $d_0$  and  $d_1$   $J = 1-2$  transition frequencies have been reported.<sup>9</sup> Those of the  $d_2$  species were calculated from the rotational constants given by Hirota and Morino.<sup>11</sup> The moments of inertia of the  $d_3$  species were calculated using the structure of Lide and Christensen<sup>9</sup> and corrected by the difference between calculated and observed moments of the normal species. The rotational constants from these were used to predict the  $J = 1-2$  frequencies to within about 2 MHz. The calculated  $d_2$  and  $d_3$  frequencies are shown in table 6.2.

Each line is recorded three times to minimise random error, and more often if these are not consistent. The  $1_{01}-2_{02}$  transition of the most abundant species is repeated regularly throughout an analysis to monitor adsorption on the interior surfaces of the cell, and any drift in the phase sensitive detection system. If the phase control requires adjustment, the reference line is recorded at the new setting. Correction for any line recorded prior to this is made by assuming a constant rate of drift. This assumption is reliable, as no drift in phase greater than 10% has been observed.

The intensities of the  $1_{01}-2_{02}$  transitions of the various species are then measured and multiplied by the appropriate correction factor, taking account of any drift in phase or change in recorder sensitivity or attenuator setting. The results are then evaluated on a percentage basis, including in the total any  $d_4$  and  $d_5$  concentrations from the mass spectrometric analysis.

Table 6.2.

Calculated Transition Frequencies,  $d_2$ - and  $d_3$ -Propenes.

Species	$1_{01}-2_{02}$	$1_{11}-2_{12}$	$1_{10}-2_{11}$
$d_2(1,2)$	31070.98	29958.28	32244.84
(1,3)	32382.78	31013.60	33862.16
(1,4)	31475.28	30432.72	32754.56
(1,6)	32905.34	31391.77	34567.23
(2,3)	31040.10	29954.53	32182.79
(2,4)	30266.61	29468.32	31092.80
(2,6)	31632.14	30414.51	32928.65
(3,4)	31701.22	30655.79	32803.77
(3,6)	33011.92	31509.44	34658.56
(4,5)	30951.76	30224.05	31705.19
(4,6)	32169.33	31003.00	33413.08
$d_3(1,2,3)$	30037.99	28841.91	31316.05
(1,2,4)	29244.00	28325.97	30205.75
(1,2,6)	30566.91	29239.81	32005.27
(1,3,4)	30527.91	29378.91	31757.45
(1,3,6)	31805.89	30214.63	33587.65
(1,4,5)	29755.55	28907.79	30643.21
(1,4,6)	30940.37	29672.06	32316.18
(2,3,4)	29315.35	28410.53	30261.91
(2,3,6)	30526.81	29228.24	31929.20
(2,4,5)	28653.09	28016.07	29309.09
(2,4,6)	29786.77	28775.35	30854.93
(3,4,5)	30053.80	29195.99	30952.37
(3,4,6)	31141.98	29871.97	32518.71
(4,5,6)	30423.00	29465.44	31435.52

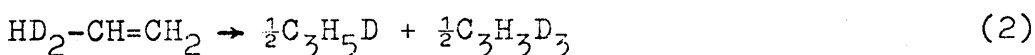
### 3. Example of Mechanistic Studies of Catalytic Exchange Reactions by the Tracer/Microwave Technique.

Microwave spectral analysis of the products of the exchange reaction between normal propene and deuterium on magnesia and rutile showed that exchange proceeded to an equilibrium distribution between the five terminal positions, with no deuterium detected at the (6) position.<sup>14</sup> The intermediate adsorbed species must be either prop-2-yl or carbonium ion species, or an allyl anion with rapid double bond shift. From consideration of other reactions on these catalysts, the allyl anion intermediate, formed by abstraction of a methyl proton, was selected as most reasonable in both cases. In an attempt to confirm this and further elucidate the reaction mechanisms  $\text{CD}_2=\text{CH}-\text{CH}_3$ , ( $\text{d}_2(1,2)\text{propene}$ ), was reacted on each catalyst in the absence of gaseous deuterium.<sup>15</sup>

There are several points of interest in the mechanisms of these reactions. The abstracted proton may be closely associated with the allyl anion on the surface, giving rise to an intramolecular double bond shift process, or there may be a pool of adsorbed protons free to move about the surface, giving an intermolecular mechanism for exchange and double bond shift. It is also of interest to determine whether a kinetic isotope effect operates on the double bond shift. Three processes must be considered;



- double bond shift (H loss - H gain)



- cross exchange (H loss - D gain + D loss

H gain)



- deuterium scrambling (D loss - D gain)

The cross exchange is monitored by mass spectrometry and when the required extent is achieved, the propene mixture is condensed and removed for analysis by microwave spectroscopy.

The results of the microwave analyses are shown in tables 6.3 and 6.4, reproduced here for convenience from Appendix 2. As in the appendix, reactions on magnesia at 195 K are designated  $M(\tau)$ , where  $\tau$  is the duration of reaction in minutes, and those on rutile at 453 K,  $T(\tau)$ .

In Appendix 2 a full discussion of these results in terms of the reaction mechanisms, kinetics and isotope effects are presented. Here some qualitative conclusions will be drawn from the analyses.

It is evident from examination of the  $d_2$  analyses that, for both reactions, double bond shift to give  $\text{CHD}_2-\text{CH}=\text{CH}_2$  is by far the fastest process, the ratio of  $\text{CD}_2=\text{CH}-\text{CH}_3$  to  $\text{CHD}_2-\text{CH}=\text{CH}_2$  reaching its statistical value of 1:3 before appreciable deuterium scrambling took place. This effect is somewhat less pronounced in the case of rutile. For the exchange over magnesia, double bond shift is fastest, cross exchange considerably slower, and deuterium scrambling the slowest. The latter two were reversed in order for the reaction over rutile. This implies that the intermolecular exchange is faster than the intramolecular process over magnesia, while the reverse is true for rutile.

Table 6.3.

Microwave Analyses of d<sub>2</sub>-Propenes.

Normalised Deuterium Distribution (%).

Sample	(1,2)	(3,4)+(4,5)	(1,4)+(1,3)	(2,4)+(2,3)
M(0)	100	0	0	0
M(4)	53.3	46.7	0	0
M(21)	28.0	66.4	2.7	2.8
M(49)	21.2	69.3	4.4	5.3
M(76)	19.8	65.0	7.3	8.0
M( $\infty$ ) <sup>a</sup>	9.4	33.4	26.2	31.0
M( $\infty$ ) <sup>b</sup>	10.0	30.0	30.0	30.0
T(1)	49.0	51.0	0	0
T(5)	25.4	59.1	7.7	7.8
T(27)	12.5	37.6	23.1	26.8

Table 6.4.

Microwave Analyses of d<sub>3</sub>-Propenes.

Normalised Deuterium Distribution (%).

Sample	(3,4,5)	(1,3,4) +(1,4,5)	(2,3,4) +(2,4,5)	(1,2,4) +(1,2,3)
M(21)	48	17	15	19
M(49)	43	19	14	24
M(76)	37	23	17	22
M( $\infty$ ) <sup>a</sup>	14	31	31	24
M( $\infty$ ) <sup>b</sup>	10	30	30	30
T(5)	42	20	11	26
T(27)	19	36	17	28

a. Sample reacted at 195 K for 85 min then 298 K for 70 min.

b. Equilibrium distribution for 5 exchangeable hydrogen atoms.

Over both catalysts  $\text{CD}_3\text{-CH=CH}_2$  constituted 50% of the initial  $\text{d}_3$  products, slowly decreasing to an equilibrium value of 11%, suggesting that this species is considerably more stable than the other positional isomers. This provides evidence for a kinetic isotope effect, the effect being less marked in the exchange over rutile.

This work demonstrates the power of microwave spectroscopy as a technique for analysis of catalytic exchange reaction products, particularly when a specifically labelled molecule is used. The postulated exchange reaction mechanisms<sup>14</sup> have been confirmed, and information on the adsorbed species obtained.

#### REFERENCES.

1. Y. Hironaka, K. Hirota and E. Hirota, Tetrahedron Letters, 1966, 2437.
2. K. Hirota, Proc. 5<sup>th</sup> International Congress on Catalysis, 1972, 37.
3. K. Tamara, Annals N.Y. Acad. Science, 1973, 213, 161.
4. F.H. Field and J.L. Franklin, "Electron Impact Phenomena", Acad. Press, New York, 1957.
5. K. Hirota and Y. Hironaka, J. Catalysis, 1965, 4, 602.
6. P.B. Wells and G.R. Wilson, Disc. Far. Soc., 1966, 41, 237.
7. D.R. Lide, Jr. and D.E. Mann, J. Chem. Phys., 1957, 27, 868.
8. D.R. Herschbach and L.C. Krisher, J. Chem. Phys., 1958, 28, 728.
9. D.R. Lide, Jr. and D. Christensen, J. Chem. Phys., 1961, 35, 1374.
10. E. Hirota, J. Chem. Phys., 1966, 45, 1984.
11. E. Hirota and Y. Morino, J. Chem. Phys., 1966, 45, 2326.

12. C.H. Townes and A.L. Schawlow, "Microwave Spectroscopy", McGraw-Hill Book Co. Inc., New York, 1955.
13. A.R. Gordon, J. Chem. Phys., 1934, 2, 65.
14. B.T. Hughes, C. Kemball and J.K. Tyler, J. Chem. Soc., Faraday I, 1975, 71, 1285.
15. C.S. John, R. Dickinson and J.K. Tyler, J. Chem. Soc., Faraday I, 1976, 72, 1782.